Determination of a normal orogenic palaeo-geothermal gradient with clay mineral and organic matter indices: a review

Rafael Ferreiro Mählmann, Meinert Rahn, Sébastien Potel, Lan Nguyen-Thanh, Rainer Petschick

SGG SGS sc | nat
Swiss Journal of Geosciences

ORIGINAL PAPER

Open Access

Determination of a normal orogenic palaeo-geothermal gradient with clay mineral and organic matter indices: a review

Rafael Ferreiro Mählmann[1*], Meinert Rahn[2], Sébastien Potel[3], Lan Nguyen-Thanh[1] and Rainer Petschick[4]

Abstract

A collection of large data sets from different orogenic belts was compiled for a correlation between organic matter (OM) versus clay mineral (CM) indices calibrated with the vitrinite reflectance, (VR) vs Kübler-Indices (KI) method. Data selection was based on a normal geothermal gradient (25 to 35 °C/km) as determined in previous studies, e.g. by maturity modelling and clay mineral reaction progress calculations. In the Lower Austroalpine (Eastern Switzerland, European Alps) a 20 myr lasting metamorphic overprint caused an OM–CM thermal equilibrium among the indices used. The observed correlation enables to determine gradual changes in metamorphic factors such as pressure, temperature and time causing sensitive shifts of the gradient slope in the range of normal gradients. For New Caledonia, an identical correlation has been determined. Prior to re-equilibration of the VR/KI indices, sediments in New Caledonia of diagenetic to incipient metamorphic grade underwent a high-pressure subduction event. VR/KI indices are in or close to equilibrium, while slight differences in OM vs CM indices allow for a better understanding of polyphase conditions, especially with respect to pressure. Temperature estimations are identical despite of their poly-phase metamorphic history, which was mainly controlled by the last orogenic thermal event lasting > 5 to < 10 myr. In the eastern Helvetic Alps and Northern Calcareous Alps similar correlations were found with slightly different slopes. Comparison between different regions is possible when using KI standardization and same data discrimination. In both parts of the Alps a complex thermal history of short durations (< 5.0 myr for the Northern Calcareous Alps to 10 myr for the Helvetic Alps) caused similar VR/KI trends, but disequilibrium is suggested by weaker regression parameters. The following correlation is calculated for a moderate geotherm (55 to 74 mWm^2, mean = 61 mWm^2) and normal temperature gradient conditions (25 to 35 °Ckm^{-1}): $KI = 1.134e^{-0.305VR}$, ($R^2 = 0.880$, n = 462) with VR given as $\%R_{max}$, KI as Δ°2θ (limited to values between 0.2 to 1.0 Δ°2θ). With increasing depth (z) a VR gradient of $1.4 \pm 0.2\%R_{max}km^{-1}$ is determined and a KI gradient of 0.09 ± 0.002 Δ°2θ km^{-1} is observed. The study illustrates that a normal geotherm can be described by VR/KI correlation, even if different heating episodes may occur. For the detection of a poly-phase or plurifacial thermal history, several indices of clay minerals and organic matter with very different kinetics should be used, as e.g. demonstrated by strong differences in smectite content at equal VR/KI values versus structural depth. A specific interest is given to the correlation of vitrinite like solid bitumen reflectance as an alternative method to VR, the persistent preservation of liptinite macerals and the stability range of clay minerals and sub-greenschist facies

Handling editor: Paola Manzotti.

Dedicated to Hans Krumm.

*Correspondence:
Rafael Ferreiro Mählmann
Ferreiro@geo.tu-darmstadt.de
Full list of author information is available at the end of the article

critical minerals compared with VR/KI data. Until now, despite the Alps in this study, systematic liptinite maceral studies have not been published in other orogenic settings.

Keywords Normal heat flow, Organic matter reflectances, Maceral preservation, Kübler-Index, Clay minerals, Austroalpine nappes, Helvetic nappes, New Caledonia

1 Introduction

Following a round-table discussion at the Mid-European Clay Conference (MECC) in Dresden 2014, new recommendations for Kübler index standardization have been agreed upon (Warr & Ferreiro Mählmann, 2015). Based on this international agreement a preliminary attempt to define grade of diagenesis and incipient metamorphism considering geothermal gradients calibrated with clay mineral, mineral and maceral index data was presented in a keynote lecture at the MECC in Zagreb 2018. The question was then raised (e.g. by Béla Raucsik, Darko Tibljaš, Goran Durn and Ömer Bozkaya) whether the conclusions represent a rough general estimate, a mean including all geodynamic settings or indicate predictions for a normal geotherm at steady state conditions. The latter question is the main focus of the study presented here.

Cooperation established by the working groups of Hans Krumm (Goethe University, Germany) and Martin Frey (Basel University, Switzerland) between 1984 and 1994 led to several studies and Ph.D. theses, which compiled a large amount of data on very low-grade metamorphism in different orogens. In these days it was assumed that the combination of solid organic matter (OM) and clay mineral (CM) indices would allow generating a universally applicable geo-thermometer to better determine sensitive temperature differences in sedimentary and meta-sedimentary rocks.

Organic matter petrography is the study of solid OM and vitrinite reflectance (VR) the most robust analytical method to determine maturity (Suárez-Ruiz et al., 2012; Hartkopf-Fröder et al., 2015; Hackley et al., 2015). The potential to determine maturity in sedimentary rocks (shales) was proposed first by Teichmüller (1958), referring to a traditional method used in coal mining since Hoffman & Jenkner (1932). Vitrinite like solid bitumen reflectance (VlBR, according to Ferreiro Mählmann & Le Bayon, 2016), a maturity determination method hardly considered in very low-grade metamorphic (VLGM) studies so far is especially outlined, because solid bitumen (SB) is the most frequent OM found in clay rocks, mudstones, shales, slates and phyllites (Hackley & Cardott, 2016). Such rocks also represent the main lithotype (pelites, meta-pelites) used in VLGM rocks to determine the grade of diagenesis and incipient metamorphism by clay mineralogy (Ferreiro Mählmann et al., 2012). Measuring the sharpness ratio of the 10 Å-basal peak of illite is the most popular method used for VLGM rocks (Weaver, 1961; Kübler, 1967; Frey, 1987a). The terms diagenetic zone, anchizone, and epizone are defined strictly by KI values (Frey, 1987a). The anchizone lower and higher boundary are given with the KI values of 0.42 and 0.25 $\Delta°2\theta$ (Kübler, 1967). The combination of OM petrography and clay mineralogy can be used for predicting relatively precise temperatures in diagenetic to incipient metamorphic terranes. Limitations of the illite Kübler Index (KI, Kübler, 1967, 1968) and the VR method are extensively discussed in reviews such as Ferreiro Mählmann et. al. (2012). It was demonstrated that one single method is not sufficiently indicative to be used as a geo-thermometer (see also Árkai, 1991). Despite routine application as maturity index, VR data need to be calibrated with other mineralogical and geochemical parameters, if used for thermal modelling (Ferreiro Mählmann, 1994, 2001).

When comparing VR/KI, VR/VlBR and VlBR/KI correlations from different geodynamic settings from diagenesis to low-grade greenschist and low-grade blueschist facies (according to Winkler, 1979), the relationships show significant different trajectories in correlating graphs (Fig. 1, and Ferreiro Mählmann et al., 2012). Thus, temperature (T) and pressure (P) differences cause discrete regression formalisms, in particular if one thermo-tectonic event was predominant. Plurifacial (metamorphic events crossing different metamorphic facies along one P–T path) or poly-thermal (occurring at different time periods, "poly-metamorphic", according to Bucher & Frey, 1994) diagenetic/metamorphic histories are much more difficult to record. Different kinetic rates of reaction progress controlling the OM and CM indices, especially for short thermal episodes, cause disequilibrium conditions between the indices used (Frey et al., 1980a; Krumm et al., 1988; Ferreiro Mählmann, 1994, 1995, 1996; Potel et al., 2006, 2016; Potel & Trullenque, 2012). Long lasting thermal events at relatively lower temperatures may result in the same values of the thermal indices as short-term thermal tectonic-metamorphic events with relatively higher peak temperatures (Rahn et al., 1994) and the precision of the determined temperature increases with heating time (Ferreiro Mählmann, 2001). Several studies (Wolf, 1975;

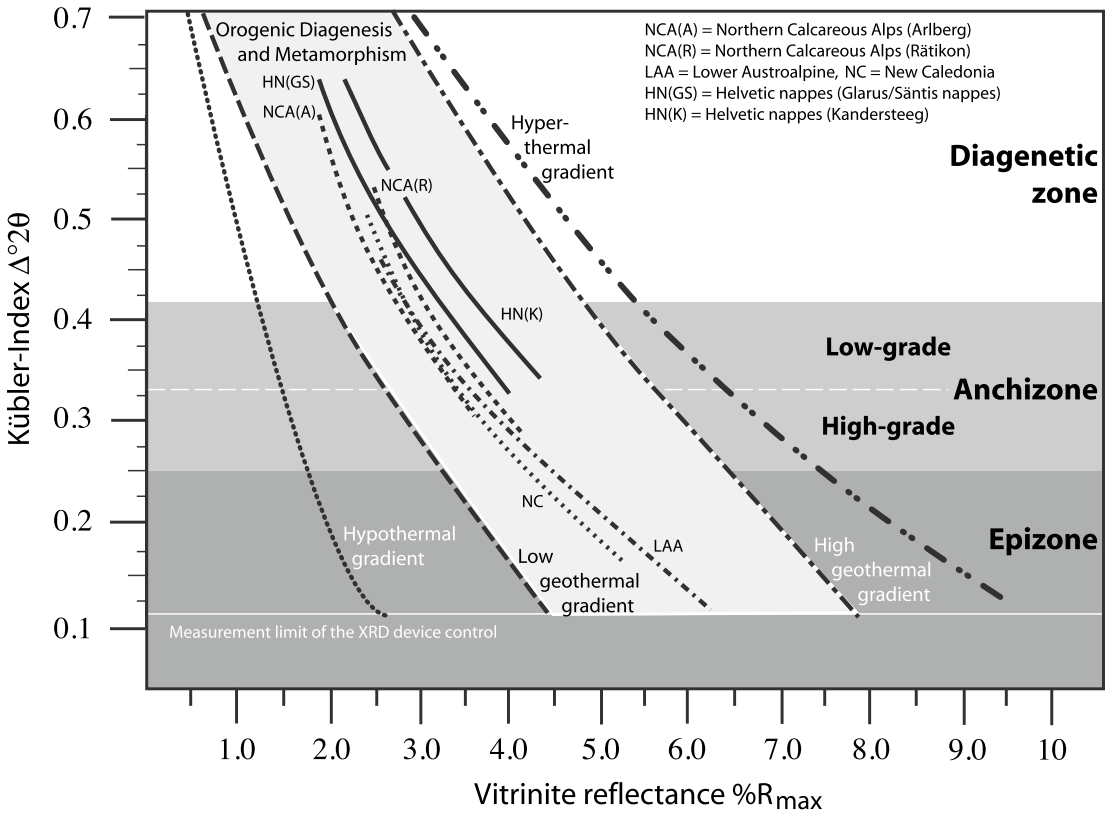

Fig. 1 Kübler-Index (KI) vs. vitrinite reflectance (VR) diagram and determined geothermal gradients; modified from Ferreiro Mählmann et. al. (2012, Fig. 15). The zones of diagenesis, anchizone, and epizone are based on the division by Kübler (1967), with the limits at KI = 0.42 and 0.25 Δ°2θ (Kisch, 1987). Methodical limits are given by VR = 6.5 R_{max}% and KI = 0.115 Δ°2θ (representing the technical limits of the XRD measurement device and the corresponding VR value for normal geothermal gradients). The diagram is calibrated until a KI of 0.6 Δ°2θ

Kisch 1980a, b; Teichmüller, 1987) have demonstrated that the equilibration in VR acts faster than KI or clay mineral aggradation (Frey, 1987a; Petschick, 1989; Ferreiro Mählmann et al., 2012). Considering these factors contolling the VR/KI relationship, only tectonic units were selected for the review being affected by a single metamorphic event or tectonically buried during a long time at normal heat flow conditions (assuming steady state conditions). Establishing a zoning of metamorphic grade based on VR/KI boundary-values is currently the best option to determine metamorphic conditions between 100 and 350 °C in different geodynamic settings, including contact metamorphism and extensional diastathermal basins (e.g. Warr et al., 1991; Belmar et al., 2002; Bozkaya & Yalçin, 2004a; Belmar & Morata, 2005), as well as subduction-related convergent margins (e.g. Kisch, 1980b, 1981; Dalla Torre et al., 1996; Potel et al., 2006).

In Fig. 1, gradients from different areas compiled for this study show a "moderate" orogenic VR/KI gradient (cf. Figure 15 in Ferreiro Mählmann et al., 2012) reflecting normal geothermal/palaeo-geothermal heat flow conditions as demonstrated in the study of Ferreiro Mählmann & Le Bayon (2016). Note that a specific VR value corresponds to a range of different KI values varying with respect to the geothermal gradient, and vice versa. According to earlier reviews (Frey, 1987a) the limit of the diagenetic zone/anchizone varies from 180 to 230 °C with a proposed mean of 200 °C (Frey & Robinson, 1999; Merriman & Peacor, 1999). Based on FI data in the Glarus Alps (Helvetic nappes) a temperature of 230 °C was calibrated (Merriman & Frey, 1999). In more recent studies of the former working groups of Martin Frey and Hans Krumm boundary temperatures of 240 ± 15 °C were deduced (Mullis et al., 2017 and references therein). From these studies, it is evident that very different temperatures may be derived for individual VR and KI values, but a specific VR/KI pair of values should be indicative for one spot in P/T space. In this study the correlation of methods to determine diagenesis to incipient metamorphism will be constrained and characterised for "normal" geothermal conditions, i.e. a range from 25 to 35 °Ckm^{-1} and heat flow values around 65 ± 20 mWm^2. Furthermore, a universal application for orogenic P/T conditions will be proposed.

After presentation of the compiled database the temperature–pressure histories of the different areas from

which the samples originate are discussed briefly. It will be demonstrated that small differences in pressure, heat-flow, and the duration of the thermal peak (interval of nearly same peak temperatures) cause significant correlation differences in the same range of temperature.

In this study the terms "high" and "low" will be used with respect to grade of metamorphism, grade of diagenesis, and stage of maturity. For the characterisation of a geothermal gradient the terms "hypothermal" for <25 °Ckm^{-1} and "hyperthermal" for >35 °Ckm^{-1} (Robert, 1988) are applied. The terms "upper", "middle" and "lower" will be used to define tectonic, structural, and geographic altitude or depth positions, while "early", "mid" and "late" will be restricted to time, (e.g., time of diagenesis/metamorphism or deposition).

2 Database

Areas in agreement with P–T-conditions of a normal geothermal gradient defined in the introduction (Fig. 1) include in Switzerland and Austria (Fig. 2) the western part of the Northern Calcareous Alps (Upper Austroalpine nappes, Vorarlberg, Eastern Austria), the Lower Austroalpine and South Penninic nappes of the Oberhalbstein (Grison, Western Switzerland), the Helvetic nappes (Säntis and Glarus Alps, Switzerland and Bregenzer Wald Helvetic nappes, Austria), the Dauphinois nappes (Pelvoux Massif, France), and NW New Caledonia (France).

First KI values from the Northern Calcareous Alps west of the Arlberg region (Fig. 2) were published by Schramm (1980, 1982a, 1982b), Krumm (1984), Kralik et. al. (1987), and Kralik & Schramm (1994), first VR measurements by Gaupp & Batten (1985), and Henrichs & Richter (1993). As we do not have KI values from the same locality for all VR analyses (Krumm et al., 1988; Petschick, 1989, Ferreiro Mählmann, 1994), closest KI samples from the same stratigraphic unit and same lithofacies type were included from the first VR and KI studies cited above. The same strategy was applied to all other areas listed below.

Using different illite "crystallinity" indices, first data sets from the Lower Austroalpine of the Grisons were published by Dietrich (1969), and Dunoyer De Segonzac

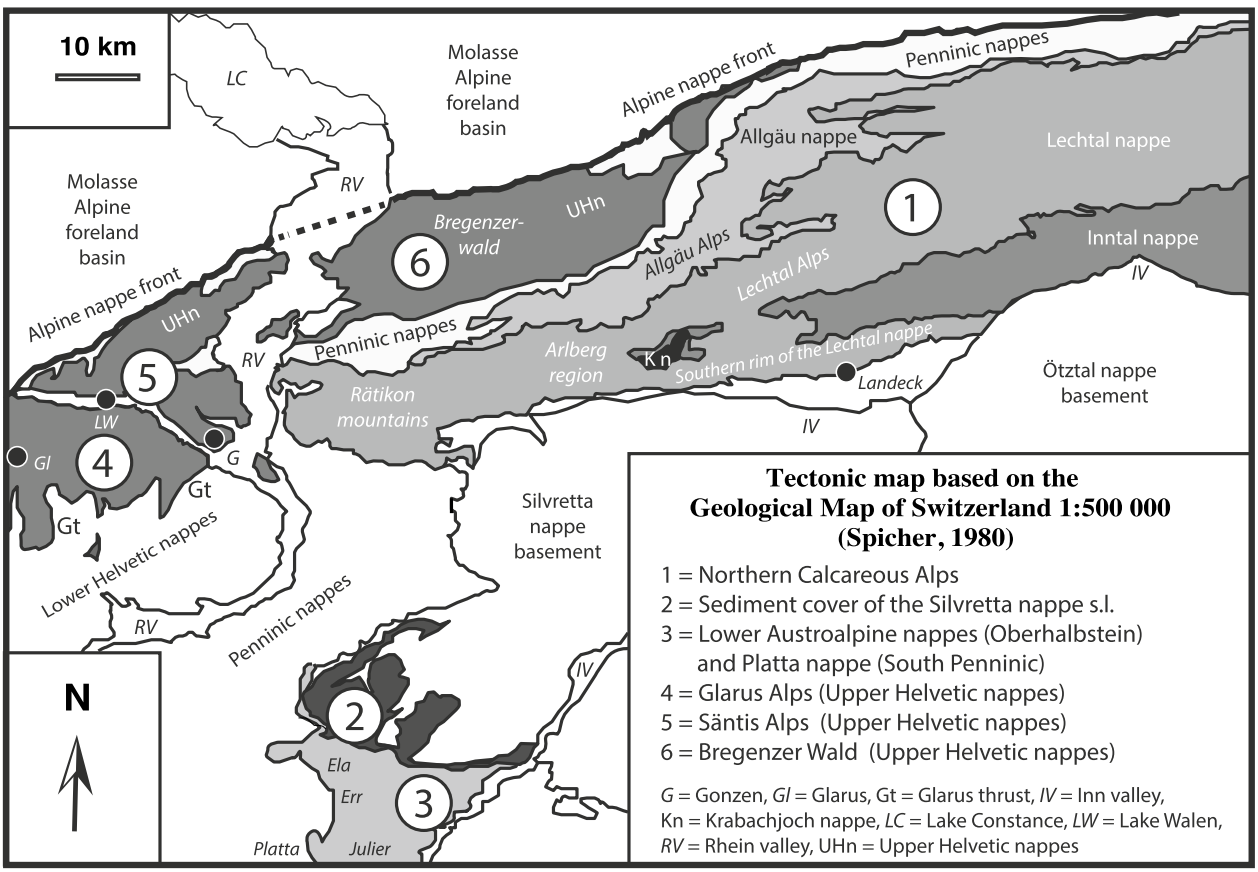

Fig. 2 Tectonic map with the highlighted Alpine nappes shown with different grey scales. The numbers indicate the different data sets compiled in the study and related to nappe stacks of the Helvetic and Austroalpine units. In the large nappe stack of the Northern Calcareous Alps four nappe units are separately shown, the Allgäu-, Lechtal-, Inntal- and Krabajoch nappe

& Bernoulli (1976). The data set was later extended by VR measurements by Henrichs (1993), and Kürmann (1993). A large number of VR and KI values listed by Ferreiro Mählmann (1995, 1996) complete the data set. Included in metamorphic studies from the southernmost area (but north of the Engadine line) Nievergelt et. al. (1996), and Handy et. al. (1996) published VR and KI values. Data were used to propose first published coalification, illite aggradation, clay mineral transformation and organic matter trends with increasing P–T-grade at a normal thermal gradient of 30 ± 2 °C (Ferreiro Mählmann, 2001). New measurements are presented in this study extending the dataset to lower tectonic units and more to the south for a better understanding of conflicting results with Handy et. al. (1996).

The third area, the Helvetic nappe system is one or the most prominent study area of low temperature metamorphism and a frequently referenced area in the VLGM community. Shortly, after publication of the basic studies on illite "crystallinity" (Kübler, 1964, 1967, 1968), redefined as Kübler-Index (Guggenheim et al., 2002), the first diagenetic to metamorphic field gradient from the Jura mountains across the Central Helvetic Alps following one single stratigraphic lithology was studied by Frey (1969). A second section across the Alps presented by Kübler et. al. (1979a) included VR data. Several thousand KI samples and several hundreds of VR samples were measured in the Helvetic domain since and are part of an extensive data file including new and unpublished measurements (for new measurements, see Tables 1, 2, 3 and 4). In a landmark study, Frey et. al. (1980a) demonstrated that VR/KI correlations show regional differences within the Helvetic domain when calibrated against fluid inclusion and mineral paragenesis data. Within the Helvetic realm different Helvetic/Ultrahelvetic nappes and nappe stacks occur, and VR/KI relationships must be explained assuming different tectonic burden and geodynamic conditions or thermal regimes. In the study of Frey et. al. (1980a) it was implicitly suggested that the thermal gradient might be an important controlling factor. It was demonstrated that VR/KI correlations are different in orogenic settings with respect to coal basins (Kübler et al., 1979a, Środoń, 1979). This led to many regional studies in orogenic settings and especially in the Helvetic Alps. In a compiling paper (Ferreiro Mählmann et al., 2012) some areas show a VR/KI correlation resulting from normal geothermal heat flow conditions, as e.g. observed in the Kandersteg area (Árkai et al., 2002) and the Glarus Alps (Rahn et al., 1994). Due to

Table 1 Samples from around the Toissa Outlayer, partly provided by Daniela Krieg (BSc thesis)

Sample	VR %Rmax	n	s	KI Δ°2Θ	n	Tectonic unit	mNN
Flysch F 70	7.4	16	0.65	0.13	3	Platta	2408
Palombini Pa 46	4.9	52	0.38	0.26	3	Carungas	1232
Aptychus J 85	6.5	22	0.62	0.15	3	Carungas	1245
Palombini Pa 47	7.0	28	0.47	0.13	3	Platta	1952
Aptychus J 83	7.2	15	0.56	0.13	3	Platta	1952
Flysch F 58	8.0	18	0.72	0.18	1	Platta	1792
Raibl RS 159	8.6	3	–	0.17	1	Toissa	1851
Palombini Pa 42	7.9	6	–	0.20	1	Platta	1361
Palombini Pa 44	9.5	5	–	0.20	1	Platta	2288
Palombini Pa 45	8.7	25	0.66	0.17	1	Platta	1942
Flysch F 67	8.2	38	0.42	0.20	1	Platta	1642

Table 2 Samples from Piz Ducan, partly provided by Patrik Meister (diploma thesis)

Sample	VR %Rmax	n	s	KI Δ°2Θ	n	Tectonic unit	mNN
Platten Limest	3.5	24	0.42	0.37	3	Silvretta	1885
Platten Limest	3.3	21	0.38	0.40	3	Silvretta	1885
Kössen Fm	2.9	34	0.35	0.38	3	Silvretta	1935
Kössen Fm	3.2	72	0.21	0.38	3	Silvretta	1935
Kössen Fm	3.2	50	0.27	0.45	3	Silvretta	1935
Kössen Fm	3.0	28	0.34	0.42	3	Silvretta	1935
Kössen Fm	3.1	50	0.22	0.38	3	Silvretta	1935

Table 3 Samples from around the Vrenelisgärtli, provided by Martin Frey

Sample	VR %Rmax	n	S	KI Δ°2Θ	n	Tectonic unit	mNN
MF 1321	3.6	39	0.19	0.34	1	Glarus	856
MF 1322	3.2	41	0.12	0.39	1	Axen	1200
MF 1322k	3.3	23	0.08	0.32	1	Axen	1202
MF 1322 b,c,d	3,3	55	0.16	0.39	1	Axen	1202
MF 1323	3.6	19	0.19	0.41	1	Axen	1230
MF 1324	3.6	11	0.10	0.43	1	Axen	1340
MF 1325	3.4	26	0.21	0.40	1	Axen	1792
MF 1326	3.1	45	0.18	0.40	1	Axen	1805
MF 1327	3.1	47	0.13	0.40	1	Axen	1818
MF 1328	2.9	7	0.21	0.43	1	Axen	1820
MF 1329	2.7	10	0.27	0.47	1	Axen	1825
MF 1330	3.0	39	0.15	0.42	1	Axen	1908
MF 1331	2.1	24	0.12	0.85	1	Axen	2860
MF 1331 b	2.5	32	0.24	0.72	1	Axen	2860
MF 1332	2.7	18	0.28	0.55	1	Axen	2632
MF 1336 bit	2.4	34	0.30	1.06	1	Axen	2200
MF 1337 bit	2.8	29	0.34	0.89	1	Axen	2150
MF 1338 bit	3.0	22	0.29	0.70	1	Axen	2070
MF 1340	3.8	14	0.08	0.43	1	Axen	1520
MF 1341	3.5	52	0.19	0.43	1	Axen	1082
MF 1342	3.1	42	0.27	0.45	1	Mürtschen	820
MF 1343	3.4	18	0.32	0.38	1	Glarus	750

Three samples, bold letters, are very rich in solid bitumen (see text)

Table 4 Samples from the Walenstadt–Hinterrugg (2306 m) section, sampled in a project with Martin Frey

Sample	VR %Rmax	n	s	KI Δ°2Θ	n	Tectonic unit	mNN
QK 1 WS (CH)	3.9	9	0.48	0.27	3	Axen	885
QK 2 WS (CH)	3.7	11	0.38	0.35	3	Axen	1685
ZS 1 WS (CH)	3.0	16	0.16	0.37	3	Axen	1700
ZS 2 WS (CH)	2.9	17	0.19	0.45	3	Axen	1735
ZS 3 WS (CH)	2.6	43	0.21	0.45	3	Axen	1780
ZS 4 WS (CH)	2.9	28	0.14	0.41	3	Säntis	1825
SK 1 WS (CH)	2.2	28	0.24	0.59	3	Säntis	2109
SK 2 WS (CH)	2.3	55	0.18	0.55	3	Mürtschen	1355
VM 1 WS (CH)	2.7	52	0.21	0.57	3	Mürtschen	1175
QK 3 WS (CH)	3.1	11	0.19	0.48	3	Axen	1050
QK 4 WS (CH)	3.6	19	0.30	0.37	3	Axen	955
ZS 5 WS (CH)	3.4	42	0.22	0.37	3	Mürtschen	710
QK 5 WS (CH)	3.4	13	0.32	0.29	3	Mürtschen	580
QK 6 WS (CH)	3.5	8	0.33	0.40	3	Mürtschen	425

an integrated large data set, the focus is on the Glarus and Säntis Alps (Rahn, 1994; Wang, 1994), but comparisons will be made with the Kandersteg (Oeschinen Lake, Fig. 1) section including neighbouring areas (Frey et al., 1976, 1980b; Burkhard, 1987; Suchý et al., 1997; Árkai et al., 2002) and the Bregenzer Wald (Ferreiro Mählmann, 1994; Zerlauth et al., 2015; Mullis et al., 2017).

In the Glarus and Säntis Alps higher structural units (i.e. above the Glarus thrust plane) are characterized by normal thermal VR/KI gradients, while the lower structural units are controlled by increasing strain and

lithostatic pressure (Ferreiro Mählmann et al., 2012). Thus, this study is focusses on the higher structural units. These were studied by Frey (1970, 1987a, 1987b, 1988), Frey & Niggli (1971), Frey et. al. (1973, 1980a), Hunziker et. al. (1986), Rahn (1994), Wang et. al. (1996), and Árkai et. al. (1997). Additional KI and CM studies were combined with VR measurements reported by Ferreiro Mählmann (1994); Erdelbrock (1994); Rahn et. al. (1994, 1995), Ferreiro Mählmann et. al. (2012), and Ferreiro Mählmann & Le Bayon (2016). Both methods were also calibrated against fluid inclusion (FI) data (Frey et al., 1980a; Rahn et al., 1995; Mullis et al., 2002, 2017) and critical (clay) mineral parageneses (Rahn et al., 1994).

The sedimentary cover of the Dauphinois domain (French Alps) was one of the very early studied VLGM areas of the Alps (Aprahamian, 1974; Aprahamian et al., 1975, one of the very first pioneers using the KI and CM data in metamorphic petrology). For this study, data from Aprahamian (1988), Waibel (1990), Ceriani et. al. (2003), and Potel & Trullenque (2012) were included. Fission track data are available from tectono-metamorphic studies by Seward et. al. (1999), Fügenschuh et. al. (1999), and Fügenschuh & Schmid (2003). No VR data have yet been published, but CM data can be compared with aggradation grade of illite by KI data to support the database for normal orogenic palaeo-geothermal gradients.

Finally, data from the northern part of New Caledonia are included, an area well known from studies by Brothers (1970), Brothers & Black (1973) and many others cited in Potel et. al. (2006) for its low-grade blueschist (sub-blueschist) to eclogite facies field gradient. Potel (2001), and Potel et. al. (2006) demonstrated that VR and CM data showed reactivated reaction progress towards higher thermal conditions after pressure peak conditions during a sub-greenschist to greenschist facies event (Potel et al., 2002). Equilibration of different indices under diagenetic conditions was observed along a cross section from the external part of the orogen towards its foreland. Results are important to understand the time–temperature–pressure evolution of chemical and mineralogical reactions and the approach towards steady state conditions along the P–T gradient.

From most of the study areas, vitrinite like solid bitumen (VlB) and migra-bitumen investigations are available (Ferreiro Mählmann, 1994, 1995, 2001; Ferreiro Mählmann & Le Bayon, 2016) to allow formulation of a correlation equation between VR and VlBR for normal geothermal heat flow conditions. Not many attempts were made so far to correlate stages of coalification as defined by optical microscopy with changes of graphitic structures/textures (Wada et al., 1994; Kahr et al., 1996; Petrova et al., 2002; Ferreiro Mählmann et al., 2002).

3 Geologic setting, pressure–temperature evolution, and duration of thermal episodes

For a better understanding of the differences found among the integrated study areas with respect to effective heating-duration at peak temperature conditions, a short overview on the tectonic history and its deciphering by radiometric age dating is given below. For the five study areas a short overview is given. It will be remembered that the structural and starigraphic position in the nappe pile and geologic section is not important. For the compilation the determined thermal grade, tectonic burial pressure, and time of maximum diagenesis and incipient metamorphism is essential. For geological details, structural sections, and maps the cited literature may be used.

3.1 Tectono-metamorphic evolution of the Northern Calcareous Alps

The Austroalpine nappes were part of the northwestern and northern shelf of the Austroalpine-Apulian plate (Adriatic promontory of the African continent, Dercourt et al., 1986) bordering the Piemonte-Liguria Ocean during Jurassic and Early Cretaceous. The Piemonte-Liguria Ocean was situated between the Eurasian and African plates. The Upper Austroalpine of the western Northern Calcareous Alps consists, from bottom to top, of the Allgäu, Lechtal, Inntal and Krabachjoch nappes (Ampferer, 1902, 1914, 1940; Ampferer & Hammer, 1911). The Krabachjoch nappe (Fig. 2) is characterised by a monometamorphic pattern (Fig. 3) and an allochthonous position with respect to the nappes in the footwall (Petschick, 1989). The mainly carbonaceous platform sediments (Permian to Triassic-Jurassic boundary) are part of the distal Austroalpine-Apulia passive margin of the Neothethys region (Oberhauser, 1968; Trümpy, 1975; Froitzheim et al., 1994). The Northern Calcareous Alps form the structurally highest allochthonous nappe system of the Alps, independent of the tectonic model postulated (Zyndel, 1912; Tollmann, 1959; Frank, 1983; Müller-Wolfskeil und Zacher, 1984; Schmid et al., 2004). In synclines and on top of the sediment stacks syn-orogenic Albian to Turonian flysch sediments are occasionally preserved. The structural position on the Northern Calcareous Alps in the Alpine orogen impeded a deep tectonic burial and Cretaceous orogenic metamorphic overprint.

Krumm et. al. (1988), and Petschick (1989) concluded that preserved palaeo-geothermal gradients observed with increasing stratigraphic depth occurred syn-depositionally prior to Alpine deformation. Burial heating in the Upper Austroalpine units inducing peak temperatures on sedimentary rocks took place mainly during the Permian, Anisian to Ladinian and Norian diastathermal subsidence episodes. Burial hyperthermal heat flow, characterized by flat VR gradients in the lower stratigraphic

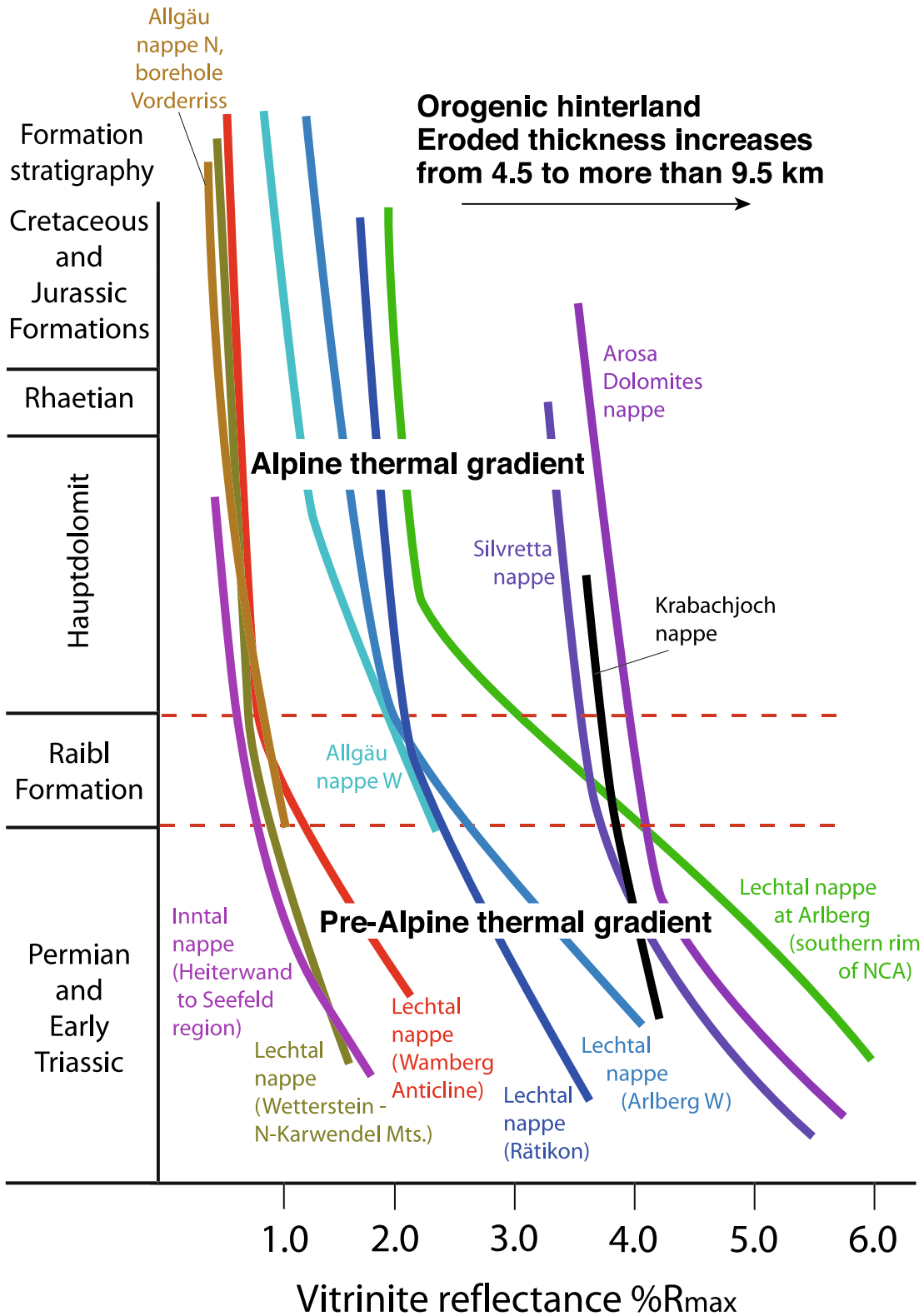

Fig. 3 Vitrinite reflection (VR) gradients from the Austroalpine nappes, plotted along a standardised stratigraphic section. In the formation level of the Raibl and Hauptdolomit formation a prominent change in the VR gradient slope is visible. The flat lower part reflects a pre-orogenic hyperthermal event and the steep upper part was formed during an orogenic Alpine normal geothermal gradient. The compilation uses gradient determinations published by Krumm et. al. (1988), Petschick (1989), Ferreiro Mählmann (1994, 1995, 2001), and Ferreiro Mählmann et. al. (2012)

sections, are shown on Fig. 3 and were extensively described by Petschick (1989), and Ferreiro Mählmann (1994). Sediment deposition not affected by hyperthermal burial conditions (Krumm et al., 1988) ceased during the Late Cenomanian to Turonian (Caron et al., 1982; Ortner, 2003).

During Late Cretaceous Alpine nappe stacking and folding, attributed to the first Austroalpine deformation (AD1) phase, the burial metamorphic pattern was disturbed along tectonic structures. Discontinuous VR or KI data at nappe boundaries or important faults are widely observed within the western Northern Calcareous Alps, especially where Permian to Middle Triassic rocks are not detached at the base of the nappe piles. The onset of thrusting (AD1) is of Albian to Turonian age (Tollmann, 1976; Trümpy, 1980a, 1980b; Froitzheim et al., 1994).

Jurassic to Early Cretaceous sediments underwent post-depositional thermal alteration to higher grades during Alpine orogenesis (Petschick, 1989). A thermal anomaly with a high heat-flow existing in the lower structural parts of the Austroalpine crust is postulated for the Jurassic rifting period (Ferreiro Mählmann, 1994). Thus, for most units of the Upper Austroalpine (Fig. 2) VR gradients observed for Permian to Carnian formation sequences differ from those measured for the Norian to Jurassic/Cretaceous formation successions (the latter is less well reflected in KI aggradation gradient plots, Petschick, 1989). Along the southern border of the Northern Calcareous Alps the gradient subdivision is less evident, but a more continuous gradient pattern from the Permian to the Jurassic (Cretaceous rocks are not cropping out) has been measured (Fig. 3, Rätikon section). In this area, patterns of high-grade anchi- to epizone along folds point to local hydrothermal activity and do not relate to normal geothermal conditions. The technique and discrimination rules applied in this study are explained in Sect. 4.

Epizonal conditions at the southernmost Northern Calcareous Alps (Schramm, 1980, 1982a, 1982b; Kralik et al., 1987; Petschick, 1989) led to Cenomanian to Turonian K/Ar ages for the smallest white mica grain size fraction ages (Ferreiro Mählmann, 1994). Mixed ages from Rb/Sr dating of the same size fraction could not be attributed to a geologic event, but point to a short orogenic peak temperature interval (the same was found using K/Ar analyses from coarser grain size fractions). TTI modelling (Lopatin, 1971; Waples, 1980) based on the timetable of Haq et. al. (1987) with an Alpine orogenic interval >5 myr completely levelled out any maturity differences (Ferreiro Mählmann, 1994). The lower structural nappes of the Walsertal/Arosa zone (South Penninic, Piemonte-Liguria Ocean) remain at much lower maturity. Thus, a short heating duration (<5 myr) must be assumed (Ferreiro Mählmann & Giger, 2012). This is also reflected by high-grade diagenesis KI values for the "Walsertal zone" according to Winkler (1988) and for the Cenomanian/Turonian flysch (Richter, 1957; Winkler, 1988) in the "Arosa zone s.s." according to Ferreiro Mählmann & Giger (2012). In the hanging wall a short orogenic thermal interval of the northern Austroalpine units (Silvretta nappe, Northern Calcareous Alps, Fig. 2) prior to thrusting onto South Penninic units is evident (Ferreiro Mählmann, 1994). The South Penninic Walsertal zone and Arosa zone in the fodwall of the main trust of the Silvretta nappe and the Northern Calcareous Alps is not schown on Fig. 2 because it is a relative thin tectonic mélange unit.

A similar stratigraphy, tectonic and thermal history (Ferreiro Mählmann, 1994, 1995, 1996) is reported for the sediment cover of the Silvretta nappe (Fig. 2), belonging to the Upper Austroalpine (Froitzheim et al., 1994). The main difference controlling metamorphic grade from the foreland to the orogenic hinterland is shown in Fig. 3. Eroded tectonic loads increase from 4.5 to 9.5 km from the Northern Calcareous Alps (N) to the Silvretta nappe (S). A large number of clay mineral and coal petrological data is available (Henrichs & Richter, 1993; Henrichs, 1993; Kürmann, 1993; Ferreiro Mählmann, 1994, 1995, 1996). Between the Silvretta nappe s.l. (including the Silvretta nappe s.s., the Arosa Dolomites nappe and the Rothorn nappe) and the Lower Austroalpine a prominent metamorphic inversion was mapped and related to late Alpine thrusting (Ferreiro Mählmann, 1995). Due to metamorphic inversion and based on tectono-thermal reasons, the Ela nappe was assigned to the Lower Austroalpine nappe system. Diagenesis to metamorphic results were included as follows in the Lower Austroalpine data group.

3.2 Tectono-metamorphic evolution of the Lower Austroalpine

In the Oberhalbstein area "stockwerk tectonics" (Liniger & Nievergelt, 1990) controls the pattern of diagenesis and metamorphism (Ferreiro Mählmann, 1995). Tectonic boundaries were detected by gaps of progressive metamorphism or metamorphic inversion ("transported metamorphism" sensu Frey, 1988) as revealed by using KI, VR, BR, FI, clay mineral and metamorphic mineral assemblages (Frey & Ferreiro Mählmann, 1999). A stack of Lower Austroalpine nappes together with the South Penninic Platta nappe (Fig. 2) corresponds to the middle "stockwerk". Different to the Northern Calcareous Alps the continent–ocean transition of the Austroalpine-Apulia continent plate to the Piemonte-Liguria Ocean plate is preserved in the Platta nappe of the Cretaceous nappe stack.

In the Lower Austroalpine Permian and Mesozoic basins were formed by lithospheric stretching. Sedimentation started during intra-continental rifting with detrital deposits in Permian pull-apart basins accompanied by volcanism (Handy et al., 1996). During the Triassic, dolomite platform sediments were deposited in a passive margin setting of the Hallstatt–Meliata–Vardar Ocean. Assuming intra-oceanic subduction according to Stampfli et. al. (1998) the ocean closed during the Late Jurassic to Early Cretaceous (Channell et al., 1990) in the E of the Austroalpine. This geodynamic event caused the initiation of the Austroalpine nappe formation (Ferreiro Mählmann, 1994; Schmid et al., 2008) triggered by the Vardar obduction (Handy et al., 2010). Pre-rifting to the Piemonte-Liguria Ocean caused the formation of neritic to littoral deposits, mainly carbonaceous platform sediments (Triassic). In the Triassic the Austroalpine was part of the northern shelf of the Tethys. The increase in subsidence passed into the opening of the Piemont-Liguria Ocean in the W of the Austroalpine (Weissert & Bernoulli, 1985). In the new plate tectonic configuration, the Austroalpine nappes where in the Jurassic part of the proximal Austroalpine-Apulia passive margin (Froitzheim et al., 1994, Froitzheim & Manatschal, 1996). In the Early Jurassic, syn-rift conglomerates, shales and turbidites were deposited leading to the formation of a mature continental margin in the Late Jurassic (Froitzheim et al., 1994), while post-rift sediments (radiolarites, limestones, and shales) and Cenomanian to Turonian flysch sediments demonstrate the change to an active margin setting.

In the Platta nappe, ophiolitic rocks are part of the Early Jurassic oceanic crust of the Piemonte-Liguria Ocean (Tollmann, 1978; Trümpy, 1980a, 1980b; Schmid et al., 2004). The Platta nappe is considered a part of the oceanic Piemonte-Liguria basin and is probably an oceanic slice obducted and accreted very early during Cretaceous Alpine orogenesis (Ferreiro Mählmann, 1995). It includes mantle rocks (serpentinite, pyroxenite and peridotite rocks), exhumed and denuded immediately during Middle Jurassic continental break-up (Froitzheim & Manatschal, 1996). The development of the Middle Jurassic to Cretaceous sedimentary cover was the same as described for the Lower Austroalpine nappes.

The thermal overprint of the tectonic "middle stockwerk" is here defined according to data by Ferreiro Mählmann (1995), which comprises the South Penninic Platta nappe together with the Lower Austroalpine Ela, Carungas, Err and Julier nappes (Fig. 2). Ferreiro Mählmann (2001) showed that their maturity pattern (VR and VlBR) is best modelled when postulating more than one heating period (Ferreiro Mählmann, 1994, 2001), including (1) pre-orogenic burial due to thermal subsidence during Permian to Triassic, (2) hyperthermal heat flow during Jurassic rifting, (3) orogenic Early to Late Cretaceous tectonic burial during alpine deformation AD1 nappe stacking, induced by the closure of the Hallstatt-Meliata-Vardar oceanic realm since the Late Jurassic and initial Turonian Austroalpine nappe thrusting (AD1a) from E to W (Dercourt et al., 1986; see references in Dallmeyer et al., 2008), (4) Cretaceous orogenic diagenesis to metamorphism (Cretaceous Alpine orogenesis) triggered by the closure of the Piemonte-Liguria Ocean (Weissert & Bernoulli, 1985; Winkler, 1988; Schmid et al., 2004). The latter phase (AD1b) is considered the main source for forming the maturity pattern found in the area (Ferreiro Mählmann, 1995, 1996, 2001), (5) high heat flow conditions during crustal thinning (AD2) subsequent to orogenic collapse (Nievergelt et al., 1996), preserving temperatures at the same level as during AD1b, and (6) a final retrograde thermal event in the Tertiary when the Austroalpine nappe stack was passively transported to the N, folded and thrusted onto metamorphosed rocks in the footwall (AD3). Metamorphism below the Austroalpine "orogenic lid" according to Laubscher and Bernoulli (1982), and Laubscher (1983) is the result of a second Alpine orogenic cycle. For more details on the tectonic history, see reviews in Froitzheim et. al. (1994), Steck and Hunziker (1994), and Schmid et. al. (1996).

Mineral parageneses and illite-mica ages of epizonal structures gave K–Ar ages of 90 ± 10 Ma for AD1b and quartz-mylonite ages of 70 ± 5 Ma for AD2 (Ferreiro Mählmann, 2001). The Austroalpine is generally characterised by a diagenetic to metamorphic event between 100/80 Ma (e.g. Thöni, 1981; Frank et al., 1987; Kralik et al., 1987; Handy et al., 1996) and 90/60 Ma (Frank et al., 1987; Hunziker et al., 1992). In those parts included in this study, ages of 90 Ma and 70 Ma are interpreted to determine formation and cooling ages. Zircon FT data indicate fast cooling at 60 Ma (Spiegel et al., 2004). Peak thermal conditions endured for a period of 20 myr. An eroded nappe pile of 5 to 7 km was estimated with the onset of exhumation and during orogenic lid tectonics (Ferreiro Mählmann, 2001). The diagenetic to metamorphic Cretaceous pattern is post AD1 and AD2 and pre AD3 (Ferreiro Mählmann, 1995, 2001, see also Frey et al., 1999; Frey & Ferreiro Mählmann, 1999; Oberhänsli et al., 2004; Ferreiro Mählmann & Giger, 2012).

3.3 Tectono-metamorphic evolution of the eastern Helvetic Alps

The Helvetic belt, including the Glarus and Säntis Alps (Fig. 2), represents a stack of sedimentary nappes with sediments deposited during the Mesozoic and early Cenozoic at the northern border of the Penninic Oceans, between the Eurasian and Austroalpine-Apulian plates.

The Penninic realm is palaeo-geographically subdivided from north to south into the Valais basin, the Briançonnais continental plate, and the Piemonte-Liguria basin with oceanic crust (Frisch, 1979). Movement of the Apulian-Austroalpine microplate towards Europa caused accretion of parts of the Piemonte-Liguria Ocean, the Briançonnais continental plate, and Valais basin. Crustal shortening since the Late Cretaceous led to closure of the oceans and eventually to continent–continent collision in the Early Cenozoic (Schmid et al., 2004; Pfiffner, 2009). Continuous orogenic shortening involved the Helvetic shelf, causing a separation of most of the Triassic to Cretaceous/Early Cenozoic sediments from their pre-Mesozoic metamorphic basement and nappe transport from S to N leading to a propagating orogenic front with flysch formation towards the north as the last episode of sedimentation before emergence above sea level.

Tectonic burial under a thick stack of nappe units from more southern proveniences is documented today by the presence of allochthonous Penninic and Austroalpine klippes on top of the autochthonous to parautochthonous Helvetic nappe stack (but nearly completely eroded away in the Glarus and Säntis Alps). From the Säntis Alps in the N to the Glarus Alps in the S an eroded nappe stack of 4.0 to 7.5 km is estimated (Erdelbrock, 1994, Rahn, 1994, Wang, 1994). Burial led to conditions from diagenesis to low-grade greenschist facies metamorphism, generally increasing in grade from N to S. However, several unconformities in the diagenetic/metamorphic pattern illustrate post-metamorphic thrusting ("transported metamorphism" sensu Frey, 1988).

Initial data on the metamorphic gradient within the Glarus and Säntis Alps were gathered by Frey (1969, 1970, 1978), and Frey et. al. (1973, 1980a), while more regional studies were published in the 1990s (Frey, 1988; Erdelbrock, 1994; Rahn, 1994; Rahn et al., 1994, 1995, 1997, 2002; Wang et al., 1996). Metamorphic P–T-conditions determined by Frey & Ferreiro Mählmann (1999), and Mullis et. al. (2017) are based on extended data sets on KI, VR, fluid inclusion composition and homogenization temperatures, and minerals reactions such as kaolinite/pyrophyillite (Frey, 1987b) or the neo-formation of chloritoid (Frey & Wieland, 1975; Rahn et al., 2002). These data demonstrate that diagenetic/metamorphic zones crosscuts nappe boundaries (Frey et al., 1973), while the metamorphic pattern was later dissected by thrusting, in particular along the Glarus thrust plane (Fig. 2; Frey, 1988), for which difference in metamorphic grade allowed to estimate a post-metamorphic thrusting distance of 10 km towards N (Rahn et al., 1995). From the Helvetic napes and cover nappes of the Bregenzer Wald (Fig. 2) maturity studies were published (Eggert et al., 1976; Kuckelkorn et al., 1990; Kuckelkorn & Hiltmann, 1990; Ferreiro Mählmann, 1994; Hiltmann et al., 1995; Krumm et al., 1995; Zerlauth et al., 2015). The results demonstrate a similar tectono-thermal history as found in the Glarus and Säntis Alps (Mullis et al., 2017).

Concordant K–Ar and Rb–Sr ages of around 35–30 Ma were interpreted to represent the main phase of Alpine metamorphism in the Glarus Alps, while a second age group between 25 and 20 Ma was tentatively attributed to movements along the Glarus thrust (Hunziker et al., 1986). Since youngest flysch sediments accumulated in the Glarus Alps (Taveyannaz sandstone) contain zircons of the same age (Lu et al., 2018), it must be assumed that the previous K–Ar and Rb–Sr ages are still biased by a detrital age component, and the second age group may be a more realistic estimation for the age of peak metamorphism. This was recently corroborated dating peak metamorphism in the Helvetic Flysch below the thrust plane at 27.1 ± 0.6 Ma by compiling radiometric ages and new K–Ar and Ar–Ar ages (Akker et al., 2021). Correlations between VR and fluid inclusion data suggested that the maximum thermal peak endured for significantly less than 10 myr (Rahn et al., 1995). Ages from apatite FT dating reflect late exhumation and continued thrusting along the Glarus thrust (Rahn et al., 1997).

The combined application of the various techniques led to several attempts of cross calibration of the methods. A first correlation was presented Frey & Niggli (1971), while data from different areas of the Helvetic Alps (including the Glarus and Säntis Alps) were compared in Frey et. al. (1980a). More regional correlations were published later (e.g. Rahn et al., 1995), but an overview compilation and correlation of the large data sets measured in the 1990s is yet missing here.

3.4 Tectono-metamorphic evolution of the Dauphinois domain

During Mesozoic rifting, the margin of the European plate (Helvetic shelf) became substantially thinned towards east. The formation of major tilted crustal blocks allowed for the deposition of thick Mesozoic sedimentary series in asymmetric half grabens (Davies, 1982; Gillcrist et al., 1987; Tricart et al., 1988; Butler, 1989; Coward et al., 1991; Huyghe & Mugnier, 1995; Lazarre et al., 1996; Sue et al., 1997). The half grabens were inverted during the Alpine orogeny, but relics are preserved within the Pelvoux Massif and immediately north of it. Palaeo-normal faults, such as the "Col d'Ornon" fault (Barféty et al., 1979) are mostly NE–SW striking.

Mesozoic strata are discordantly overlain by a conglomerate formation (Gupta, 1997), followed by a "Priabonian trilogy" (Ravenne et al., 1987; Apps et al., 2004), which comprises, from base to top: (1) shallow water

nummulitic limestone, (2) hemipelagic globigerina marls, (3) the Champsaur sandstone formation, a regular alternance of turbiditic sandstones and shales (Perriaux & Uselle, 1968; Waibel, 1990). In some areas immediately south of the Pelvoux Massif, the siliciclastic deposits contain up to 50% of volcanic detritus (Debrand-Passard et al., 1984; Bürgisser, 1998). The intense volcanism, the increase in subsidence and lithospheric thinning during the Cretaceous in the later Penninic basin was followed by the opening of the Valais Ocean in the S of the Dauphinois (Helvetic) shelf and subsequently the turbidite formation predate the propagation of the Alpine deformation front (Schmid et al., 2004).

The Subriançonnais domain formed the northern Briançonnais passive margin during the opening of the Valais Ocean, representing an intermediate position between the tectonically underlying Dauphinois domain units and the overlying Briançonnais continental plate. The stratigraphically youngest formation of the Subriançonnais units is the Lutetian "black flysch" unit. Shortening of the Valais Ocean and later thrusting on the Dauphinois started in the late Eocene. In map view, the Subriançonnais unit usually forms a narrow zone bordering the Briançonnais domain east and south of the Pelvoux Massif. Crustal thinning along the bordering zone might be explained by late normal faulting, dissecting the Subriançonnais and Briançonnais front (Tricart, 1986), or alternatively, by intense lateral shearing of the units at the eastern rim of the Pelvoux Massif (Rocher de l'Yret shear zone, Trullenque et al., 2006).

The Dauphinois domain SE of the Pelvoux massif underwent VLGM conditions (Potel & Trullenque, 2012), comparable to facies-critical mineral stability fields (Aprahamian, 1988; Waibel, 1990). According to Frey et. al. (1991), and Potel et. al. (2002), the coexistence of zeolites (and in this case laumontite) and prehnite-pumpellyite is restricted to a rather small P–T range below 240 °C (lower part of low-grade anchizone). The reassessment of such low peak temperatures raises doubts on the interpretation of zircon fission track (FT) ages as cooling ages, as proposed by Seward et. al. (1999), and Fügenschuh and Schmid (2003) and see discussion on zircon FT annealing in Brandon et. al. (1998), and Rahn et. al. (2004, 2019). Consequently, existing FT-data do not allow to bracket the duration of the thermal episode (see discussion). The measured K-white mica *b* cell dimension values infer an intermediate geothermal gradient with 25–35 °C/km when comparing with the correlation of Merriman & Peacor (1999). This geothermal gradient was the gradient occurring during peak metamorphism in this part of the Dauphinois domain. The comparison of KI, FT and fluid inclusion data led to the conclusion that the SE of the Pelvoux massif experienced conditions of high-grade diagenetic zone to low-grade anchizone.

Locally, three Alpine deformation phases (D1, D2 and D3) can be recognized (Trullenque, 2005). Available data on metamorphism and deformation SE of the Pelvoux massif indicate that D1 corresponds to the first penetrative schistosity. The observed metamorphic gradient is related to this deformation phase. Burial in the Dauphinois domain reached a maximum of 9 km, caused by tectonic overburden due to overthrusted Penninic units along the D1 Roseland thrust (Potel & Trullenque, 2012). The D2 phase recorded within the investigated area results in SW-directed movements that overprint the top-WNW D1 nappe displacement. D3 normal faults related to the Durance fault system (High Durance Faulted Zone, Tricart, 2004) are the latest deformation pattern found in the investigated area. D2 and D3 deform the metamorphic field gradient observed in the Penninic domain. This observation coroborates the results that peak metamorphism was established earlier, as observed by Ceriani et. al. (2003) further to the N. If the deformation events can be parallelised with the Eastern Helvetic Alps (Sect. 3.3) a similar thermal period can be expected. Therefore, the data from the Dauphinois can help to not only better correlate with Helvetic samples, but also generally compare data sets of normal thermal regimes as needed for the study.

3.5 Tectono-metamorphic evolution of the NE New Caledonia

New Caledonia is a dispersed fragment of the eastern margin of Gondwana resulting from the opening of the Tasman Sea by rifting of New Caledonia and New Zealand from Australia. In Late Eocene time, the New Caledonian fragment collided with an intra-oceanic island-arc system (Cluzel et al., 1994, 2001; Aitchison et al., 1995; Clarke et al., 1997) after a period of subduction tectonics. The collision, responsible for the main deformation of the continental basement of New Caledonia, generated a High-Pressure (HP) schist belt coeval with the southwestwards thrusting of two nappes over the basement, the Poya nappe or "formation des basalts" (Paris, 1981) and the peridotite nappe (an ophiolite complex). The basement is composed of terranes of Palaeozoic to Mesozoic age of varying metamorphic grade, transgressively overlain by Late Cretaceous to Eocene sedimentary rocks deposited during Gondwana dispersal (Aitchison et al., 1995; Clarke et al., 1997). The basement is affected by Late Jurassic high-pressure metamorphism (ca. 150 Ma, Cluzel & Meffre, 2002). A second Eocene HP metamorphism overprinted only the northern part of New Caledonia (Cluzel et al., 2001), i.e. the northern part of the investigated terranes (Potel, 2007).

The post-Early Cretaceous tectonic units comprise the Poya and peridotite nappes and the Koumac, Diahot and Pouébo basement terranes. The Koumac terrane (Cluzel et al., 1994) is a sedimentary terrane preserved as olistrostromes in the collisional structure of northern New Caledonia according to Fitzherbert et. al. (2003). It consists of an intensely tectonized Late Cretaceous to Early Eocene flysch sequence. The Diahot terrane contains an interbedded sequence of Cretaceous to Eocene metasediments and felsic volcanics metamorphosed under high P–T conditions (Fitzherbert et al., 2003). The easternmost Pouébo terrane is composed by a mélange containing large mafic eclogite tectonic slices enclosed in an argillaceous or serpentine-rich matrix (Maurizot et al., 1989). According to Ghent et. al. (1994) the time of metamorphism is bracketed between Early Eocene (youngest Sediments) and Late Eocene (37 ± 1 Ma $^{40}Ar/^{39}Ar$ white mica cooling ages).

Bell and Brothers (1985) demonstrated an increase of temperature during exhumation after peak pressure metamorphism in the lawsonite zone. At the transition between lawsonite and epidote-blueschist zone, all organic matter changed to a well-ordered graphite structure (Diessel et al., 1978). Yokoyama et. al. (1986) presented a P–T path for the higher metamorphic zones, including a temperature-prograde phase of climax crystallisation that prevailed during pressure decline. The eclogite to blueschist facies metamorphism was followed by a collisional orogenic greenschist to sub-greenschist facies event with preserved high grade diagenetic to anchizonal rocks in the foreland structural zone (Potel et al., 2006). This structural part has been included in this correlation study. In contrast, data from the hinterland must be evaluated with caution due to the subduction related HP event. During the collisional stage metamorphic temperatures increased. Thus, during the temperature-prograde path part of the mineral assemblage re-equilibrated under higher temperatures at normal heat flow conditions (Potel et al., 2006). Consequently, it is thought that at least coal indices and clay mineral indices followed the same process.

4 Methods

In all the areas described in Sect. 3 a careful sample selection was performed. Samples selected without (I) signs of weathering (see guidelines in Littke, 1993; Ferreiro Mählmann & Le Bayon, 2016), (II) detrital vitrinite or mica populations, (III) indication for red bed facies, (IV) the evidence for migra-bitumen or migrated solid bitumen (bituminous rocks), and (V) without evidence for prograde hydrothermal activity (for methodical details, see Ferreiro Mählmann et al., 2012). Samples with fluid-driven retrograde processes as described by Nieto & Peacor (1993), Środoń (1999), and Árkai et. al. (2012), commonly found along faults and high permeable psamitic rocks, were also rejected. Many of these five reasons can be observed in the outcrop and hand specimen, and the grade of alteration of a measured value estimated (Fig. 4). Wherever the presence of detrital VR/KI material or weathering effects, not observed in the field, were evident after subsequent analytical steps based on the discrimination graph by Ferreiro Mählmann and Giger (2012, Fig. 5) corresponding samples were discarded too. Additional statistical reasons for data discriminations are reported as follows.

The analytical methods are described in detail in the original sources of the data. 95% of the data have previously been published, and the reader is referred to the cited references. New measurements from the Lower Austroalpine and Helvetic nappes are listed in Tables 1, 2, 3 and 4.

1051 samples (more than 700 samples represented by the mean value of 3 separate measurements per sample) provided KI analyses. Despite their production within different study groups using different preparation techniques, different analytical measurement devices, and different analogue and digitalised XRD (x-ray diffraction) equipments, an inter-laboratory comparison and calibration revealed well compatible results (Ferreiro Mählmann & Frey, 2012). For the KI value compilation, the following aspects were included:

- Recommendations by Kisch (1991), Krumm & Buggisch (1991), and Kisch et. al. (2004); according to Kübler (1967, 1968) the full width at half maximum (FWHM) of the 10 Å illite peak is measured and presented as KI Δ°2θ (Guggenheim et al., 2002).
- KI values from the old mm scale were re-calculated into Δ°2θ (Frey, 1988; Frey & Burkhard, 1992).
- Wherever needed, data were re-calibrated to the Kisch standards (Kisch, 1983) after their transformation to Kübler-Frey values (Ferreiro Mählmann & Frey, 2012; Warr & Ferreiro Mählmann, 2015).
- Application of CIS standards (Warr & Rice, 1994), e.g. in Potel & Trullenque (2012),
- Translation of CIS values based on a calibration formulism to KI values (Warr & Ferreiro Mählmann, 2015).

Therefore, in this study a uniformly calibrated and standardised KI is accomplished for further correlation with VR. The same strategy of standardisation is applied to other diagenetic to incipient metamorphic indices and mineral phase stability limits.

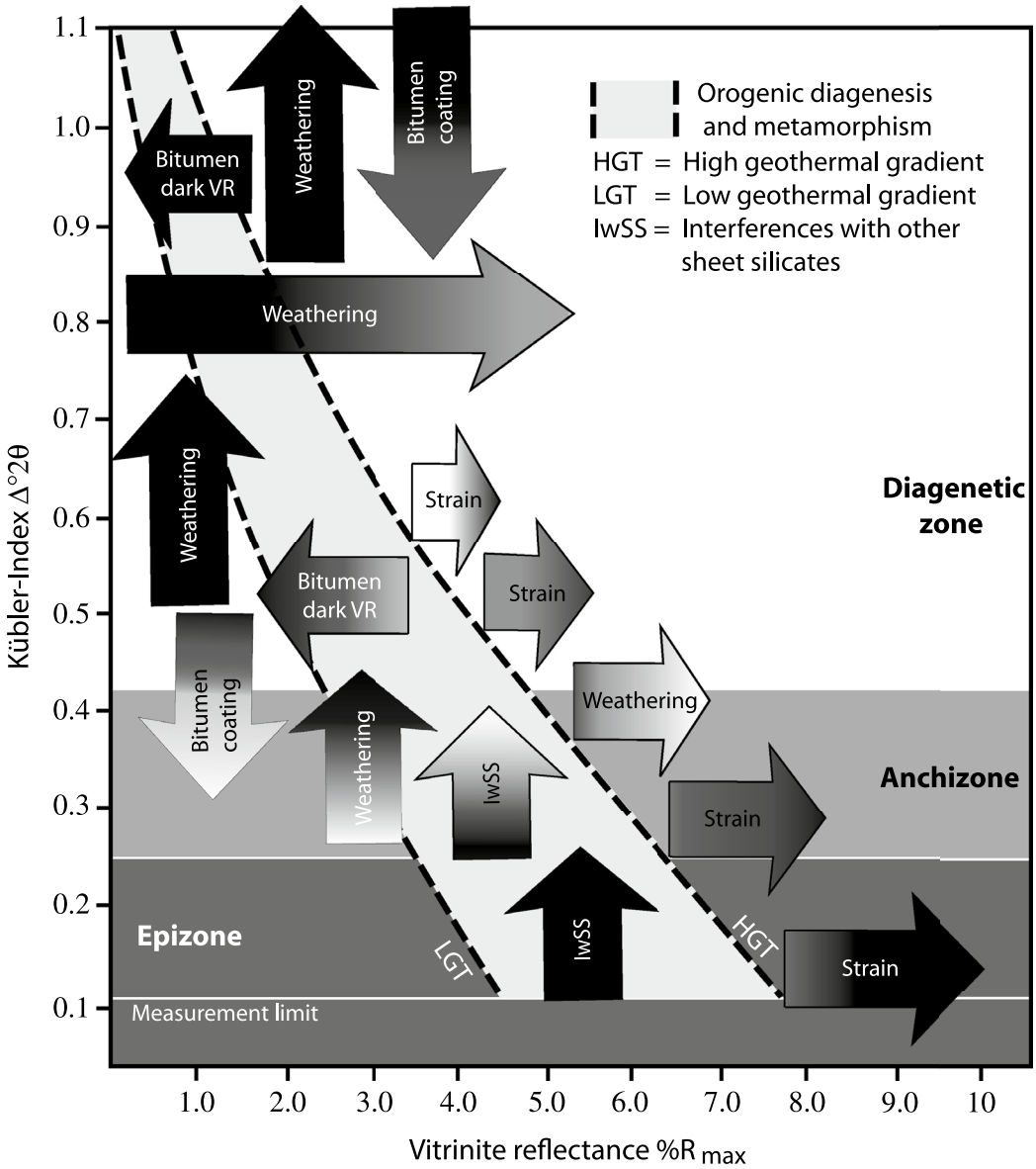

Fig. 4 Influencing factors altering vitrinite reflectance (VR) or the Kübler-Index (KI). The limits for orogenic diagenesis and metamorphism by the high geothermal gradient (HGT) and the low geothermal gradient (LGT) were taken from Ferreiro Mählmann & Le Bayon (2016). Red-bed facies, hydrothermal overprint and detrital populations of illite or organic matter may strongly change mean KI and VR values but can be discriminated easily (by field evidence). Size and direction of the arrows indicate the importance and changes caused by the influencing factor, respectively. White to black shading indicates: white = not observed, grey = occasionally observed, black = frequently observed. This is shown in relation to the KI or VR values with one or several arrows. Example for KI: bitumen coating on illite hinders illite aggradation. The arrow at the anchizone/diagenesis boundary indicates nearly no influence in the anchizone, but an increasing influence in the diagenesis zone. The "bitumen coating" arrow at the top of the graph indicates the occasionally observed influence on KI at values of 1.0 Δ°2θ and the frequently observed influence on KI at low-grade diagenetic grade (KI > 1.0 Δ°2θ). Example for VR: in high-grade diagenesis a very prominent increase of Δ 4.5%R_{max} of VR is caused by weathering

568 samples were incorporated into a uniform data set of VR values. Calibration and standardisation are described in Ferreiro Mählmann & Frey (2012, see also Teichmüller, 1987). As recommended in OM studies reflectance below a VR of 1.3 is measured as random reflectance under monochromatic white light (%R_r) and at higher maturity under polarised light as maximum reflectance (%R_{max}). Measuring VR is a relatively subjective method and, thus, slight differences may occur among different analysts (commonly in the range of the

methodical error, Ferreiro Mählmann & Le Bayon, 2016). In the study areas, different analysts cross-calibrated their measurements on the same samples. Very few cases show results beyond statistical tolerance ($\sigma^2 > 10\%$ of the mean value). Such measurements from e.g., the southern anchizone part of the Helvetic nappes (Permian–Triassic) are excluded from final correlation (see discussion in Ferreiro Mählmann et al., 2012). In other cases literature data were not included due to unknown relationships with other illite- "crystallinity" values ("Weaver-Index", Weaver, 1960; "Weber-Index", Weber, 1972; see discussion in Ferreiro Mählmann & Frey, 2012). Other illite-"crystallinity" methods should show close agreement to KI in principle (Kübler, 1968; Loeschke & Weber, 1973; Weaver, 1984), but they have more restrictions due to measurement errors depending on the XRD peak geometry than KI (Frey, 1987a). An extended comparison based on 1385 samples with 3 measurements per sample Ferreiro Mählmann (1994), support prior results. The same was observed for studies using deviating methods to determine mean reflectance values on vitrinite (see discussion in Ferreiro Mählmann & Frey, 2012). As a precondition prior to VR measurements, a precise OM characterisation by maceral analyses of the physical (and chemical) individual components of OM is required (Spackman, 1958).

158 measurements of VIBR values form a third uniformly available data set. As for VR the same standardisation and calibration was applied. In this study the first VR/VlBR correlation equation (n = 95 VR/VlBR values) will be determined for a normal orogenic geothermal gradient (Sect. 5.2). In Mastarlerz et. al. (2018) the term bituminite is by definition restricted to a primary organic matter, similar to other maceral groups, such as vitrinite, liptinite and inertinite, and the term solid bitumen used for secondary organic matter. For this study, samples, for which bituminites could not be resolved optically (mostly from the low-grade diagenesis zone), were rejected from correlation. Thus, the VR/VlBR correlation starts with solid bitumen measurements at the low-grade to high-grade diagenesis zone boundary.

According to Mastarlerz et. al. (2018) the term "bituminite" has frequently been used in petrologic studies instead of "solid bitumen". In low-temperature petrology the terms "bituminite" and "meta-bituminite" have a long tradition (Teichmüller, 1987; Ferreiro Mählmann, 1994 and references therein; Ciulavu et al., 2008). In the Alps, bituminite (exudatinite) reflectance and solid bitumen reflectance (BR) were first applied and correlated with VR and KI by Ferreiro Mählmann (1994, 1995, 2001). Ferreiro Mählmann & Le Bayon (2016) proposed that the term bituminite should no longer be used in VLGM studies (see inconsistend critical comment of Mastarlerz et al., 2018), if the bitumen matter is a secondary product. According to the proposal, solid bitumen was subdivided into three optical determined categories. In this study only VlB will be used as recommended. Measured "bituminite" of Ferreiro Mählmann (1994, 1995, 2001) corresponds to VlB. Thus, for this study a large data set is available.

Additional clay mineral, organic matter, and mineralogical indices as well as mineral paragenesis (including a total of 250 thin sections) were used in this study to propose subdivisions of the KI zones, to define the grade of diagenesis, anchizone and epizone in more detail. A second focus of the study is to show stability limits of selected clay minerals and minerals critical for determination of the metamorphic facies with respect to VR and KI. Special emphasis is given to discrete smectite, smectite mixed layer minerals and illite polytype occurrences along a normal geothermal gradient from low-grade diagenesis to epizone (sub-greenschist facies). When using smectite as an indicator for the degree of burial, some preconditions must be defined. Many processes may form smectite and control the smectite to illite (illitisation) or chlorite (chloritisation) reaction progress. During progressive burial and tectonic burial in the context of orogenic metamorphism, the decrease of smectite and increase of illite content is a diagnostic parameter (Hower et al., 1976; Hoffmann et al., 1976; Altaner et al., 1984), but also dependent on the geothermal gradient (Jennings & Thompson, 1986; Inoue et al., 1988), K^+, Ca^{2+}, Na^+ and Mg^{2+} activity in the fluid, and rock composition (Robertson & Lahann, 1981; Frey, 1987a; Huang et al., 1993). The transformation rate increases with increasing temperature (Pytte, 1982; Pytte & Reynolds, 1989; Elliot et al., 1991) and may also increase with H_2O activity (Whitney, 1990). In this study only solid-state transformation scenarios are used for correlation, if a series of interstratified phases of illite/smectite (I/Sm) changes from Sm to illite (according to Reynolds & Hower, 1970) has been observed. In such cases, the percentage of Sm in illite may be applied as a semi-quantitative geo-thermometer (Hoffman & Hower, 1979; Pollastro, 1993; Elliot & Matisoff, 1996). As shown by Frey (1987a), the percentage of smectite may be a useful inorganic maturity index to determine maximum T [°C] (Pollastro, 1993; Środoń, 1995, see also Waliczek et al., 2020 and references therein).

Kinetic models based on this solid-state concept (Huang et al., 1993; Hillier et al., 1995) can be easily compared with VR modelling giving comprehensive results (Fereiro Mählmann, 2001). The sensitivity of smectite content-determination depends on the method applied. In the Northern Calcareous Alps simple peak fitting by comparing air-dried and glycolated samples was applied,

but provides only restricted information (Petschick, 1989; Ferreiro Mählmann, 1994). In the Lower Austroalpine and Platta nappe, the sophisticated XRD method of Środoń (1984) was practiced on many samples (Ferreiro Mählmann, 2001). In the Helvetic nappes the ordering type according to Moore & Reynolds (1989) was determined (Wang et al., 1996) by applying the program NEWMOD (Reynolds, 1985). For the clay mineral study in New Caledonia (Potel et al., 2006) the classification of Moore & Reynolds (1997) was used.

In case of hydrothermal alteration of the rocks, smectite may have formed by fluid–rock interaction. This process is evident along E–W striking faults at the southern border of the Northern Calcareous Alps (Ferreiro Mählmann, 1994), at the AD1 basal thrust of the Lower Austroalpine (Eppel & Abart, 1997), in the basal trust of the Platte nappe and along internal AD1 digitations (Ferreiro Mählmann, 2001), along the tectonised zone of the Gellihorn nappe mylonite (Árkai et al., 2002) in the Helvetic nappes (first Helvetic deformation, HD1), and along the Glarus thrust plane (Abart & Ramseyer, 2002; Hürzeler & Abart, 2008). Smectite may transform to illite by a dissolution and re-precipitation process (Boles & Franks, 1979; Nadeau et al., 1984) or by Ostwald ripening (Morse & Casey, 1988, Eberl et al., 1990). Accordingly, if a hydrothermal event was detected or must be assumed based on indicators of thermal anomalies, samples were excluded from this correlation study.

All X-ray diffractograms characterised by an illite 10 Å-peak interfering with other sheet silicates were also excluded (see also Árkai et al., 2004). Such interferences include the presence of (1) paragonite, as found in the southern Helvetic nappes and lowermost Lower Austroalpine nappes and Platta nappe, (2) rare biotite in the epizone, (3) occasional stilpnomelane, and (4) rare occurrence of pyrophyllite in the anchizone. Despite being discarded for correlation, the stability range of the minerals in the field will be compared with the prograde change of illite aggradation, vitrinite and vitrinite like solid bitumen maturity.

135 samples have measurement of illite/K-white mica *b* unit-cell dimension. Velde (1965) suggested that the phengite mol% in white mica is significantly related to pressure. Thus, a *b* unit-cell dimension (*b* parameter) measure should be pressure dependent. Since the introduction of the lattice illite "b_0 parameter" (Sassi, 1972; Sassi & Scolari, 1974) to predict the baric type of very-low grade (Guidotti & Sassi, 1976) to low-grade metamorphic conditions (Padan et al., 1982) many authors (see e.g., references in Kisch et al., 2006) have used the method for Na poor illite/muscovites to semi-quantitatively estimate pressure. A "cumulative b_0 value plot" with reference lines for specific baric conditions from selected areas published by Sassi & Scolari (1974) was frequently used. No crystallographic rational could be related with this value, therefore the universally accepted symbol *b* will be used as follows. With the help of this method the very-low grade to low-grade metamorphic zone could be sub-divided into a low-, intermediate-, and a high-pressure facies series (Guidotti & Sassi, 1986). Frey & Kisch (1987) discussed the advantages and limits of the method, being one of very few methods to estimate pressure in VLGM studies. Despite the recommendation of Essene (1989) to avoid the method while not knowing the illite chemistry (in particular its Si content and $Fe^{2+}/(Mg+Fe^{2+})$ ratio, both strongly controlling the *b* parameter (Kisch et al., 2006), the method gives reasonable results in this study fitting with pressure estimations from fluid inclusions and tectonic burial modelling. The Ph.D. studies of the authors are the main database (re-evaluating clay mineral XRD analyses). At that time (Petschick, 1989; Ferreiro Mählmann, 1994; Rahn, 1994) the *b* parameter was controversially discussed and the *b* parameter not routinely used (see also Wang, 1994; Erdelbrock, 1994). Therefore, *b* values are not available for most tectonic units in this study. The authors have later used the parameter in many studies, in which the *b* parameter results have been supportive for the geologic interpretation (e.g., Potel et al., 2006, 2016; Potel & Trullenque, 2012; Ferreiro Mählmann & Giger, 2012).

5 Results

In Fig. 4 a schematic VR/KI plot illustrates the range of values of all included study areas. The arrows in the figure demonstrate the direction of influencing factors including red-bed facies, bitumen-rich rocks, weathered rocks, deformed rocks with high strain rates, rocks with signs of hydrothermal transformations taken along faults and within tectonised zones, and rocks showing detrital populations. Including these samples, resulted in a large variation of VR/KI relationships and thus in the studies of Wang (1994), and Erdelbrock (1994) a statistically and significantly constrained VR/KI gradient could not be detected. As indicated in Sect. 3, samples showing

(See figure on next page.)

Fig. 5 Vitrinite reflectance (VR) vs. Kübler-Index (KI) correlation plot showing all data used from the different areas to characterise the orogenic normal geothermal gradient. Low-grade and high-grade diagenesis KI zones are shown according to the division proposed by Merriman & Kemp (1996). In the VR/KI correlation this limit reflects the transition from high to medium volatile bituminous coal (Ferreiro Mählmann & Le Bayon, 2016). For explanation to the data group in the fine dashed line ellipses, see text. The sub-division of the anchizone is shown at KI = 0.33 Δ°2θ according to Ferreiro Mählmann (1994, 2001; see also Potel et al., 2006, 2016)

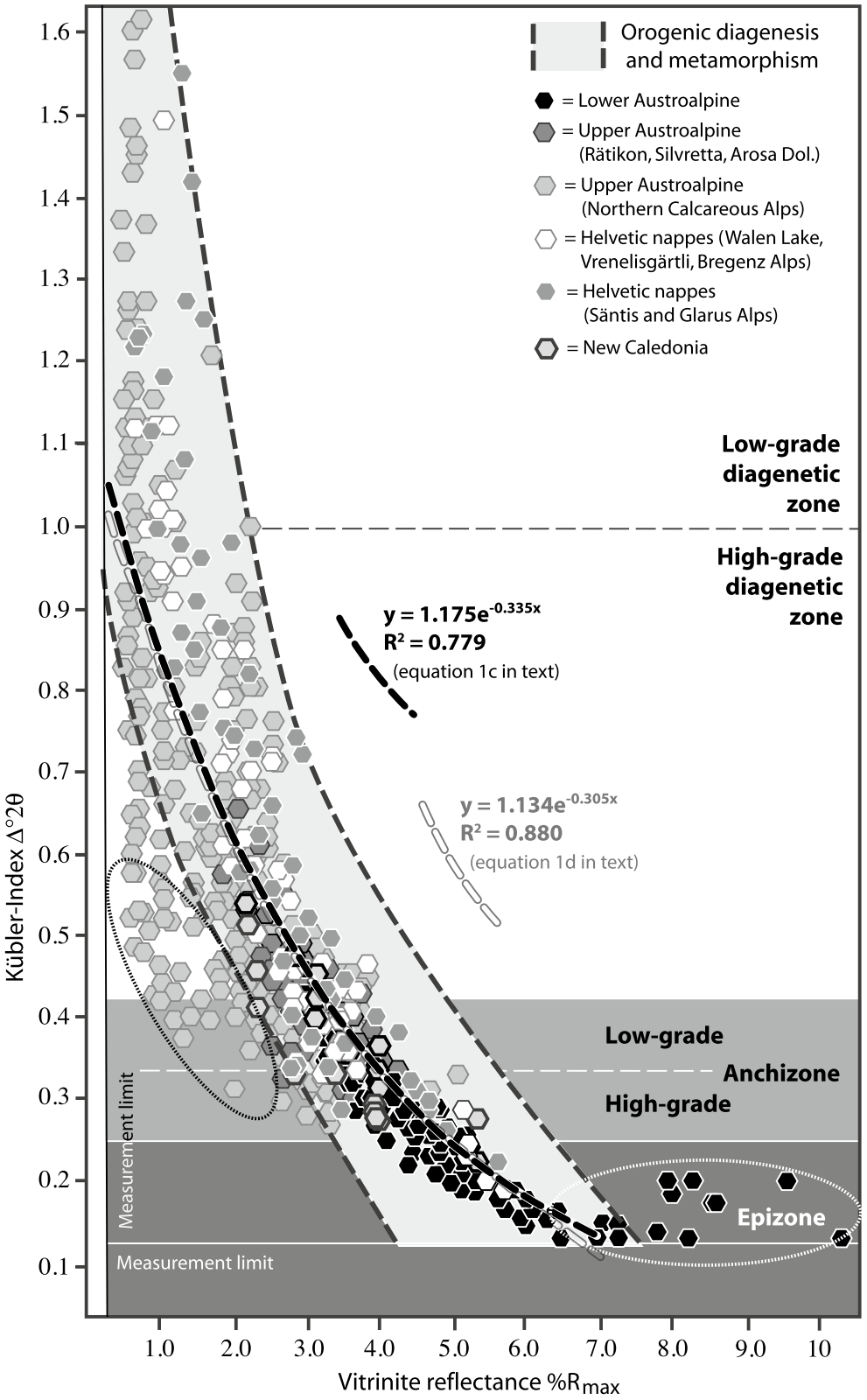

Fig. 5 (See legend on previous page.)

such influencing factors are not included in the study. Thus, the light grey area between the lower and higher geothermal gradient-limits of orogenic geothermal gradients in the Figs. 4 and 5 presents the unaffected samples assumed to mark values only controlled by temperature, time, and pressure in an orogenic setting. In Fig. 5, all values from the study areas plot in the middle of the interval of orogenic gradients (Fig. 1) as shown by Ferreiro Mählmann et. al. (2012). Thus, it is proposed that a "moderate geothermal gradient" sensu Ferreiro Mählmann et. al. (2012) can be interpreted as a normal orogenic gradient (Fig. 1).

5.1 Vitrinite reflectance and Kübler-Index values

5.1.1 Data from the Northern Calcareous Alps and Silvretta nappe

In the Northern Calcareous Alps of Bavaria and Northern Tyrolean outside the western and southernmost regions studied (Rätikon to Lechtal Alps and southern rim, Fig. 2) there is a wide spread of KI and VR data sets of diagenetic grades collected from late Triassic to Cretaceous fine clastic and marly sediments. VR values ranges from 0.45% to 0.9%R_r. KI values scatter from 0.6 to > 1.5 Δ°2θ pointing to considerable amounts of illite–smectite mixed layers and their swellable parts who broaden the FWHM of most illite peaks. According to palaeogeothermal model calculations (TTI of Lopatin, 1971; Waples, 1980) palaeo-temperatures required to explain the coal rank and illitisation stage range between 60 and 100 °C which were reached under moderate palaeodepths after nappe stacking. Earlier Triassic rocks buried closer to the detachment planes reached maximum temperatures before the end of sedimentation as estimated based on palaeo-geothermal gradients between 25 and 40 °C/km (Petschick, 1989) or 50 °C/km (Silvretta nappe; Ferreiro Mählmann, 1996).

From the Rätikon mountains to the Arlberg region, central Lechtal and southernmost Allgäu Alps (Fig. 2) the complete set of Raetian to Cretaceous rocks are higher coalified as in other regions of the Northern Calcareous Alps (Fig. 3). Thermal maturity is indicated by VR %R_{max} values of around 2.0% (sometimes up to 2.5% when approaching the southern rim of the Northern Calcareous Alps). The grade of diagenesis is determined by KI values from 0.4 to 0.8 Δ°2θ, which indicate a substantial loss of smectitic layers within the illite–smectite mixed layer structures. Different slopes of VR gradients (Fig. 3) demonstrate the existence of a two-step thermal history, i.e. a pre-orogenic thermal VR gradient in Triassic rocks and a post-orogenic, post-nappe formation gradient (Petschick, 1989). The pre-orogenic gradient was hyperthermal and thus not of interest for this study. Towards the southern border of the Northern Calcareous Alps the post-nappe thermal event also re-heated Norian to Rhaetian sedimentary rocks to a higher maturity grade, thus samples from these stratigraphic units are considered part of the post-orogenic VR gradient. Similarly, samples of post-Norian age collected at the southernmost rim of the Lechtal nappe show VR values exceeding 4.0%R_{max}. The KI values do not reflect any re-heating (Ferreiro Mählmann, 1994) and these data cause a large data variance in the VR/KI correlation. The re-coalification of the organic matter causes a steep VR-gradient slope for the Permian to Cretaceous rocks, which follows a single second order regression line (Fig. 3). Accordingly, only post-Norian to Cretaceous samples were used for further correlation. Maximum maturity is given by VR values of 3.5%R_{max} (Rätikon area) to 5.05%R_{max} (near Landeck, Fig. 2) corresponding to KI values of 0.27 to 0.39 Δ°2θ (near Landeck 0.24 Δ°2θ).

In the sedimentary cover of the Silvretta nappe s.l. (Fig. 2), the same procedure for the VR/KI values as for the Northern Calcareous Alps is applied and data reflecting the pre-orogenic hyper-thermal event are neglected. Ferreiro Mählmann (1995) demonstrated that in the Silvretta nappe s.l. the post nappe tectonic orogenic thermal event can be traced in all sub-units, as evidenced by only plotting the VR/KI data using the measurements from the Raibl Formation to the youngest sediments preserved (Kössen Formation and Allgäu Formation) only. Apart from the Kössen Formation, rocks are commonly poor in clay minerals and vitrinite, resulting in a limiting data set, which is amended to the result of the Northern Calcareous Alps (Fig. 3, Table 2). In fact, this set of values is important because they assist to sharpen the important boundary of the diagenetic zone/anchizone at 0.42 Δ°2θ (Kübler, 1967; Guggenheim et al., 2002). Furthermore, it helps to bracket the occurrence of anthracite (White & Thiessen, 1913 in Stach, 1935), defined by a large range of VR values. The values of the Silvretta nappe s.l. overlap with data found in the Northern Calcareous Alps (low volatile bituminous coal, semi-anthracite, and anthracite) and in the Lower Austroalpine and Platta nappe (anthracite, meta-anthracite, and optical graphite).

5.1.2 Data from the Lower Austroalpine of Grisons (Oberhalbstein)

The VR/KI gradient crosscuts nappe boundaries of the Lower Austroalpine/South Penninic nappe pile. The metamorphic grade determined by VR/KI measurements is therefore dependent on the structural position of the tectonic unit, varying from the diagenesis/anchizone boundary (VR = 2.9%R_{max}, KI = 0.46 − 0.42 Δ°2θ) at mountain summit to conditions of the upper limit of the sub-greenschist facies (VR %R_{max} > 6.5, KI 0.125 to 1.20 Δ°2θ) in deep valleys. Ferreiro Mählmann (2001) used the

data to estimate maximum temperatures and to discuss nappe tectonic scenarios. The study served as a reference for normal geothermal orogenic gradient comparisons including OM and clay mineral stability relationships (e.g. Potel et al., 2006; Malinconico et al., 2009; Środoń et al., 2018). The VR/KI correlation of the previous regression calculation for a normal orogenic metamorphic gradient (Ferreiro Mählmann, 2001) between KI 0.19 and 0.48 Δ°2θ can be expressed by the following equation:

$$\text{VR } \%R_{max} = 8.6 - 17.7\ (\text{KI}) + 11.1\ (\text{KI})^2, \quad (n = 47,\ r = 0.87). \tag{1a}$$

This relationship is well defined within the study range of this VR/KI correlation. At the structural basis of the nappe pile the methodical limit is reached (Fig. 5, Table 1) with VR values at around 6.5%R_{max}. Towards this limit (meta-anthracite rank) KI amounts to 0.15 Δ°2θ, corresponding to the technical limit of the XRD measurement device (KI = 0.13 Δ°2θ). Independent of the maturity increase from VR = 6.5 to > 11.0%R_{max} (not shown in Fig. 5 and not included for further VR/KI correlation) the KI values scatter between 0.15 and 0.20 Δ°2θ. The scatter of values in the southernmost area (see also Handy et al., 1996) illustrates the loss of significance of KI changes with respect to metamorphic grade (Ferreiro Mählman, 2001; Montmartin et al., 2021).

It is observed that gradient slopes frequently change along strike and perpendicular to nappe structures. The gradient determined in the Err section (Ferreiro Mählmann, 2001) was reported with 28 °Ckm^{-1}, but to the north (Ela section, Ferreiro Mählmann, 1995) or to the south (Platta, Julier section (Fig. 2), Ferreiro Mählmann, 1995; Handy et al., 1996) thermal gradients between 25 and 35 °Ckm^{-1} were predicted, respectively. Similarly, in the Northern Calcareous Alps (Fig. 3), thermal gradients may differ considerably in a single nappe pile or nappe unit depending on the tectonic-thermal history and/or the structural geometry at crustal scale, the palaeo-geographic position along the ocean-continent transition, and the geodynamic history within the orogen.

5.1.3 Data from the Helvetic nappes (Glarus, Mürtschen, Axen, and Säntis nappe)

North of Lake Walen (Säntis Alps, Fig. 2), in the Mürtschen, Axen and Säntis nappes, KI data demonstrate field gradients with a topographic top-down trend parallel to a general increasing metamorphic trend from NW to SE from the low-grade diagenesis to the high-grade anchizone/epizone boundary. KI demonstrates increasing grade from 1.75 to 0.25 Δ°2θ (corresponding to VR = 0.60 to 4.88%R_{max}). In the studies of Erdelbrock (1994), Rahn et. al. (1995), and Wang et. al. (1996), a post-nappe and post-fold metamorphic overprint is indicated.

A data group at Gonzen and from the southeasternmost part of the Axen and Säntis nappe, east of Gonzen (Fig. 2) gave very high VR values. After the studies of Erdelbrock (1994), Ferreiro Mählmann (1994), and Rahn et. al. (1995) it was demonstrated that the area was part of a fossil migration system of hydrocarbons (solid bitumen) and partly also hydrothermal fluids (Árkai et al., 1997). Tobelite causes a broader KI (Árkai et al., 1997) and hydrothermal pulses a short-term heat supply increased VR. For this study, samples from hydrothermal fossil systems and tobelite-bearing samples were excluded from further correlation.

Discriminating both data groups, the remaining samples from Erdelbrock (1994), and Rahn (1994) show a well-established and statistically significant correlation parallel to the data from other eastern Helvetic nappes (data group Walen Lake, Vrenelisgärtli, Bregenzer Alps, Fig. 5). However, data from the Säntis and Axen nappes by Erdelbrock (1994), and Rahn (1994) tend to have slightly elevated VR values at similar variance of the VR/KI values (data group "Säntis and Glarus Alps", Fig. 5).

In the Glarus to Säntis nappe stack (Linth and Sernft valleys) at the south of Glarus (Fig. 2) post-nappe tectonic metamorphism (Frey et al., 1973) is documented with a KI trend from high-grade anchizone (Glarus nappe, close to the Glarus thrust) to high-grade diagenesis at the mountain summits (Frey, 1988; Rahn, 1994; Rahn et al., 1994). KI decreases from valley bottom to the summit peaks from 0.32 to 0.55 Δ°2θ (locally to 0.85 Δ°2θ, Table 3). A parallel trend of decreasing VR values is established with data from Rahn (1994) and new measurements (Table 3) along the Vrenelisgärtli ridge at Glarus (Frey et al., 1973; Ferreiro Mählmann et al., 2012, Fig. 8). VR decreases from 3.6 to 2.1%R_{max} (mountain peak).

To include the structurally highest Helvetic nappe, a new section from the Mürtschen to the Säntis nappe at the northeastern end of Lake Walen (Fig. 2) was sampled and provided a similar trend with 3.9%R_{max} at valley bottom to 2.2%R_{max} at mountain peak (Table 4). KI values show little scatter and a well-defined trend with altitude.

Discrepant results exist between Árkai et. al. (1997), and Erdelbrock (1994) SE of Glarus in the Linth valley in the Verrucano and Axen nappes (see also review by Ferreiro Mählmann et al., 2012). As observed at the Glarus thrust south of Gonzen a similar VR/KI pattern is probably a thermal fossil-anomaly. Therefore, data are not used for further correlation (see discussion in Abart & Ramseyer, 2002; Ferreiro Mählmann et al., 2012; Mullis et al., 2017).

5.1.4 Data from NE New Caledonia

In northern New Caledonia, KI values generally range from low-grade diagenesis to epizone. In the Koumac terrane, the KI data indicate low-grade diagenesis to low-grade anchizone values, ranging from 2.33 to 0.33 Δ°2θ (VR = 1.39%R_r to 3.34%R_{max}). In the Diahot terrane, KI values vary between low-grade anchizone and epizone (VR = 3.95 to 14.9%R_{max}, observation of optical graphite). A trend of increasing grade from diagenesis to epizone is observed in a traverse from southwest to northeast along the Koumac-Ouégoa road. An overall prograde sequence for the terranes is documented, with KI decreasing and VR increasing from southwest to northeast. The VR/KI trends reflect the post-nappe and post-terrane tectonic collisional and post-kinematic orogenic metamorphic event.

5.1.5 Vitrinite reflectance/Kübler-Index correlation defined for a normal geothermal gradient

After rigorous data discrimination refusing all samples not reflecting orogenic diagenesis to metamorphism (Sect. 4) 568 VR/KI data pairs can be related to an orogenic normal heat flow setting. The resulting equation is:

$$KI = 1.0693e^{-0.318VR},\ (R^2 = 0.552,\ n = 568). \quad (1b)$$

The equation is very similar to Eq. 1a but based on a much larger sample number. One data group (dasched black line ellipse in Fig. 5) must be discussed separately. The VR/KI data come from the Austroalpine and mostly from Cretaceous syn-orogenic (e.g. turbidite) sequences. Most of the corresponding samples have small amounts of discrete smectite or low mixed-layer content in illite. Thus, any mineral reactions (smectite diagenesis) can only have a low impact on the 10 Å peak form and any aggradation is limited to crystal structural (domain size, particle thickness) and chemical ordering (Merriman & Frey, 1999; Ferreiro Mählmann et al., 2012). Furthermore, a low illite-FWHM may be explained with very fine-grained mica detritus. A high detrital contamination is well known in clay, mudstone, and shale of these formations (Achtnich, 1982; Gaupp, 1982; Gaupp & Batten, 1985; Petschick, 1989; Ortner & Gaupp, 2007).

As next the measurements with a VR > 7.0 R_{max}% VR must be extracted (pointed white line elipse in Fig. 5, see Sect. 6.1). Approaching the limit of the XRD measurement device, KI does no longer change with increasing maturity (see also Montmartin et al., 2021), but continue to show values between 0.13 and 0.20 Δ°2θ. Excluding both groups, the values follow a gradient defined between VR 7.0 and 0.25%R_{max} with the following regression (Fig. 5):

$$KI = 1.175e^{-0.335VR},\ (R^2 = 0.779,\ n = 521). \quad (1c)$$

In the VR/KI thermal gradient graph of Ferreiro Mählmann et. al. (2012) the calibration below KI = 0.6 Δ°2θ was based on 1200 samples. The extrapolation to KI = 1.1 Δ°2θ (Ferreiro Mählmann & Le Bayon, 2016), based on many cited publication results, was signficantly narrower than the correlation presented in this study (Fig. 5). The presentation in Fig. 5 is extended to KI = 1.6 Δ°2θ. With the help of this VR/KI correlation graph low- and high-grade sensitivity limits are determined for the first time. At VR < 0.85%R_r, KI values scatter from 0.6 to 2.4 Δ°2θ. At VR = 1.0%R_r, the scatter decreases to 0.6 to 1.28 Δ°2θ, and with increasing grade of metamorphism the VR/KI value is increasingly diagnostic to determine metamorphic grade up to VR = 6.5%R_{max}. At 1.0%R_r the correlation gradient is still represented in the range of plottet values. Accepting VR limits of 1.0 and 6.5%R_{max}, the correlation follows an equation:

$$KI = 1.134e^{-0.305VR},\ (R^2 = 0.880,\ n = 462). \quad (1d)$$

Equation 1d is proposed for general use. Commonly, research is based on smaller sample numbers and thus data discrimination more complex and/or limited. Plotted together versus structural depth a KI gradient versus depth (z) per km is formulated as follows:

With increasing depth (z) the KI gradient for the calibration interval 1.10 to 0.20 Δ°2θ is:

$$z\ (km) = 0.09 \pm 0.002\ \Delta°2\theta. \quad (2)$$

The corresponding VR gradient for the calibration interval 1.00 to 6.5 R_{max}%) is:

$$z\ (km) = 0.66 \pm 0.05\ \%R_{max}. \quad (3)$$

For the Lower Austroalpine, a much higher VR gradients approaching 1.4 R_{max}%/km (Ferreiro Mählmann, 2001) was later re-interpreted with VR increased by strain effects (Ferreiro Mählmann et al., 2012). Samples close to shear zones are here excluded. In New Caledonia, it is not possible to determine a VR or KI gradient in the field in direction of a palaeo-surface (defining the direction of the geotherm), because topographic differences are too low. However, a field gradient can be determined in the same order of magnitude, assuming to reflect a similar VR and KI gradient.

5.2 Solid bitumen reflectance

Only vitrinite like solid bitumen (VlB) measurements are used for the reflectance correlation with vitrinite (both measured as %R_r – random reflectance, when the organic matter used shows isotropy and as %R_{max} if anisotropic, Fig. 6). In most cases (study areas) the solid bitumen

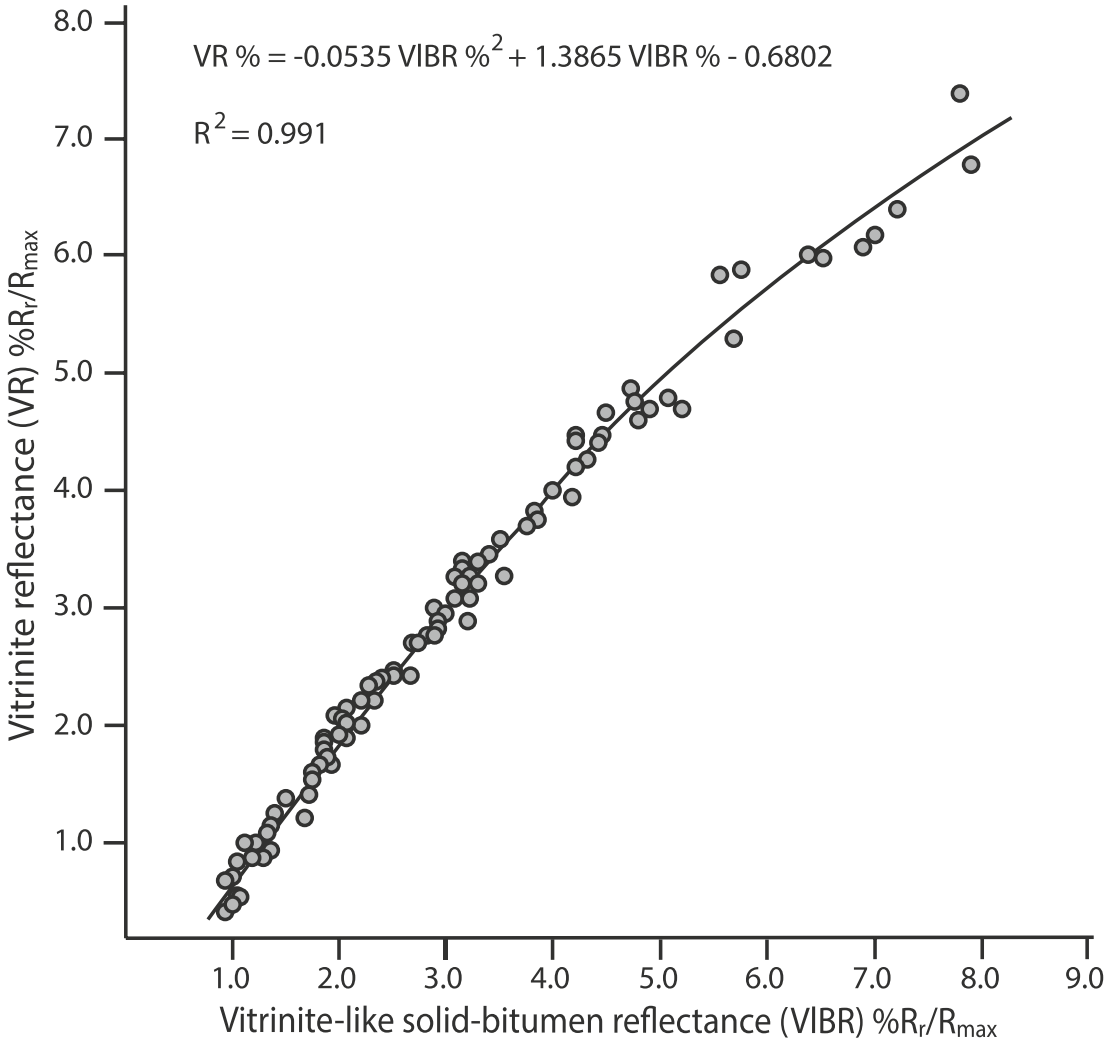

Fig. 6 Vitrinite reflectance and vitrinite-like solid-bitumen reflectance correlation plot showing all data used from the different areas to characterise the orogenic normal geothermal gradient

classification of this study is not organo-geochemically tested according to Taff (1909), Abraham (1918), Jacob (1967), and Landis & Castaño (1995). In no one of the studies of the authors compiled for the VR/KI correlation an extraction test is documented and oil generation found. In Ferreiro Mählmann & Le Bayon (2016) controled samples were reported, and the oil prone genetic information was assumed to be valid for all the VlB in this study derived from the optical surveillance. Mastalerz et. al. (2018) has pointed out that the upper maturity limit for solid bitumen with the isotropic characteristics was initially limited to reflectance values of VR 0.7% and that the boundary is imprecise and should be shifted to BR of 1.5% (VR = 1.5%R_0, Lewan & Pawlewicz, 2017, and references therein), while in the study of Ferreiro Mählmann & Le Bayon (2016) the first anisotropy is measurable in the range of VR %R_r of 1.0 to 1.7 (VlBR = 0.7 to 1.55%R_r) depending on the geothermal gradient (i.e. "heating rate" sensu Mastalerz et al., 2018). The range agrees with observations on reflectances from different liptinite macerals lower than VR (Petschick, 1989; Ferreiro Mählmann, 1994).

The term pyro-bitumen at higher maturity according to Mastalerz et. al. (2018) is not applicable in the study areas. None of the characteristic features (fine-grained mosaic, coarse-grained mosaic, coarse flow mosaic and domain anisotropy) were observed. The anisotropy of the VlB is a uniform plane change from minimum to maximum reflectance and mostly characterised by a lower bi-reflectance than determined in the same sample for virtinite. The terminology used in this study is purely based on optical properties without supporting organo-chemical analysis (Ferreiro Mählmann & Le Bayon, 2016).

Solid bitumen and VlBR data are recorded from samples of a VR = 0.45%R_r to 7.5%R_{max} range (KI 1.45 to 0.13 Δ°2θ). In the meta-anthracite stage (epizone) all kind of solid bitumen (except migra-bitumen of allochthonous generation) disappeared in more than 50% of the samples. In the optical graphite stage (high-grade epizone, lower greenschist facies) 8 samples had relics of solid bitumen (in 8 of more than 150 samples). The predominance of vitrinite or solid bitumen depends on the sedimentary facies. In the Austroalpine, the Raibler and Kössen Formation are occasionally very rich in vitrinite, respectively (with occasional fine coal beds). In the Helvetic domain, this is observed in the Wang, Amden, Palfris and Zementstein Formations and partly in the Quarten Formation. In most other formations (excluding pure carbonate and psammite facies) solid bitumen is the dominating maceral. For shales the general postulate that with maturities of VR > 0.8%R_o (≈0.8%R_r) bitumens becomes the dominant OM (Cardott et al., 2015; Mastalerz et al., 2018) cannot be confirmed. In formations and depocenters close to terrestrial areas and e.g., an approaching orogenic front vitrinite becomes very frequent. In deep neritic formations (radiolarites, Apthychus limestone, Palombini Formation, distal Drusberg Formation, distal Palfris Formation, and in distal formations of schales and schists of the Early and Middle Jurassic) vitrinite may be absent, but also solid bitumen (VlB) may be scarce (while e.g., alginites dominate). In these rocks between 1.0%R_r and 4.0%R_{max} solid bitumen is more abundant than vitrinite. At higher maturity the trend changes to vitrinite dominance (see Petschick, 1989; Ferreiro Mählmann, 1994; Erdelbrock, 1994), as is reflected in the number of vitrinite measurements (organic matter reflectance measurements: n ≈ 850, 158 samples documented with VlBR measurements).

Differences between VR and BR/VlBR due to chemical different rock composition and sediment lithology (Wenger & Barker, 1987; Bertrand 1990, 1993; Bertrand & Malo, 2001) have been proposed as a possibility to explain contrasting results (Mastalerz et al., 2018). Such differences cannot be confirmed by this study. When plotting data groups of marl/marly schist, clay stone/schist, clayey limestone/calcite phyllite, and silty claystones/silty schist separately, the variance is in the range of error, independent from sedimentary formation, study area and operator.

In contrast to Mastalerz et. al. (2018) we must correct the false statement that the VR/VlBR correlation equation used to calculate the equivalent VR by Ferreiro Mählmann & Le Bayon (2016) is "restricted to values between 0.2 and 2.5%R_r/R_{max}", and from "multiple samples from sedimentary basins in USA and Germany". Such implementation would be misleading, because the equation formulated (Eq. 1a) was given by Ferreiro Mählmann & Le Bayon (2016) for a much more general use for sedimentary and inverted basins (orogenic conditions) and for VR values between 0.4 and 6.9%R_r/R_{max}.

In orogenic settings pressure is an important factor. At VR 6.0%R_{max} (Fig. 7) pressures of 3.5 kbar (Helvetic nappes), 4.0 (Upper Austroalpine) and 4.0 to 6.0 kbar (Lower Austroalpine) have been estimated (Handy et al., 1996; Frey & Ferreiro Mählmann, 1999; Ferreiro Mählmann, 2001). Thus, the equation of Ferreiro Mählmann & Frey (2012)

$$\begin{aligned} BR\%R_{max} = &-0.519 + 1.341\ (VR\%R_{max}) \\ &- 0.0977\ (VR\%R_{max})^2 \\ &+ 0.0151\ (VR\%R_{max})^3. \end{aligned} \quad (4)$$

should be used for orogenic heat flow conditions at pressures between 3.5 and 6.0 kbar only. The here presented correlation between VR and VlBR incorporates recent measurements from the study areas, by at the same time excluding samples from hypothermal and hyperthermal heated areas. The resulting equation is (Fig. 6):

$$VR = -0.0535\ VlBR^2 + 1.3865\ VlBR - 0.6802,\ (R^2 = 0.991). \quad (5)$$

In Sect. 5, we have shown that all included data sets have been generated in a post-nappe stacking setting, thus the VR and KI gradients are considered to represent post-nappe thrusting and folding maturation (except for late thrusting event such as e.g. the Glarus thrust). Consequently, VR are related to the thickness of the corresponding degree of tectonic burial. At VR > 1.5 R_{max}% both reflectance values (VR, VlBR) are equal within their range of error. Plotted together versus structural depth a VR/VlBR gradient is:

$$z\ (km) = 0.7 \pm 0.2\ R_{max}\%. \quad (6)$$

As shown in most correlations in this study, at least a second or even third order regression gives a better fit. The precision of Eq. 6 is lower than for Eq. 3 when using VR values only. Linear regressions should be seen as rough adaptation to geothermal gradients (Reinhardt, 1991), only to accept if the geological database is rudimentary. This is postulated if the gradient represents a geotherm (Bucher & Frey, 1994; Allen & Allen, 2005). Geotherms in the first 30 km of the crust have a second order slope and perturbations in the deeper crust can lead to third order regressions depending on deep crustal structure, lithospheric thickness, and MOHO temperature cotrolled by mantle heat flow (e.g. Balling, 1985; Stern et al., 1987; Rolandone et al., 2002). The slope increases with depth. Thus, the linear regressions (like Eqs. 2, 3 and 6) should not be overestimated.

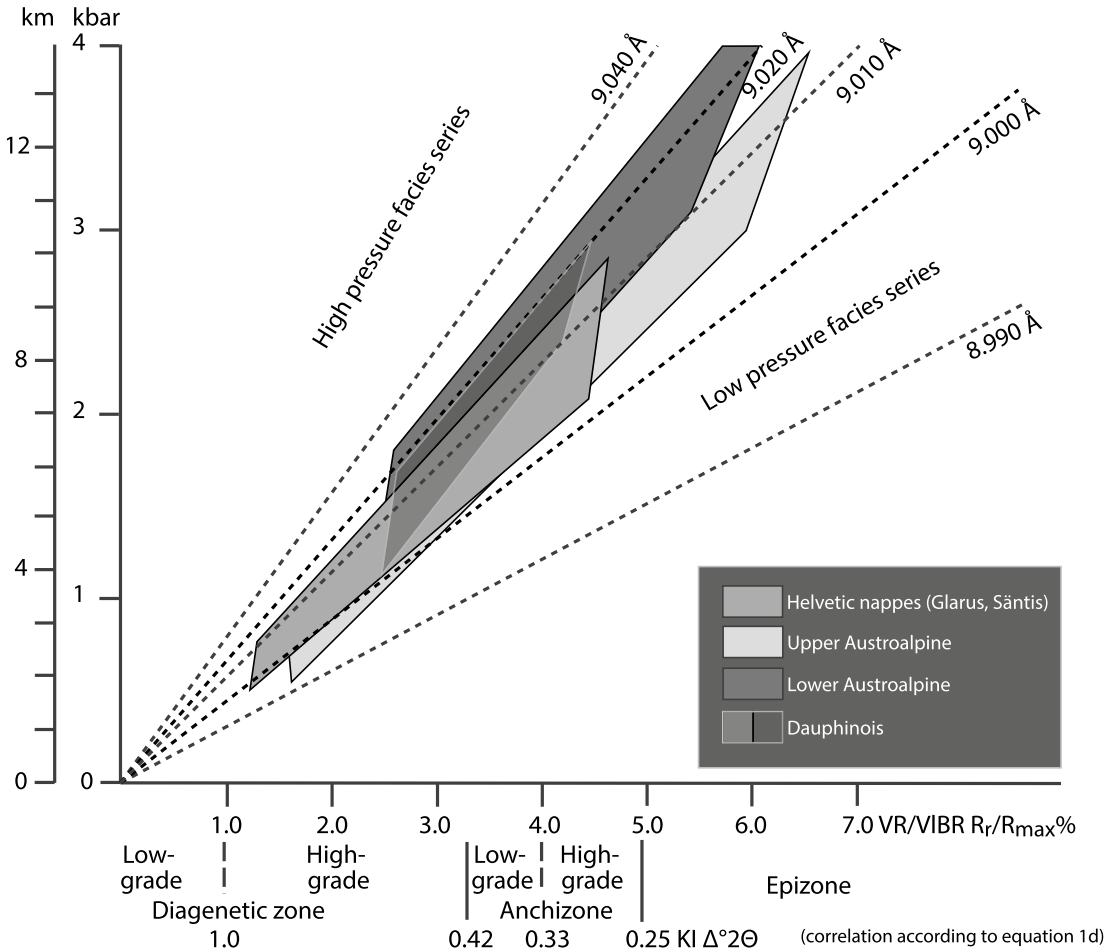

Fig. 7 Illite *b* Å-values (*b* parameter) determined in the different study-areas plot in the intermediate pressure facies series (*b* = 9.000 to 9.040 Å) related to normal geothermal gradients (25 to 35 °C km^{-1}). The plot shows the illite *b* facies series according to Sassi & Scolari (1974), revised by Guidotti & Sassi (1986), and using the terminology of Miyashiro (1961). The pressure relation on the y-axis corresponds to the graphs presented by Merriman (1991), and Merriman & Peacor (1999) and is reappraised by fluid inclusion data at low-grade (diagenesis) and petrogenetic grids at high-grade (metamorphism) in the different study areas (Mullis, 1979; Rahn, 1994; Ferreiro Mählmann, 1994, 2001; Rahn et al., 1995; Frey & Ferreiro Mählmann, 1999; Potel & Trullenque, 2012; Mullis et al., 2017). The vitrinite reflectance (VR)/vitrinite like solid bitumen reflectance (VlBR) vs. Kübler-Index (KI) correlation along the x-axis (instead of temperature) corresponds to Figs. 5 and 6. The correlation reflects the general mean determined from all geodynamic settings presented in the study of Ferreiro Mählmann & Le Bayon (2016)

5.3 *b* parameter and pressure constraints

Taking up the previously claimed criticism on the original plot of Sassi and Scolari (1974) (see Sect. 4), an alternative presentation of the *b* parameter data set is shown in Fig. 7. Kisch et. al. (2006) referred to more recent studies demonstrating that reference cumulative lines for baric types in the original plot of Sassi & Scolari (1974) do no longer reflect the P/T conditions of the areas as presented by the authors. Modern revisions of the reference areas used by both authors have suggested contrasting P/T estimates.

In Fig. 7 *b* parameter iso-lines are plotted versus pressure and related to the facies series of Guidotti & Sassi (1986) according to the terminology of Miyashiro (1961). Pressure was (i) determined by fluid inclusion studies from Mullis (1979), Rahn et. al. (1994), Ferreiro Mählmann (1994, 2001), Potel & Trullenque (2012), and Mullis et. al. (2017), (ii) derived from mineral reaction iso-grades from the same cited literature and Frey (1987b), and (iii) calculated from petrogenetic grids and P/T path reconstructions from the Alps (see review by Frey & Ferreiro Mählmann, 1999). Like the graphic presentation of Merriman (1991) the plot includes a correlation with VR data and KI zone boundaries. Due to the small data set in each study area the illite *b* parameter Å-iso-lines are plotted as straight lines with respect to the KI-VR/kbar-depth graph (for the danger of oversimplification by linear relationships, see Sect. 5.2).

The different areas are represented with n = 25 samples for the Helvetic nappes, n = 21 for the Dauphinois, n = 28 for the Upper Austroalpine and n = 33 for the Lower Austroalpine. 28 analyses from New Caledonia are not shown, as these *b* parameters are correlated with the HP/LT mineral facies paragenesis and did not undergo re-equilibration (re-crystallisation) in contrast to KI and VR (Potel et al., 2006). None of the data groups (Fig. 7) is statistically based on the recommended number of 30 to 50 samples (Merriman & Peacor, 1999), but fulfil the second criteria of 1σ = 0.010 Å. Therefore, the graph (Fig. 7) should be used for semi-quantitative pressure estimations only. Here, the *b* parameter method is used as an auxiliary result to better interpret differences between the integrated study areas.

80% of the *b* determinations in the Lower Austroalpine give vaues of 9.020 ± 0.01 Å (Kürmann, 1993 and new data). In the Upper Austroalpine 60% of the values plot between 9.005 and 9.015 Å. Determinations of *b* parameter from the epizone tend to higher values and in the high-grade diagenesis zone the variance increases (Henrichs, 1993, and new data). In the Helvetic nappes the *b* parameter plots mostly between 9.005 and 9.010 Å. (Fig. 7). In the high-grade diagenesis zone, most values are below 9.008 Å. In the Dauphinois, 80% of the values range between 9.010 and 9.020 Å, showing a shift to higher Å values of *b* with increasing grade of metamorphism, as indicated for all other incorporated study areas. The homogeneity of the values in the Dauphinois and the strong consensus with the data range of the Lower Autroalpine is remarkable. The similarity regarding the *b* parameter and the KI led to the interpretation of a coinciding thermal history with long lasting peak metamorphic temperatures as in the Lower Austroalpine of Grisons (Potel & Trullenque, 2012). This was an important reason to include this study to the presented compilation.

When correlating the *b* parameter with the VR/KI subdivision of thermal gradients (Ferreiro Mählmann et al., 2012 and Fig. 1) the low-pressure facies series (< 9.000 *b* Å) corresponds to hyperthermal gradients (> 35 °Ckm^{-1}), the intermediate facies series (9.000 to 9.040 *b* Å) to normal thermal gradients (35 to 25 °Ckm^{-1}), and the high-pressure facies series (> 9.040 *b* Å) to hypothermal gradients (< 25 °Ckm^{-1}), see also Merriman & Peacor (1999). In Fig. 7, all data sets plot along *b* *i*so-lines of normal geothermal settings (intermediate facies series).

5.4 Comparison with stability fields of macerals, clay minerals and facies critical minerals

During optical examination of polished resin mounted rock sections, thin sections as well as powder whole rock x-ray diffractograms and clay fraction x-ray diffractograms including texturated samples, additional information on macerals, clay minerals and facies critical minerals was collected. The observations were ordered in relationship with the KI data of the same sample and are here discussed with increasing grade of diagenesis and metamorphism (Figs. 8 and 9). VR and VlBR values were used as internal control based on the correlation shown by Eq. 5 (Fig. 6).

5.4.1 Optically distinguishable macerals

At the limit from low- to high-grade diagenesis it is thought that **liptinite macerals** can no longer be distinguished optically from huminite/vitrinite macerals by their lower reflectance, darker appearance, or anisotropy (Alpern & Lemos de Sousa, 1970; Jacob & Hiltmann, 1985; Robert, 1988). In the review ICCP System 1994 of Pickel et. al. (2017) a convergence of reflectance and gray color is reported for VR values of 1.3 to 1.4%R$_r$. and may be indicative for coal basins. Petschick (1989) showed for the studied orogenic inverted basins that dark liptinite in maceral reflection-histograms (Fig. 8) is observed up to VR = 2.1%R$_{max}$. An increasing homogenisation to the same grey shades as observed for **vitrinite** is also observed with increasing maturity/diagenesis first for **cutinite**, then for **sporinite** and at higher maturity for **alginite** (Ferreiro Mählmann & Le Bayon, 2016). In the Lower Austroalpine homogenisation in grey shades is observed at VR = 2.4 ± 0.3%R$_{max}$ (sporinite and liptodetrinite). Sporinite at higher rank was still distinguished by size and shape and is evidently very resistant to degradation (Shaw, 1971). In the Upper Austroalpine cutinite was still optically distinguishable up to VR = 2.08%R$_{max}$, sporinite and alginite/"proto-bitumen" (Bertrand, 1993) up to VR = 2.93%R$_{max}$. Alginate at higher rank was still distinguished by fibrous microstructures and shape when anastomosing appearance parallel to bedding and cell structures where observed (Pickel et al., 2017). In the Helvetic nappes the same trend was observed at slightly lower reflectance values. Cutinite was still optically different from vitrinite up to VR = 1.88%R$_{max}$, sporinite at VR = 2.03%R$_{max}$ and alginite/"proto-bitumen" up to VR = 2.72%R$_{max}$. Cutinite in coals is rarely abundant (Pickel et al., 2017) and in the studied samples locally detected, thus the preservation probably more casual. Until now, systematic liptinite maceral studies have not been published in other orogenic settings. A large dataset is only available from the Upper and Lower Austroalpine (Petschick, 1989; Ferreiro Mählmann, 1994, 1996, 2001 and Ferreiro Mählmann & Le Bayon, 2016).

According to the discussion (see Sects. 4 and 5.2) about the persistence of **resinite**, **exsudatinite** and **bituminite** discriminated from migrabitumen and solid

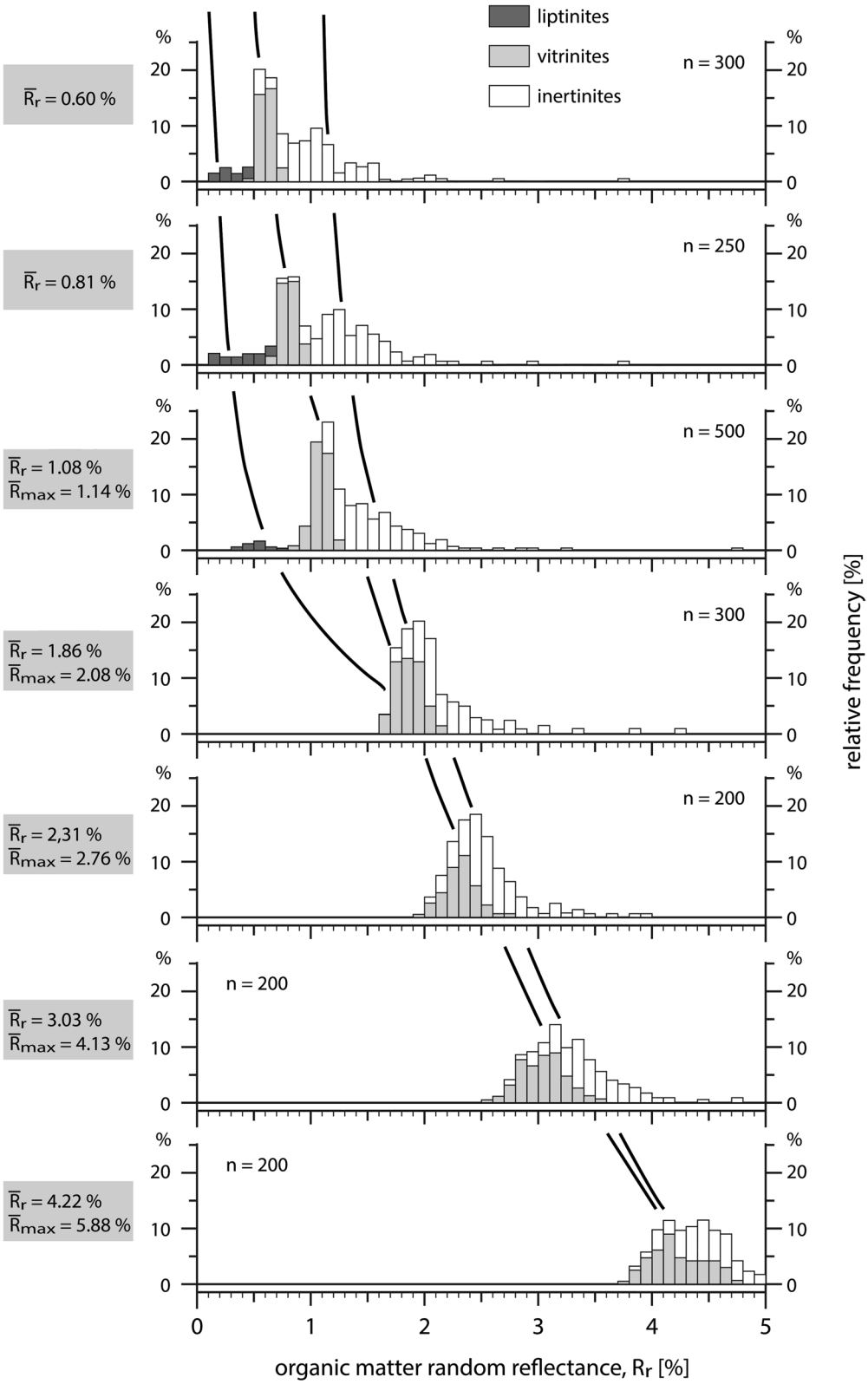

Fig. 8 Reflectance measurement histograms of liptinite, vitrinite and inertinite maceral groups along the maturation path from the sub-bituminous coal stage to anthracite/meta-anthracite (after Petschick, 1989, Fig. 9)

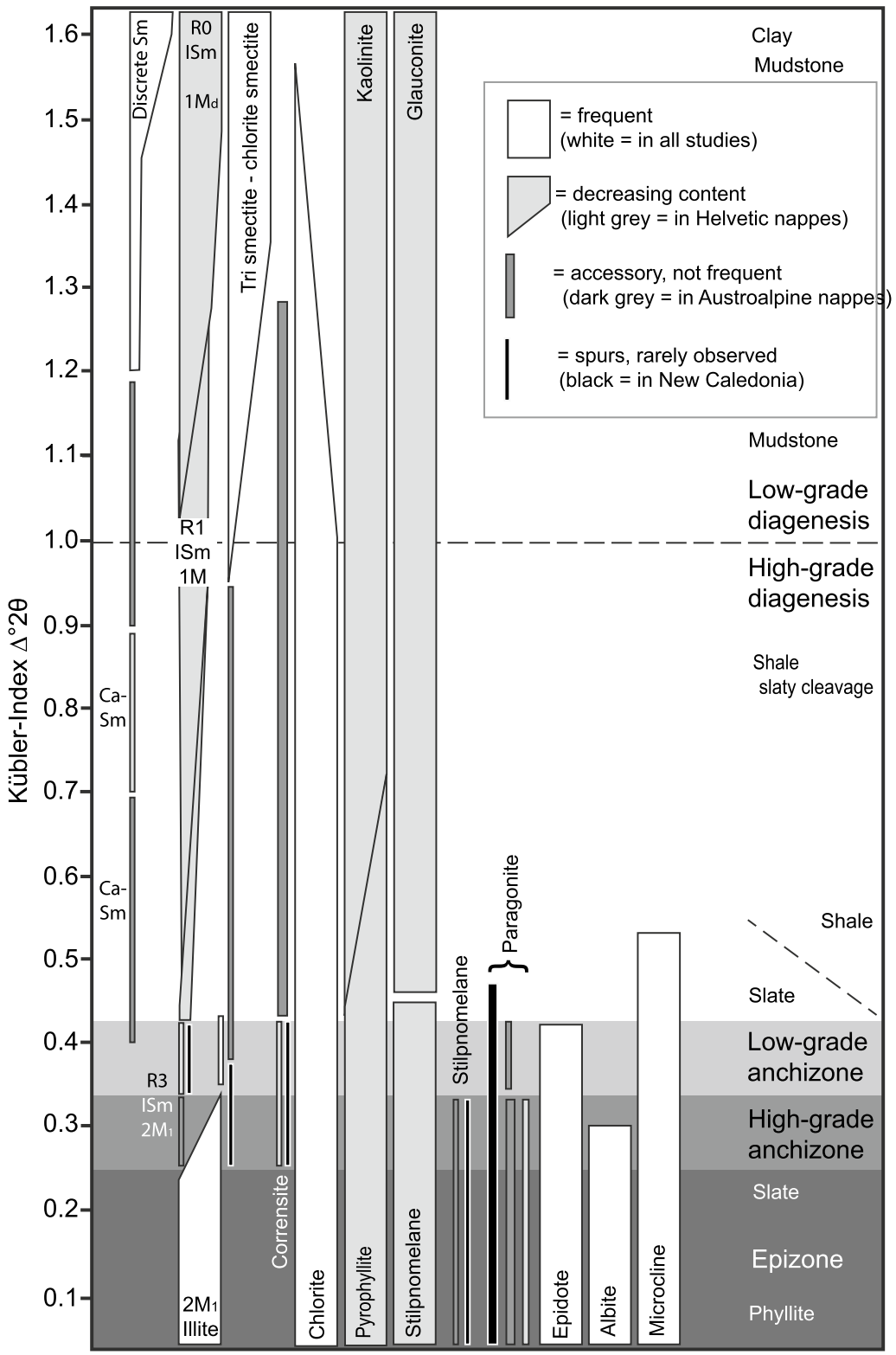

Fig. 9 The graph shows the stability ranges of clay minerals and facies indicative minerals correlating with the Kübler-Index (KI). The KI was chosen because all samples used (n = 1051) can be related to a KI-value. *Sm* smectite, *ISm* illite/smectite, *R* reichweite

bitumen a special focus was set during data compilation on reported detections of this liptinite macerals. It was attempted to adapt the results to the terminological use presented by ICCP System 1994 (Pickel et al., 2017). During the new reflectance measurements, the recommendations were applied. In any case it is very difficult to distinguish these macerals fragmented and dispersed in sedimentary rocks in the study areas. In general, these macerals can only be identified when the relation to the source maceral is obvious (Pickel et al., 2017). Probably an early deformation at low-grade diagenesis forming a slaty cleavage may enhance this problem. It is interesting to note that at same deformation stage and diagenetic grade **micrinite** was often mentioned in the developing foliation. Micrinitization is an indicator for bituminite at VR > 1.3%R_r (Pickel et al., 2017). VR/KI correlations are different in orogenic settings with respect to coal basins (Kübler et al., 1979a; Środoń, 1979; Ferreiro Mählmann & Le Bayon, 2016). The persistence of a lower reflectivity of many liptinie macerals and different optical characteristics at higher VR/KI grade are additional fundamental criteria to predict specific orogenic conditions (Petschick, 1989). The determined KI, VR, and VlBR gradients in this study thus defines normal orogenic gradients.

5.4.2 Stability fields of clay minerals

In low-grade diagenesis **discrete smectite** (17.0 Å, Dunoyer De Segonzac, 1970) is frequently observed and in the Helvetic nappes forms a major clay mineral phase (Wang, 1994; Erdelbrock, 1994). A strong decrease of smectite amounts between 1.6 and 1.4 Δ°2θ (0.65 to 0.85 VR %R_r, Petschick, 1989) was observed in several nappes. In the diagenesis zone at 1.2 Δ°2θ in the Helvetic nappes and at 1.0/0.9 Δ°2θ in the Austroalpine nappes the 17 Å peak disappears completely (Fig. 9). At the same diagenetic grade-level the Reichweite R1 of I/Sm replaced the Reichweite R0 and the illite polytype 1Md (turbostratic orientation) is replaced by 1M (block wise orientation). The illite/smectite (IS) interlayer succession and its order are determined by the Reichweite parameter (Jagodzinski, 1949) from random (IS-R0) to short-range ordered (IS-R1), and then to long-range ordered (IS-R3) illite/smectite mixed-layer (I/S-ml) interstratified crystallites (Reynolds & Hower, 1970; Pytte & Reynolds, 1989).

Minor amounts (< 5%) of smectite, however, could be found in three subsurface outcrops (Ferreiro Mählmann, 1994) in absolute fresh samples (i.e. without solid bitumen oxidation). One sample group comes from the Walgau underground aqueduct in the Northern Calcareous Alps (low-grade anchizone, ≈0.40 Δ°2θ) and the other two sample sets are from the Helvetic nappes, from the Au 1 well (high-grade diagenesis zone, ≈0.70 Δ°2θ) and from the potable water-well Brunnenbüchel (Schaan, Liechtenstein, ≈0.62 Δ°2θ). Chemical analyses of the CaO rich smectite-illite-quartz samples suggested that CaO is located within the smectite interlayers (Kaufhold & Dohrmann, 2008), forming **Ca-smectite**. Most clay specimens containing accessory smectite in the high-grade diagenetic zone and low-grade anchizone have been sampled from clay-bearing limestones or marly mudstones (e.g. Quinten Limestone, Drusberg Formation (limestone, marl), Kössen Formation, Aptychus Limestone). The KI values in these samples were frequently higher than in the clay-rich formations at the footwall or hanging wall (Säntis Alps, Northern Calcareous Alps). It is assumed that the smectite in the illite/smectite mixed-layer contains interlayers of Ca-smectite and broadens the KI peak. It is concluded that Ca-smectite predominance in these samples may be predicted.

At the transition from low- to high-grade diagenesis **chlorite-smectite** disappears in the Helvetic nappes. In the Northern Calcareous Alps chlorite-smectite is still present in samples from the anchizone up to KI = 0.39 Δ°2θ (VR ≈ 3.1%R_{max}). Detected as expandable portions in chlorite. In New Caledonia it was still present in samples close to the epizone boundary. The lowest grade/maturity in the Lower Austroalpine preserved is the high-grade diagenetic zone/semi-anthracite to anthracite, at which grade chlorite-smectite minerals is no longer present as individual crystallites.

Trioctahedral smectite behaves like chlorite-smectite in the low-grade diagenetic zone but is completely absent in the high-grade diagenetic zone. Smectite in the mixed-layers illite–smectite is still present. The illite–smectite Reichweite ordering is predominantly R1 and the illite polytype is 1M (Helvetic nappes). In illite/smectite mixed-layers the smectite content decreases drastically from 100% smectite (VR = 0.6/0.8%R_r, KI = 1.7 to 1.2 Δ°2θ) to 50% smectite at the low- to high-grade diagenesis zone boundary (KI = 1.0 Δ°2θ, Środoń & Eberl, 1984). It is thought that the evolution from R0 to R1 parallels the polytype change from **illite $1M_d$** to **$1M$**, together with the transformation from mudstones to shale (Fig. 9). With increasing grade of diagenesis, the illite–smectite Reichweite transforms to R3 and the illite–smectite type is ISII (according to Środoń, 1984). Smectite in mixed-layer illite minerals decreases at the diagenesis to anchizone boundary to amounts of 10 to 20%. At the same range of metamorphic grade the illite 1M polytype transformation to **illite $2M_1$** advances from 100% 1M in the high-grade diagenetic zone (KI < 0.50 Δ°2θ) to 75% (25% $2M_1$) at the diagenesis/anchizone boundary and to 0% in the high-grade anchizone (100% $2M_1$) of the Helvetic nappes at KI = 0.33 Δ°2θ (VR ≈ 3.70%R_{max}) and in the Lower Austroalpine at KI = 0.28 Δ°2θ. Few data from the Upper Austroalpine seam to substantiate small amounts

of illite 1M in the high-grade anchizone. In New Caledonia the smectite content is around 62% at the diagenetic/anchizone boundary and decreases to 0% (100% $2M_1$) at the low- to high-grade anchizone transition.

Kaolinite is not a common phase in the Austroalpine and dispersely found in few samples within the diagenetic zones (no Reichweite ordering measured). In the Helvetic nappes, kaolinite is a frequent clay mineral within the low- to intermediate high-grade diagenetic zone. It is still present in some samples up to the upper limit of diagenesis (KI = 0.42 Δ°2θ, VR ≈ 3.0%R_{max}). According to the method by Środoń (1984) the mixed-layer illite smectite type in these samples is IS. The Reichweite IS-R1 may be more common in the Austroalpine in the high-grade diagenetic zone than in the Helvetic nappes, where kaolinite smectite KS-R1 is abundantly detected. Kaolinite is also present in the lowest part of the low-grade anchizone in the Northern Calcareous Alps and in New Caledonia (KI = 0.33 Δ°2θ). In these samples mostly illite/smectite mixed-layer ordering of 1:1 layer stacks (**rectorite** according to Bailey, 1982), is stable during a wide VR/KI range approaching the upper limit of the diagenesis (Helvetic nappes, Lower Austroalpine). Dickite could not be recognised. In the Helvetic nappes **pyrophyllite** appears instead (Frey, 1987b) as a reaction product at the high-grade diagenetic zone (Fig. 9). In the Austroalpine nappes kaolinite seems to have undergone illitisation according to the reaction published by Chermak & Rimstidt (1990), and Ehrenberg et. al. (1993) at higher grade of diagenesis (VR > 2.5%R_{max}, KI ≈ 0.45 Δ°2θ). Thus, in both nappe stacks kaolinite can be present up to the diagenetic zone upper limit, but pyrophyllite is nearly completely missing in the Austroalpine (detected only in 8 samples in the Upper Autroalpine, in the Lower Austroalpine kaolinite was found in one sample, but no pyrophyllite was detected).

In a few samples in the Helvetic domain, in the Silvretta nappe and in New Caledonia **corrensite** was found as a minor phase within high-grade diagenetic samples and in the low-grade anchizone (New Caledonia). In metamorphosed Triassic rocks in the Austroalpine and in Helvetic rocks corrensite/chlorite and ISII (Środoń, 1984), smectite in illite < 10% can be preserved up to the anchizone/epizone boundary. **Chlorite** becomes more abundant with increasing grade of diagenesis. In the high-grade diagenetic zone and low-grade anchizone in most samples' chlorite is the dominating clay mineral until illite in the high-grade anchizone increases to equal amounts or to the dominant clay mineral phase.

Glauconite is a typical mineral restricted to several sediment formations in the Helvetic nappes (Wang et al., 1996) and an index mineral for diagenesis (Frey et al., 1973; Frey, 1987a). **Stilpnomelane** occurs at the lower anchizone boundary. In the Upper Austroalpine glauconite and stilpnomelane were not present. In the Lower Austroalpine stilpnomelane occurs as an accessory mineral in radiolarites and red meta-pelites (Jakob, 1923) of high-grade anchizonal to greenschist facies rocks outside the KI methodical limits (VR > 8.0%R_{max}). Stilpnomelane was detected in this study in the Lower Austroalpine in rocks of the same formation but at lower grade without any traces of glauconite. Accordingly, alternative reactions than the stilpnomelane formation from glauconite (Frey et al., 1973) were postulated: Stilpnomelane may be form from Fe-chlorite + hematite + K-white mica (ferri-illite/muscovite) and quartz (see Li et al., 2002). Fe-chlorite + hematite + ferri-illite/muscovite and quartz are frequent in radiolarites and red meta-pelites (Ferreiro Mählmann, 1996). Based on these educts the reaction was evidenced by Fe-stilpnomelane occurrences within high-grade anchi- and epizonal rocks from New Caledonia (Potel et al., 2006, Potel, 2007). The paragenesis stilpnomelane + **biotite** was not found in the studied Helvetic and Upper Austroalpine rocks. In the Lower Austroalpine and Platta nappe, however, the first appearance of both minerals together coincides with KI < 0.16 Δ°2θ and a VR > 6.0%R_{max}. Stilpnomelane is mostly **parsettensite** (Jakob, 1923), an Mn variety (Stalder et al., 1998; Roth & Meisser, 2011).

In the Upper Austroalpine **paragonite** occur rarely in the low-grade anchizone and more abundant in the high-grade anchizone to epizone within neritic Late Jurassic and Cretaceous formations. In some samples of the same formations of the Lower Austroalpine anchizone and epizone, paragonite may occur as the dominant clay mineral, together with Mg (Fe)- and Mg-chlorite. In the ophiolitic Platta nappe it was detected in all epizonal samples. It was also detected in the high-grade anchizone to epizone in New Caledonia with first occurrences in the upper high-grade diagenetic zone. In the Helvetic nappes paragonite is scarcely reported from the high-grade anchizone and epizone (Wang et al., 1996).

5.4.3 Stability fields of facies indicative and critical minerals

Low temperature **albite** and **microcline** (authigenic triclinic end-members as resolved from thin section, XRD and TEM analyses) first appear close to the diagenesis/anchizone boundary in the low-grade anchizone, but more abundant in the high-grade anchizone and epizone. Albite within low-grade and lower high-grade diagenetic zone was interpreted as a detrital phase based on thin-section observations (Ferreiro Mählmann, 1994). XRD studies by this author demonstrated a disappearance in the high-grade diagenetic zone, while authigenic recrystallisation was observed in the anchizone. In marine

rocks authigenic microcline may occur together with illite and paragonite, but not authigenic albite together with paragonite.

First **epidote** within clay-rich rocks appears in the low-grade anchizone and **clinozoisite** rarely in the epizone in siliciclastic pelites of the Lower Austroalpine and Platta nappe close to the KI methodical limit.

5.4.4 Temperature–pressure–time modelling and calibration

For different KI boundaries different VR modelling temperatures were determined in the publications compiled for this study. A first numerical VR-model applied Petschick (1989) for the Northern Calcareous Alps. KI zone boundaries were determined with the TTI model of Lopatin (1971), and Waples (1980) and confirmed using the same TTI-modelling method with data from other Upper Austroalpine nappes by Ferreiro Mählmann (1994). The derived temperatures were as follows:

$230 \pm 20\,^{\circ}C$ = diagenesis/anchizone
$262 \pm 10\,^{\circ}C$ = low-/high-grade anchizone
$300 \pm 5\,^{\circ}C$ = anchi-/epizone

For the Northern Calcareous Alps temperatures were measured and calculated from fluid inclusion data, smectite geothermometry, and VR-modelling (Ferreiro Mählmann, 1994), while Krumm et. al. (1988), and Petschick (1989) determined slightly lower temperatures. Fluid inclusion data from the Helvetic nappes suggest temperatures between 216 and 228 °C for the diagenesis/anchizone boundary (Rahn et al., 1994). By applying the Bostick et. al. (1978) model approach, Rahn et. al. (1994) derived KI zone boundary temperatures for the Helvetic nappes as follows:

$205\,^{\circ}C$ = diagenesis/anchizone
$257\,^{\circ}C$ = anchi-/epizone

The VR geothermometric model of Bostick et. al. (1978) used by Rahn et. al. (1994) is difficult to compare with TTI and EASY%R_0 (Sweeney & Burnham, 1990), as this model is peak temperature dependent only. The Bostick et. al. (1978) model calculated VR gradients of 0.033 to 0.09%/km, and these gradients are highly deviating from Eq. 3 (see also misfit shown in Mullis et al., 2017) and discussion in Ferreiro Mählmann et. al. (2012).

When using EASY%R_0 modelling, temperatures slightly lower to the TTI modelling were calculated. The first use of the kinetic-based EASY%R_0 model in the study areas (Ferreiro Mähmann, 2001) proposed the following temperatures:

$230\,^{\circ}C$ = diagenesis/anchizone
$280\,^{\circ}C$ = anchi-/epizone

The preferred models, frequently used in the Alpine orogenic system (Ferreiro Mählmann et al., 2012; Waliczek et al., 2019, 2020) are those of Barker (1988), and Barker & Pawlewicz (1994). With the first order function for normal-thermal burial conditions (Eq. (1) of Barker & Pawlewicz, 1994) the following temperatures are calculated:

$135.5\,^{\circ}C$, VR 1.00 R_0% = low-/high grade diagenetic zone
$225.5\,^{\circ}C$, VR 3.05 R_0% = diagenesis/anchizone boundary
$262.0\,^{\circ}C$, VR 4.81 R_0% = anchi-/epizone boundary

Oxygen isotopic dating (Black, 1974) and fluid inclusion measurements predict mean temperature values of 230 ± 10 °C for the diagenesis/anchizone boundary and 295 ± 10 °C for the anchizone/epizone boundary in New Caledonia (Potel et al., 2006). These values were used as reference for theire VR model calibration. The model of Dalla Torre et. al. (1997), the first one including the metamorphic factor pressure, resulted in the following temperature values:

$110\,^{\circ}C$ at 0.5 kbar VR 1.00 = low-/high-grade diagenetic zone
$225\,^{\circ}C$ at 2.0 kbar VR 3.05 = Diagenesis/anchizone boundary
$265\,^{\circ}C$ at 2.7 kbar VR 3.80 = low-/high-grade anchizone boundary
$> 300\,^{\circ}C$ at 3.5 kbar VR 4.81 = anchi-/epizone boundary (outside calibrated VR values)

All values are calculated for a time of diagenesis – anchimetamorphism of 10 myr.

When reducing burial times or increasing pressure, the calculated temperatures increased. As preliminary result the following VR temperature estimations fit best with fluid inclusion temperature (FIT) data and mineral reaction-isograd calibrations. The FIT, mineral paragenesis, VR, maturity-modelling result was used to construct Figs. 7 and 9. They represent mean values for all incorporated study areas:

VR 1.02 = 100 °C FIT (Helvetic nappes of the Bregenzer Wald, Ferreiro Mählmann, 1994).

VR 3.05 = 230 °C FIT (Helvetic nappes of Switzerland, Mullis et al., 2017),
+1 kbar = 240 °C FIT and first detection of paragonite (265 °C from chlorite thermometry, Lower Austroalpine, Ferreiro Mählmann, 2001),
−0.5 kbar = 210 °C FIT and first occurrence of stilpnomelane (Helvetic nappes, Breitschmid, 1982).
VR 3.75 = ≥ 248 °C and < 270 °C FIT (Austroalpine, Ferreiro Mählmann, 1994, 2001).
VR 4.81 = ≥ 270 °C FIT, 270 °C (2.5 ± 0.5 kbar) from the reaction kaolinite + quartz = pyrophyllite (Frey, 1987b),
+1 kbar = ≥ 280 °C (Helvetic nappes, Bucher & Frey, 1994; Potel et al., 2006).
+2 kbar = ≥ 300 °C with the paragenesis actinolite-chlorite-epidot/prehnite-pumpellyite out, (South Penninic, Platta nappe at the southern border of the study area).

Comparing the models with FI data and mineral reaction iso-grades the best fit is given by the P–T–t model of Dalla Torre et. al. (1997), close to it is the EASY%R_0 model (this model has much more variables can be used, but mostly parameters measured are missing). Barker (1988), and Barker & Pawlewicz (1993) overestimate temperature in the diagenetic zone but contrary underestimate it at incipient metamorphism (anchizone–epizone). The Bostick et. al. (1978) model calculates to low temperatures and TTI with increasing thermal grade to high temperatures (see also discussion in Ferreiro Mählmann, 2001). For the discussion the P–T–t model calibration data are used.

6 Discussion

In most studies cited for this data compilation, linear regressions were published (including Eqs. 2, 3 and 6). A better statistical coverage could be achieved when using a second order regression (Ferreiro Mählmann, 2001). For an even better fit in thick nappe-stack sections (thickened continental crust or deep wells) a cubic regression or applying a logarithmic scale was proposed (Reinhardt, 1991). With small sample numbers such mathematical treatment is of limited value, but a linear regression for local correlations more appropriate. Dealing with 1600 samples (Ferreiro Mählmann et al., 2012) and 568 samples in this study it was evident that an exponential function (Eqs. 1b, 1c, and 1d) is well representing the general trend (Fig. 5). This is much better adapted to a binary relation if the correlated factors approache an asymptotic limiting behaviour (Fig. 5). If data cover a large range of diagenetic to metamorphic conditions the exponential function provides a significant increase in regression coefficient. Thus, the limits of orogenic diagenesis and metamorphism in Fig. 1 are shown by curved boundaries. The orogenic VR/KI field (light grey area in Fig. 1) between < 0.6 Δ°2θ and 0.125 Δ°2θ is calibrated by more than 1200 samples.

6.1 Kübler-Index versus vitrinite reflectance

An emerging key question from Fig. 1 is, whether the relationships established will be universally applicable or, alternatively, be related to specific regional thermal conditions. To evaluate this issue, from all areas selected for the review (for references, see Ferreiro Mählmann et al., 2012) published regression lines with a moderate VR/KI gradient were depicted (Fig. 1). They are assumed to represent normal orogenic thermal gradients. Additionally, the study areas from the Northern Calcareous Alps (Petschick, 1989, Ferreiro Mählmann, 1994) and the Glarus/Säntis Alps (Rahn, 1994; Wang, 1994; Erdelbrock, 1994) were included. The corresponding VR/KI gradients plot in the centre of the field related to orogenic settings (Fig. 1). Mineralogical, geochemical, fluid inclusion data and OM indices calibration, together with illitisation modelling and maturity modelling allowed to estimate temperature gradients between 100 °C/1 kbar and 330 °C/3.5 kbar (± 20 °C and ± 0.5 kbar). Such results can be related to normal heat flow conditions between 75 and 55 mWm^2 and to a normal geothermal orogenic evolution (Fig. 10). It explains the missing of chloritoid, biotite + muscovite in meta-pelites and lawsonite in meta-sedimentary rocks of the ophiolitic Platta nappe in the P–T diagram (New Caledonia will be discussed separately).

A possible influence by the presence of detrital micas in syn-orogenic Jurassic to Cretaceous formations can be shown to have a minor influence ($R^2 = 0.717$ (not visualized) instead 0.779 (Eq. 1c) and causing a shift to higher VR of Δ 0.02%, see Sect. 5.1.5). Preparation, standardisation, and measurement errors including individual measuring differences are much more relevant (Le Bayon et al., 2012a; Ferreiro Mählmann & Le Bayon, 2016, Fig. 5). In the following discussion, Eq. 1d (considering the methodical limits at lower and higher grade) will be adopted for grade determination in orogenic settings with a normal heat flow. For such purpose, all factors of influence on VR and KI except temperature, pressure and time are to be excluded (Fig. 4), based on clay mineralogical and coal petrographic experience. Consequently, analytical procedures are not routine techniques, but require a more profound knowledge on the potential pit falls and methodical flaws to gather high quality data sets.

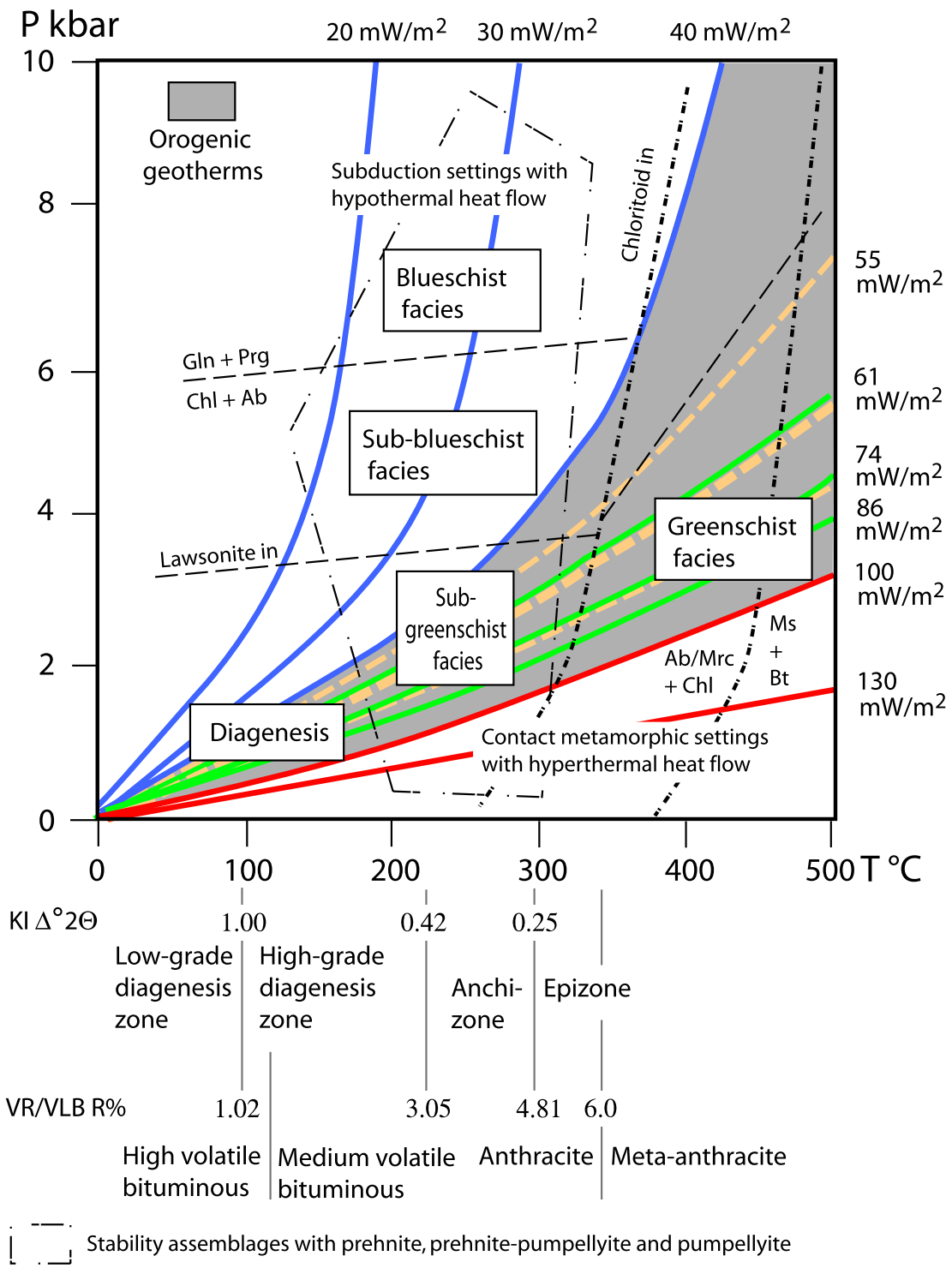

Fig. 10 Shows the subdivision of diagenesis, incipient metamorphism and geotherms in the pressure–temperature plot as proposed by Ferreiro Mählmann & Le Bayon (2016). In the original plot the lawsonite-in isograde was shown at higher grade (we like to thank Prof. Jan Środoń for a correcting remark at Euroclay 2019). The orange bold and dashed line represents the mean normal geotherm defined as a normal geothermal gradient. The thin orange and dashed lines show the upper and lower variances found in the study areas

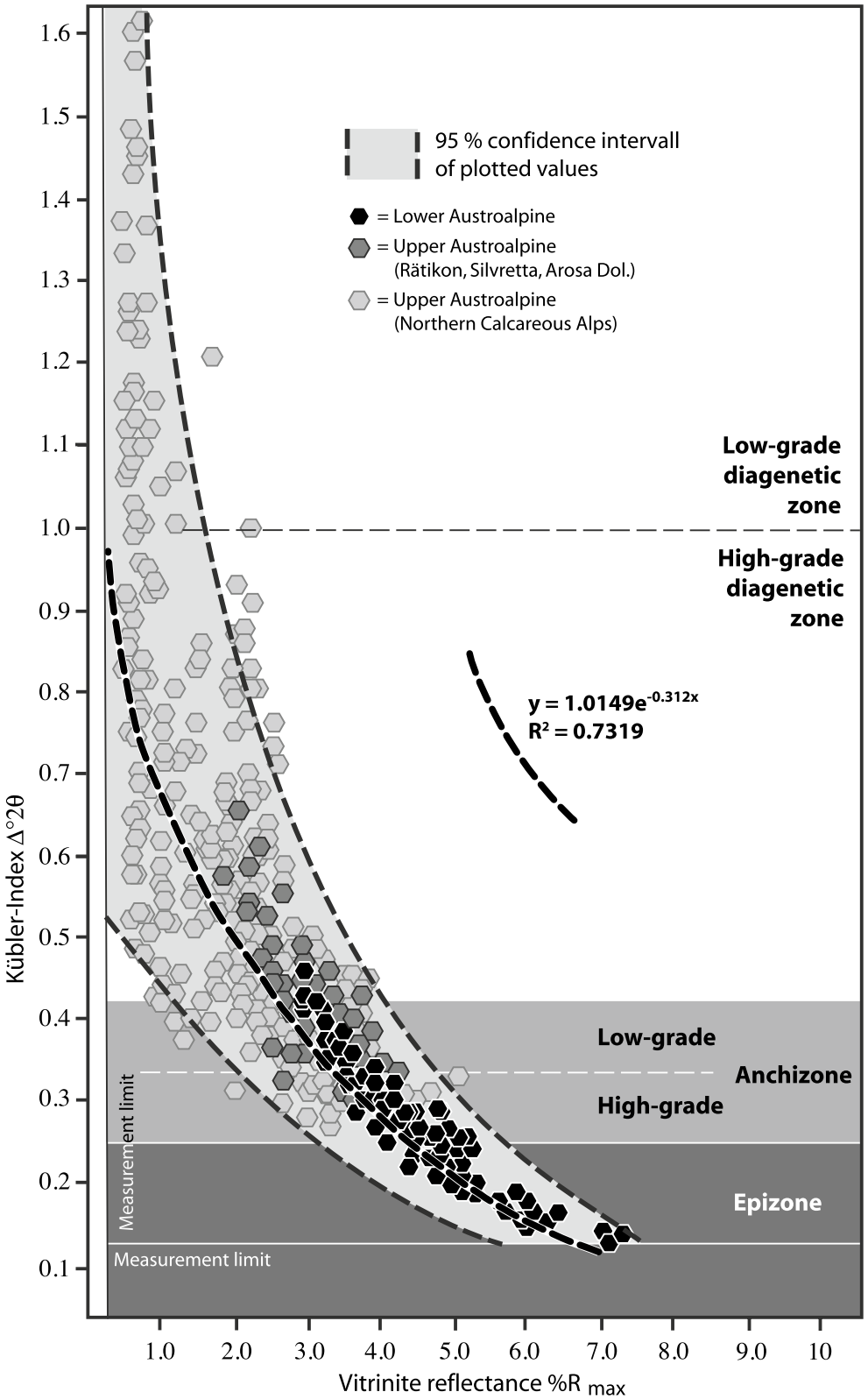

Fig. 11 Vitrinite reflectance (VR) vs. Kübler-Index (KI) correlation plots showing all data from the Austroalpine nappe units of the study areas. In this plot the regression is shown and the vales plotting in the 95% confidence area. It demonstrates the restricted use from the measurement limit of the XRD device in the epizone to the statistical significance limit close to the high-grade/low-grade diagenetic zone boundary

Some of the here included study areas show data series close to the mean, but shifted to the left (Austroalpine, New Caledonia) or to the right (Helvetic nappes, Fig. 5). Starting from the same KI value, the corresponding VR is higher for samples in the Helvetic realm (see also Fig. 1). For better understanding the regional differences, Fig. 11 displays the Austroalpine data series in a second VR/KI correlation plot (n = 439). Due to the strong scatter of the VR/KI values from the Northern Calcareous Alps (part of the Austroalpine system) within the diagenetic zone, the correlation coefficient amounts to $R^2 = 0.732$. Without the values from the Northern Calcareous Alps a much better relationship ($KI = 0.012VR^2 - 0.186VR + 0.85$, n = 142) is obtained and the correlation more significant ($R^2 = 0.888$). If plotting the values of the Lower Austroalpine only, no further change of the VR/KI equation is observed, but the regression coefficient is slightly higher ($R^2 = 0.904$, n = 103).

The epizone (KI < 0.25 Δ°2θ) is well established only in the Lower Austroalpine (Figs. 5, 11). At a VR > 6.0%R_{max} and KI < 0.20 Δ°2θ sub-greenschist facies conditions (Ferreiro Mählmann, 1996) were determined based on the paragenesis of prehnite + pumpellyite in ophiolites of the Platta nappe (Dietrich, 1969; Trommsdorf & Evans, 1974) and prehnite in Pietra Verde tuffs in Triassic formations (Austroalpine). These conditions are close to the transition to paragenesis of the actinolite + chlorite + epidot facies in the greenschist facies (Liu et al., 1987; Frey et al., 1991; Potel et al., 2002) and determined close outside of the study area of the Lower Austroalpine and Platta nappe (Dietrich et al., 1974). Thus, data comparison between different study areas is first possible in the lower grade epizone at KI > 0.12 Δ°2θ and high-grade achizone (Fig. 11) and explains the calibration limit at KI ≈ 0.15 Δ°2θ (Eqs. 1c, 1d).

For the same VR (< 5.0%R_{max}), the narrow data variance of KI in the Lower Austroalpine contrasts with a large scatter of KI values in the Upper Austroalpine of the Silvretta nappe s.l. and the SE Northern Calcareous Alps (Rätikon Mountains). The scatter in KI increases at same VR considerably in the NW Northern Calcareous Alps and coincides with a prominent increase in illite/smectite mixed-layer content. The smectite content in illite/smectite at same VR values is much lower in the Silvretta nappe s.l. and the SE Northern Calcareous Alps. The differences found between the single areas are even more prominent within the low-grade anchizone and illite peaks substantially widened by smectite interstratification within the high-grade diagenetic zone. The low-grade diagenetic zone is represented only by values from the Northern Calcareous Alps (Fig. 11). For this KI range, the VR/KI correlation becomes insignificant, and the calibration limit given at KI ≈ 1.05 Δ°2θ (Eqs. 1c, 1d).

6.1.1 Controlling factors on the correlation between different indices to determine grade of diagenesis and metamorphism

When looking for the controlling factors of metamorphism (P–T–t–D–X–aH_2O) whith respect to the differences in data discussed in Sect. 6.1, it should be kept in mind that P and T are calibrated for the same VR values (having the fastest kinetic thermal response). The influence of deformation rate (D) can be neglected because highly tectonised rocks are sorted out. Thus time (t) and the lithotype (X, geochemistry) must be considered. When comparing differences in rock chemistry, rock mineralogy, and sedimentary lithofacies "petro-variance" (Henrichs & Richter, 1993; Krumm, 1984) these petro-variances are found to be insignificant for the Lower Austroalpine, Silvretta nappe s.l. and Rätikon Mountains. The petro-variance and intra-sample variation (Kürmann, 1993) from within the same formations are much more distinct in the Northern Calcareous Alps (Petschick, 1989; Ferreiro Mählmann, 1994), minor in the Helvetic Alps (Mullis et al., 2002), than in the Austroalpine nappes in the south (Ferreiro Mählmann, 1995, 2001). The same trends are observed regarding the smectite content in illite smectite mixed-layer and Chl-Sm amounts showing high petro-variances and intra-sample differences, they are not especially restricted to a rock type (lithology) or formation (stratigraphy). Furthermore, it is known that the mineralogy of the clay fraction changes with heating time, thermal conditions (heat flow), and different fluid activities during reaction (Herbert et al., 2016). Heat flow (normal geothermal gradient) and water activity (aH_2O), excluding hydrothermal systems, are assumed to have a similar effect. Thus, the factor time will be compared as next.

In the Northern Calcareous Alps, a heating time of 5 myr would not be sufficient to equilibrate chemical differences. It is assumed that illitisation process under normal thermal conditions is slower than the tectonic burial time. Tectonic processes are faster than thermal equilibrations of mineral reactions (Walther & Orville, 1982). Posterior to Cretaceous metamorphism the subsequent tectonic cycle may have sealed the thermal pattern induced by nappe stacking. Thus, KI values, IS-R0 to IS-R1 or IS-R3 (1M to $2M_1$) ordering and smectite amounts formed at heating episodes < 5 myr may not reflect equilibrium conditions as proposed by Hoffman & Hower (1979), Pollastro (1993) or Šucha et. al. (1993) or are also not predominantly temperature dependent (e.g. Środoń, 1979, 1996; Clauer et al., 1997). Kinetic models (e.g. Hillier et al., 1995; Elliot & Matisoff, 1996; Berger et al., 1997) have demonstrated that temperatures determined by these authors represent a valid first approach, especially if little is known about the burial history. Because time is the remaining factor to explain the differences in the NW Northern Calcareous

Alps compared with the other Austroalpine units a first conclusion points on the importance of time as controlling factor. In the Northern Calcareous Alps disequilibrium is detected between the indices to determine grade of diagenesis and incipient metamorphism.

For a heating time of 5 to 10 myr (Silvretta nappe s.l., Rätikon Mountains) a significant homogenisation is observed with a slight increase in VR and a more prominent smectite % decrease in illite/smectite and a better KI aggradation order at the same temperature if compared with the Northern Calcareous Alps. The same is observed for the Helvetic nappes when comparing Säntis Alps versus Glarus Alps. At the same rank of maturity, the variance of KI and smectite % is higher in the Säntis Alps (Tertiary orogenic foreland nappes) than in the Glarus Alps (internal orogenic nappes). Thus, duration of metamorphism is assumed to decrease from the S to the N in the Helvetic nappe stack, and this must be considered in future VR modelling. The same is to be postulated for the Northern Calcareous Alps (Cretaceous orogenic foreland nappes) compared to the internal Silvretta nappe s.l. Due to the propagation of the nappe tectonic displacement to the N or NW (Tollmann, 1978; Froitzheim et al., 1994; Schmid et al., 2004; Pfiffner, 2009) this is a reasonable scenario.

At burial orogenic episodes of 10 to 20 myr (such as in the Lower Austroalpine) data homogenisation of the different indices used to determine the grade of metamorphism is reaching equilibrium. One may assume that illite aggradation continues to evolve for the same P–T-conditions (and thus equals VR) causing a flattening of the gradient in the VR/KI graph (Fig. 11), i.e., a KI decrease (sharper FWHM) at basically equal VR. Again smectite %, KI or VR modelling methods will have to consider curved gradients versus depth, and time for their numerical models. CM or OM indices equilibrium conditions where also indicated by modelling with a heating time > 10 myr, resulting in same thermal predictions (Ferreiro Mählmann, 2001). The same temperatures calculated using different models with different organic matter and clay mineral indices demonstrate for thermal condition with a duration of more than 10 myr an equilibrium state (see also Le Bayon et al., 2011; Mullis et al., 2017). Based on the selected calibration interval (KI = 1.10 to 0.20 Δ°2θ and R_{max} = 0.8 to 6.5%) the proposed range for a thermometric application is between 80 ± 10 °C and 330 ± 20 °C (Fig. 10). Montmartin et. al. (2021) demonstrated that the KI method is applicable up to epizonal temperatures around 275 °C. Their temperature restriction to 275 °C may be explained by their calibration with the Raman spectroscopic methods on carbonaceous material of Lahfid et. al. (2010), and Zhu et. al. (2016), see discussion in Mullis et. al. (2017). A possible lower temperature limit can be expected at hyperthermal conditions (Fig. 10, faster aggradation at higher heat flow) as indicated for the Permian Basin of USA (Green et al., 2020) and the Montagne Noire (Montmartin et al., 2021).

For New Caledonia (northern island) VR/KI values plot within a narrow range along the regression line of samples from the Lower Austroalpine, the Silvretta nappe s.l. and the Rätikon Mountains. Due to a very close correlation similarity and concordant CM results compared with VR an equivalent thermal history and heating time was suggested (Potel et al., 2006). Therefore, a heating episode after HP metamorphism of > 10 myr may be predicted, in line with the time between youngest sediment deposition and Late Eocene white mica cooling ages (Sect. 3.5). Independent of the metamorphic history, prior to peak thermal events of more than > 10 myr the VR/KI system equilibrates, and same thermal predictions are possible.

Finally, despite the similarities in correlation statistics between (i) the southern Helvetic nappes (Fig. 12) and the Rätikon Mountains as well as the Silvretta nappe s.l. (Fig. 11), and (ii) the northern Helvetic nappes with the Northern Calcareous Alps, one correlation difference in the VR/KI diagram (Fig. 5) is easily recognised. When plotting the data separately (Fig. 12) the Helvetic values run parallel to the Upper Austroalpine data (Fig. 11), but with a tendency to higher VR. Ferreiro Mählmann et. al. (2012) concluded that a trend to higher VR would predict higher geothermal gradients, but a trend to lower VR higher P conditions and lower thermal gradients (Fig. 1). Indeed, the *b* parameter reflects the same (Fig. 7). The Lower Austroalpine and New Caledonia areas were affected by low normal thermal gradients of 28 °C/km and 25 to 30 °C/km, respectively. The *b* parameter plots around the 9.020 and 9.015 Å line in the transitional pressure series field tending to the high-pressure series (Fig. 7, Guidotti & Sassi, 1986). The same is indicated for the Dauphinois domain showing similar clay mineral and KI trends.

The VR/KI gradient of the Upper Austroalpine is located close to the normal thermal gradient field, when taking out the data from the Northern Calcareous Alps (Fig. 11). In the centre of the *b* parameter transitional pressure series the corresponding values plot along the 9.010 Å line and therefore representing a normal thermal gradient of 28 to 32 °C/km The Helvetic nappes samples plot along the 9.008 Å line. It represents the study area with the data group closest to the low-pressure series (Fig. 7), for which higher temperature conditions are expected (Sassi & Scolari, 1974). In the field several thermal anomalies were observed within the Helvetic nappes, e.g. along thrust boundaries (Árkai et al., 1997; Abart & Ramseyer, 2002; Hürzeler & Abart, 2008). A higher geothermal gradient was derived from many studies, including hyperthermal conditions in the Helvetic nappes (Mullis et al., 2017, and references therein, but outside this study area). Indeed, differences in the VR/KI correlation

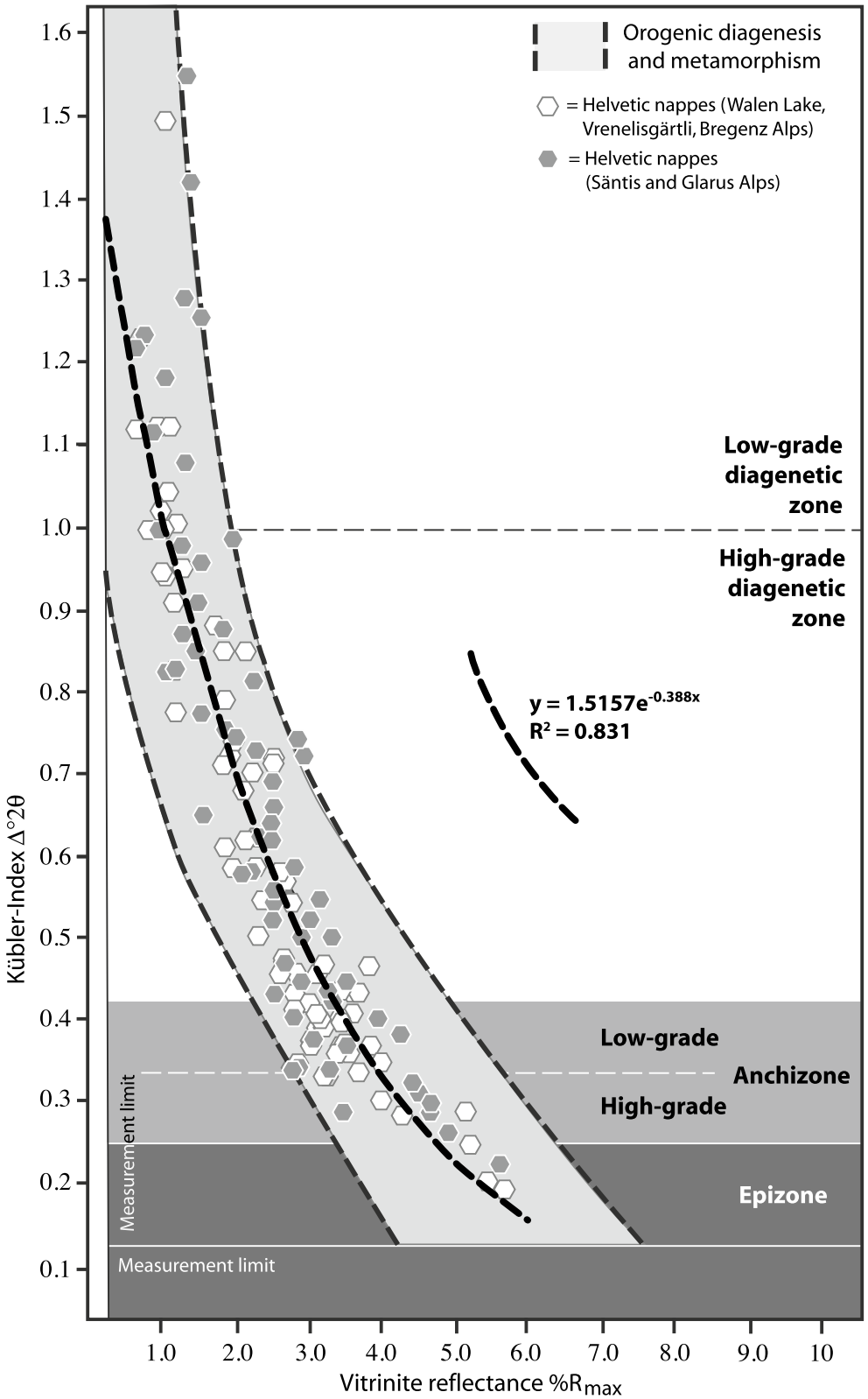

Fig. 12 Vitrinite reflectance (VR) vs. Kübler-Index (KI) correlation plot showing all data from the Helvetic nappe units of the study areas. In the Helvetic nappes a correlation can be proposed for the epizone/anchizone boundary at KI = 0.25 Δ°2θ and VR = 4.45%R_{max} to the low-grade diagenetic zone at KI = 1.20 Δ°2θ and VR = 1.0%$R_{r/max}$

correspond to differences in P–T-conditions and reciprocal heat flow during a relatively long duration (5 to 10 myr, see Sect. 5.1.3).

Pressure is not discussed separately here. Although pressure effects on VR (Huang, 1996; Dalla Torre et al., 1997; Ernst & Ferreiro Mählmann, 2004; Le Bayon et al., 2011, 2012a, 2012b) and VlBR (Ferreiro Mählmann & Le Bayon, 2016) have been observed, they are small compared to the relevant geothermal range of VR/KI gradients. During hydrocarbon generation (diagenetic KI) the differences should have a minimum influence if compared to other factors (see also Burnham, 2019), but may become more relevant in the anchizone to epizone.

6.2 Vitrinite reflectance and vitrinite-like solid-bitumen reflectance

The VR/VlBR correlation is based on 158 (Fig. 6) measurements on resin-mounted and polished rock section and its second order regression line has a very high significant regression coefficient (Eq. 5). Several studies have provided regression equations to calculate a VR equivalent from BR values (summarized in Suárez-Ruiz et al., 2012; Petersen et al., 2013; Schmidt et al., 2019). Contrasting with correlation equations from literature (Jacob, 1967; 1989; Jacob & Hiltmann, 1985; Bertrand 1990, 1993; Ferreiro Mählmann, 1994, 2001; Landis & Castaño, 1995; Bertrand & Malo, 2001; 2012; Schönherr et al., 2007; Ferreiro Mählmann & Le Bayon, 2016; Schmidt et al., 2019) most models tend to a higher gradual increase in VlBR. We propose the following explanations for the differences found:

A first reason for the better sensitivity may be due to minimizing organic matter identification errors during microscopic analysis and avoiding insufficient particle numbers measured. These methodical aspects are thought to represent primary problems (ASTM D7708-14, 2014; Hartkopf-Fröder et al., 2015). Barker and Pawlewicz (1993) determined a minimum number of 20 measurements per sample to accurately define the shape of the reflectance histogram. Figure 8 illustrates the evolution of OM histograms with increasing maturity. The shape of the reflectance histogram at oil window maturity (0.5 to 1.30%R_r) should be based on a Gaussian distribution (Fig. 8). The same is expected for VlBR measurements. Collecting 20 measurements the variance of the reflection value is mostly very high and the standard deviation > 10. Most samples would not have enough data to define a normalized distribution. The objective to determine a quantitative value is commonly acquired when approaching 50 measurements, much more than proposed previously (ASTM, 2015). At around 50 measurements the recommendation to remove outliers (ASTM D7708-14, 2014) does not need to be applied. A single value does not significanly change the mean. A mean reflectance value and its standard deviation are computed and reported from the total number of measurements. ASTM (2015) also recommends a projected diameter size of 5.0 µm. This is a minimum if the measuring spot has a 2.5 µm diameter. According to the data presented in Tables 1, 2, 3 and 4, this was also recommended to the different analysts, but in sedimentary rocks is commonly difficult to fulfil. From the study areas, only 158 samples meet this requirement, but the good regression statistics justify such strict modus operandi.

In a controverse discussion between Burnham (2019), and Hackley et. al. (2015) analyzing the same shale samples, the first author pointed out that different empirical VR/BR conversion schemes are probably the result of a mixture of VR and BR values. In a parallel discussion Ferreiro Mählmann and Le Bayon (2016) pointed out the optical similarities of resedimented solid bitumen and vitrinite. With the proposed statistic procedure and applying the second recommendation (see below), this problem, probably a much more frequent analytical error, should be minimized.

The second reason to explain the precision obtained is based on the solid bitumen selection under the microscope. Schmidt et. al. (2019) recommends restricting measurements to textures of homogeneous isotropic solid bitumen, because other solid bitumen textures can affect the reflectance values (Landis & Castaño, 1995; Schönherr et al., 2007; Sanei et al., 2015). Such recommendation is useful until a first pale bireflectance is observed, which develops within the low-grade diagenetic zone depending on the geothermal gradient (Ferreiro Mählmann & Le Bayon, 2016). With increasing maturity (e.g. within the high-grade diagenetic zone) solid bitumen may still preserve isotropy but cause serious scattering values leading to a weaker correlation (see the solid bitumen classification of Ferreiro Mählmann and Le Bayon (2016) showing optical changes with increasing grade of metamorphism). In sedimentary basins such a restriction allows diagnostic correlations (Mastalerz et al., 2018), but is not applicable to orogenic settings because strain with increasing diagenetic grade is a catalyst for anisotropy development in VlB (Fig. 4). Thus, with incipient development of anisotropy only low bireflecting solid bitumen (VlBR) was used for correlations. From high-grade diagenetic to epizonal (subgreenschist facies) conditions, anisotropic solid bitumen with a bireflectance less intensive than for vitrinite was used (Δ R% for VlB is from 0.5 to 2.0).

The third reason to explain differences is due to the mobility of solid bitumen at reservoir temperatures

(Jacob, 1989) and distinctions between pre- and post-oil textural types (e.g., homogenous, granular, coked, see Sanei et al., 2015). The here presented study focuses on pre-oil solid bitumen. The most frequently cited conversion equations are from Jacob (1989), and Landis & Castaño (1995), however, both studies are from basins with high geothermal gradients. Jacob (1989) included post-oil solid bitumen reflectance measurements from fracture-filling vein-deposits (e.g., asphaltite and asphaltic pyrobitumen), causing complications for the correlation (Schmidt et al., 2019), because such solid bitumen was generated at different times and under varying conditions. Schönherr et. al. (2007) combined data from the two studies to derive an "improved" calibration equation. Bertrand & Malo (2001) provided a correlation equation, but they noted that calculated correlations might only apply to the basin they were measured in. Ferreiro Mählmann & Le Bayon (2016) examined VR/VlBR correlations from different geodynamic settings. In the present study only pre-oil vitrinite like solid bitumen was measured and geodynamic settings were restricted to orogenic normal thermal heat flow scenarios.

The fourth reason is given by excluding VR/VlBR correlations below the value of 1.0%R_r. Jacob (1989) found bitumen to be of lower reflectance than coexisting vitrinite below VR 1.0%R_0 (see also Robert, 1988; Bertrand & Malo, 2001; Ferreiro Mählmann & Frey, 2012). In the present study VlBR below the VR of 1.0%R_r was observed to be constantly lower, but the disperse bituminitic OM was difficult to discriminate from other isotropic bitumens and vitrinite, thus data excluded (Sect. 5.4.1). So far, no VR/VlBR data were published in cross-calibration with standardized inorganic methods (e.g. KI) to determine grade of diagenesis and using well-classified solid bitumen sub-macerals.

These four reasons shown may explain the differences to the most recently conversion published by Schmidt et. al. (2019). Nevertheless, their study supports our interpretation (Ferreiro Mählmann & Le Bayon, 2016) that measurements on VlBR/BR from solid bitumen with homogeneous texture (isotropic at low maturity, anisotropic at high maturity) can be performed to improve thermal history reconstructions. The equation of Schmidt et. al. (2019) is like Eq. 4, first published by Ferreiro Mählmann and Frey (2012), but for orogenic settings at normal thermal heat-flow conditions Eq. 5 is recommended showing relative lower VlBR. The VR/VlBR regression (Eq. 5) is very close to the slope of Bertrand (1993). Other correlation equations (e.g. Jacob & Hiltmann, 1985; Robert, 1988; Jacob, 1989; Bertrand, 1990; Landis & Castaño, 1995; Bertrand & Malo, 2001) tend to predict a higher VlBR value, which seems logic when considering that hyperthermal settings are sought in hydrocarbon prospection.

An interlaboratory study (Hackley et al., 2015) was set up to stress the petrographic distinction of solid bitumen from vitrinite including the VlB used in the present study. However, the reported reflectance values of both VR and VlBR-BR turned out to be identical among all participants. The result suggested that the analysed macerals could be vitrinite-like solid bitumen (VlB sensu Bertrand & Héroux, 1987; Ferreiro Mählmann & Le Bayon, 2016; Hackley & Lewan, 2018). According to Hackley et. al. (2015), and Schmidt et. al. (2019) the vitrinite-like maceral (and our VlB) follows the solid bitumen reflectance versus temperature trend, indicating that the vitrinite-like secondary maceral probably is a solid bitumen type. Burnham (2019) calculated vitrinite and kerogen reflectances with data of Jacob (1989), Landis & Castaño (1995), Ferreiro Mählmann & Le Bayon (2016), and Schmidt et. al. (2019). Those data agree with the kerogen type II model (Burnham, 2019). Complementing previous studies by Ferreiro Mählmann (1994, 2001), Ferreiro Mählmann & Frey (2012), and Ferreiro Mählmann & Le Bayon (2016), the function (Eq. 5) reconfirms that a VlBR can be converted to an equivalent VR, but Eq. 5 provides a higher statistical rating and a VR/VlBR correlation, which is very sensitive to maturity.

Ferreiro Mählmann (1994) published the first VR/VlBR equation using exclusively orogenic diagenetic to metamorphic samples. 90% of the samples came from the Austroalpine. Later, Lower Austroalpine samples were added without causing a significant statistical difference (Ferreiro Mählmann, 1995; Ferreiro Mählmann & Frey, 2012). Predominantly the samples were collected from nappe units showing an Alpine metamorphism at pressures of 2.0 to 6.0 kbar at thermal gradients between 22 and 30 °C/km. The regression line parallels that of Eq. 5, but with a slight shift to higher VR values. Thus, the equation of Ferreiro Mählmann & Frey (2012) may be valid for slight hypothermal orogenic gradients.

For further worldwide enlargement of the sample set to orogenic inverted and sedimentary basins the measurements were extended including syn-sedimentary/early diagenetic to amphibolite facies settings. The equation established (Ferreiro Mählmann & Le Bayon, 2016) was proposed as a mean of different geothermal and geodynamic settings and will be proposed to be used if the thermal history of a study area is little known.

It is not possible to clarify, attempting to compare the data from Bertrand (1993), why his equation is very close to that of Eq. 5. Because vitrinite is missing in pre-Devonian sequences the author points out that no

universal calibration between the BR of migrabitumen and calculated VR can be suggested. Nevertheless, the new Eq. 5 should strictly be used in the case the thermal history is well known and heat flow determined to happen at normal geothermal orogenic conditions between temperatures of 100 to 350 °C. We present probably the best-calibrated VR/VlBR conversion for very specific heat flow conditions.

Comparing the correlation data of this study with other conversion equations (among others: Jacob & Hilmann, 1985; Robert, 1988; Jacob, 1989; Bertrand, 1990; Landis & Castaño, 1995; Bertrand & Malo, 2001) the different regression slopes are sedimentary basin type dependent and from basins with different hyperthermal heat flow conditions. The equation of Schönherr et. al. (2007) results from the data addition from two different geothermal settings studied by Landis and Castaño (1995), and Jacob (1989) and therefore probably better adapted for a general use in hyperthermal maturity studies when the thermal history of a basin is little known or the data base is small (e.g. Grobe et al., 2016; Waliczek et al., 2019, 2020). An important absent factor is stress in sedimentary basins ("pressure", Suárez-Ruiz et al., 2012).

6.3 Organic matter reflectance, clay mineral indices and paragenesis

In the low-grade diagenetic zone strong clay mineral composition heterogeneities are observed along a stratigraphic section in all studied areas (more than 3000 samples). Lithostartigraphic differences are prominent and a geothermal gradient trend difficult to determine. A thermal event can only be detected, if clays and mudstones are studied only (Frey, 1969), e.g. if the study is restricted to a certain formation (Frey, 1969, 1978, 1987a; Kisch, 1983; Krumm, 1984; Kralik et al., 1987). With the increase of sample numbers, it became evident that clay minerals allow recognize sedimentary clay mineral facies, palaeoclimatic, palaeooceanographic, early diagenetic and/or depositional environmental conditions (Brown, 1961; Strakhov, 1967; Grim, 1968; Krumm, 1969; Velde, 1977, 1985; Jones & Galán, 1988; Foscolos, 1990; Petschick et al., 1996; Coimbra et al., 2021). These primary influences need to be separated from the effects due to burial conditions (Krumm, 1977) and the detrital signals may also very prominently control the initial chemistry of chlorite (Krumm, 1969; Frey, 1969), illite, paragonite, mixed layer (Kulbicki & Millot, 1959; Weaver, 1967), and smectite (including Mg/Na/Ca endmembers).

The problems to discriminate different influencing factors on clay mineral chemistry and aggradation during syn-sedimentary burial diagenesis and diagenetic grade of metamorphism were illustrated by Merriman (2005). The procedure proposed allows to classify different basin types with the help of the clay mineral content (Merriman, 2005; García Romero et al., 2007; Bozkaya & Yalçin, 2010; Yalçin & Bozkaya, 2011), different series of clay mineral reactions (Schiffman & Staudigel, 1995; Merriman, 2002; Abad et al., 2003), and clay mineral habits and topologic assemblages (Bozkaya & Yalçin, 2000, 2004b; Bozkaya et al., 2007). This is best visualized in sections studied with large sample numbers (Bozkaya et al., 2002, 2007). Smectite gives a good indication for sedimentary facies (Merriman & Peacor, 1999).

Below a Kübler-Index (KI) of 1.0 Δ°2θ (boundary between low- and high-grade diagenesis, Fig. 5), KI values start to be more coherent with respect to temperature estimations and VR/VlBR (≈1.0%R_r). As shown, the variance decreases to more than half of the ΔKI (Fig. 11). Low-grade diagenesis between KI 1.6 to 1.2 Δ°2θ conditions lead to a strong decrease of around 50% of the **discrete smectite** amount. In the same KI range the amount of **IS-R0 (1Md)** decreases, but with no change in polytypism (Fig. 9), as has been shown within the Helvetic nappes (Wang, 1994; Wang et al., 1996) and Austroalpine nappes by an intensity decrease of the shifted smectite peak. Tri-smectite follows the same trend (Fig. 9). In the Helvetic domain discrete smectite disappears at 1.1 Δ°2θ (VR = 1.0%R_r), but is still present in the Northern Calcareous Alps until 0.85 Δ°2θ (Petschick, 1989). A discrete smectite stability limit at around 120 °C (Dunoyer De Segonzac, 1970; Brauckmann, 1984) is in accordance with the results of our study areas. At high-grade diagentic to anchizone grade **Ca-smectite** disappears also earlier (≈0.70 Δ°2θ) in the Helvetic than at ≈0.40 Δ°2θ in the Austroalpine units (Fig. 9). Ca-smectite is the most stable smecite type, as has been verified in an experimental bentonite study (Nguyen-Thanh et al., 2014). This corroborates earlier studies of Velde (1977), and Čičel and Novak (1977) having published field evidence for a large Ca-smectite stability range within marly clays. Within the diagenetic zone of the Lower Austroalpine, the single smectite type is found occasionally (while most samples do not have smectite or smectite mixed-layer).

The most accurate method to determine microstructural—textural differences, the electron microbeam techniques (Garcia Romero et al., 2021) were not applied for the field studies of the presented research. The thermal stability of smectites depend strongly on the distribution of octahedral cations (see discussion and references in Hoang-Minh et al., 2019, and Garcia Romero et al., 2021). This is important if Ca and much more evident if Mg in dolomitic rocks must be considered due to multiple cations position in the layer structure (Nguyen-Thanh et al.,

2017, 2021). The different smectite XRD results are discussed with caution.

IS-R1 (1M) starts to increase with the decrease in amount of IS-R0, and discrete smectite transforms continuously itself to IS-**R3** at the low- to high-grade diagenetic zone boundary. Results from the Helvetic domain published by Rahn (1994), and Wang (1994) are in line with observations from the Northern Calcareous Alps (Fereiro Mählmann, 1994). However, when looking at changes in interference geometry of reflections and peak shifts, amounts of mixed layer smectite of more than 15% (according to the method of Środoń, 1984) can be shown to still be present up to the diagenesis/anchizone boundary (Petschick, 1989) at fluid inclusion temperatures of 230 °C (Ferreiro Mählmann, 1994). Equal temperatures have also been modelled. The best fit (Ferreiro Mählmann, 2001) was obtained based on the smectite-illite model of Hillier et. al. (1995), the model calibration of which is based in a normal geothermal gradient basin study.

Using the "glycolation index" (Krumm, 1984) considerable smectite contents are still present in the low-grade anchizone and minor traces detected in the high-grade anchizone. In the Silvretta nappe and in the Lower Austroalpine intensity changes of the 10 Å-peak and FWHM allow to predict smectite interferences of lower than 5% (Moore & Reynolds, 1989), also the glycolation index shows still gradual changes (Wang, 1994; Ferreiro Mählmann, 2001). Most of the results in the Austroalpine domain are in disagrement with the generalised correlations from Velde (1977), Kisch (1987), Foscolos (1990), and Merriman & Peacor (1999) postulating an earlier consumption of the entire smectite during illite aggradation.

With the decrease of **tri-smectite/chlorite-smectite**, start to be diagnostic with increasing amounts of **corrensite** and **chlorite** at KI = 1.55 − 1.35 Δ°2θ (Fig. 9). The low content of tri-smectite/chlorite-smectite in the diagenetic zone is the result of the thermal overprint in the different tectonic settings. In early to late diagenesis of marine sediments contents are much higher (Krumm, 1969; Velde, 1985), prominent in deep basins (Petschick et al., 1996) and strongly reduced at low-grade diagenesis (Grim, 1968). According to Kübler et. al. (1979b) chlorite-smectite plus corrensite are facies indicators for Mg-rich sediments deposited in an evaporitic environment (Velde, 1985). In corresponding formations within the Austroalpine corrensite is detected at low-grade diagenesis (Krumm et al., 1988; Petschick, 1989). The main occurrences and highest amounts are observed in the high-grade diagenetic zone (see also Ferreiro Mählmann, 1994; Merriman & Peacor, 1999), but minor amounts of corrensite/chlorite are detected by XRD analyses in both tectonic units up to the high-grade anchizone.

In the Northern Calcareous Alps minor amounts of corrensite are sporadically found up to the low-grade anchizone (Petschick, 1989) and traces in a few samples within the high-grade anchizone. In the Rätikon area of the Northern Calcareous Alps a decrease in chlorite-smectite content was observed in the low-grade diagenetic zone, while it increases up to the anchizone and then disappears within a small range of anchizonal grade (Ferreiro Mählmann, 1994). The same, however less frequently, is observed for corrensite in the Helvetic domain (Wang, 1994) when compared to the Northern Calcareous Alps. This supports the observations by Kübler et. al. (1979b), and Merriman & Peacor (1999), based on which a reduction of chlorite-smectite and corrensite is postulated during burial diagenesis. Thermal induced reactions of low ordered Mg clay-minerals result in a progressive formation of corrensite and then chlorite. In both structural units the occurrence of corrensite is mostly restricted to Triassic rocks. Dependence from grade of diagenesis and an environmental/plaeoclimatic geochemical reason is suggested.

In the Helvetic domain first IS-R3 was detected at KI = 1.0 − 0.95 Δ°2θ (Fig. 9). With increasing grade of diagenesis 1M illite–smectite (IS-R1) is progressively replaced by IS-R3 or **$2M_1$ illite** and completely transformed approaching conditions of the anchizone. Concerning a possible metastable clay mineral assemblage during high-grade diagenesis and low-grade anchizone including vermiculite/chlorite-smectite (differentiated in most studies compiled for this study), IS-R1 (1M, illite/smectite mixed-layer type rectorite) and illite IS-R3, an ongoing debate is found in the literature and is here discussed based on the large data base presented. First, the reaction progress involving $1M_d - 1M - 2M_1$ illite polytypes related with IS-R0–IS-R1–IS-R3 is discussed, which is a steady progressive replacement of low-ordered to higher ordered sheet silicate structures (Fig. 9). The 1M, IS-R1-polytype does not represent an intermediate stage between $1M_d$ and $2M_1$, but is a continuous layer-by-layer replacement increasing the scheet silicate order and present at a specific diagenetic grade (e.g., Dong & Peacor, 1996; Bozkaya et al., 2012a). In the studied areas, replacement happens at KI = 1.0 to 0.33 Δ°2θ and VR 1.0%R_r to 3.80%R_{max} (Fig. 9) between ≈100 and 250 °C (Fig. 10) in agreement with observed IS-R relations coexisting at diagenetic grade in various proportions showing a lack of equilibrium (López-Munguira & Nieto, 2000). This is observed in our studies especially in the Northern

Calcareous Alps and sporadically in the northern Helvetic domain.

The occurrence of chlorite-smectite in otherwise anchizonal settings should be considered as the result of a retrograde reaction rather than of an authigenic formation (e.g. Hoffman & Hower 1979; Nieto et al., 1996; Abad et al., 2003; Bozkaya et al., 2012b). The coexisting chlorite-smectite (also vermiculite) is postulated to be incompatible with anchizone metamorphic conditions (e.g., Nieto et al., 1994, 2005; Bozkaya & Yalçin, 2004b). In the present study neither detrital biotite and chlorite-mica stacks from transformed clastic mica (Piqué & Wybrecht, 1987; Bevins & Robinson, 1988; Bozkaya et al., 2002) nor aberrant *b* parameter values (Merriman & Peacor, 1999; Abad et al., 2003) were found in thin sections or by XRD analysis. Traces of coexisting types of smectite in the achizone need to be explained differently.

At least the reaction progress involving $1M_d - 1M - 2M_1$ illite polytypes in the Helvetic domain agrees with the generalised correlations by Velde (1977), Kisch (1987), Foscolos (1990), and Merriman & Peacor (1999). However, differences of the first and last appearance with increasing grade of diagenesis exist (Fig. 9) for the Austroalpine nappes (Petschick, 1989; Ferreiro Mählmann, 1994). Based on the compilation of this study, one reason may be put forward to explain the contrasting results: the early disappearance of low-order clay mineral phases in the Helvetic domain compared to the Northern Calcareous Alps is explained with the slightly higher heat flow during diagenesis (leading to an acceleration of the reaction progress). Clay minerals with a fast reaction rate therefore reached a higher level of order than at normal geothermal gradient conditions as encountered for the Northern Calcareous Alps. Thus, transformations with a sluggish reaction process show an apparently larger stability range at lower heat flow determined. Evidently, a fast decrease in smectite content from IS to ISII is verified and the last minor amounts (Ca-smectite) decrease much slower compared to the increase in metamorphism (Środoń & Eberl, 1984) due to the deceleration of smectite reactivity. Contrasting to that, in the Rätikon Mountains, the Silvretta nappe and the Lower Austroalpine these minerals have not been detected at the same grade of diagenesis. A normal geothermal history, but stable maximum conditions during a long period allowed to equilibrate aggradation to the next level of ordering. Then, with increasing time chemical and textural order will not increase. Same results are found in nappes with a heating period of > 5, 10 and 20 myr.

The occurrence of **kaolinite** and **glauconite** in the samples with KI = 1.6 to 0.45 Δ°2θ confirms a diagenetic formation and points to their use as index minerals. The upper kaolinite and glauconite stability limit found in the Helvetic domain confirms the correlations published by Kisch (1987), Merriman & Peacor (1999), and Merriman & Frey (1999). Kaolinite disappears by illitisation and chloritisation before conditions of the anchizone are reached (< 200 °C), unless the environment is Al-rich (Środoń et al., 2006). However, kaolinite may persist in carbonate rocks, sedimentary rocks rich in organic matter, and volcaniclastic rocks until the upper diagenesis boundary < 230 °C (Kisch, 1987; Ferreiro Mählmann, 1994). Kaolinitisation of detrital plagioclase, orthoclase, and mica in a Ca-rich environment as enhanced by albitisation of plagioclase and illitisation (sericitisation) of K/Na-feldspars leads to significant potential for the kaolinite formation that is typical in low-grade diagenesis (Merriman & Peacor, 1999). Such kaolinite progressively disappears during high-grade diagenesis (Maison et al., 2019). In the sediment formations studied kaolinite amounts decrease considerably between 0.7 and 0.45 Δ°2θ (Fig. 9). Glauconite disappears within a small range of KI values close to the diagenesis/anchizone boundary.

In the same range of KI values, between 0.7 and 0.45 Δ°2θ, **pyrophyllite** is found in samples together with kaolinite. In smectite rich samples with a high amount of illite and chlorite the detected pyrophyllite tends to appear at lower KI and higher VR values. At high water activity the transformation can be shifted to 270 °C (Frey, 1987a). Thus, kaolinite transformation to pyrophyllite at higher grade can be indicative in many studies for hydrothermal pulses (Deer et al., 1962; Will et al., 2016; Zhang & Zhang, 2020). Hydrothermally altered rocks were excluded in the study and therefore the first apearence in different areas and different rock formations is attributed to burial and orogenic conditions. Missing a sharp isograde, this can be explained with different water activities dependent from the amount of OH bearing phases, may be specifically smectite. A different initial geochemical environment in the Austroalpine basins did not generate any Al- and/or Fe-rich sedimentary educts. Consequently, kaolinite and glauconite where not formed during sedimentation and could not crystallise during diagenesis (Fig. 9). Thus, also the neoformation of pyrophyllite and stilpnomelane during increasing diagenetic grade and anchimetamorphism could not be afforded.

In the Helvetic nappes alredy in the high-grade diagenetic zone **stilpnomelane** was observed by Breitschmid (1982) at 210 °C and 1.6 kbar. Also, glauconite is consumed by sliding equilibria (Frey, 1987b) but as shown in the present compilation (Fig. 9) in a narrower temperature range (210 to 230 °C) than the kaolinite–pyrophyllite

reaction. In New Caledonia stilpnomelane formation is not linked to glauconite (Frey et al., 1973), but according to Li et. al. (2002) to a reaction from Fe-chlorite + hematite + K-white mica (ferri-illite/muscovite) + quartz, as deduced from the Fe-stilpnomelane occurrences in the high-grade anchizone and epizone (Potel et al., 2006; Potel, 2007). The same reaction is assumed for the occurrences in the Lower Austroalpine, where first stilpnomelane was detected at the low- to high-grade anchizone boundary and was found to be stable into greenschist facies. The stilpnomelane-out isograde was not mappable because it is located outside the studied areas in neighbouring structural units (Niggli & Zwart, 1973; Frey, 1987b; Frey & Ferreiro Mählmann, 1999). In the Lower Austroalpine and Platta nappe Fe-chlorite, hematite, ferri-illite/muscovite and quartz are abundantly found in radiolarites, ophiolitic rocks or pelites with oceanic crust detritus. In New Caledonia (ophiolitic setting) the same is observed and a stilpnomelane-in isograd assumed to be determined at the low-/high-grade anchizone boundary at temperatures of 265 ± 10 °C. In this case a comparison with the Helvetic domain is not considered due to unequal mineral reaction conditions.

The occurrence of **paragonite** is thought to be restricted to epizonal conditions above 300 °C (Frey, 1987a; Kisch, 1987), but it is a frequent phase at low geotherms in the sub-blueschist and blueshist facies (Dietrich, 1956; Karpova, 1966, cited in Kisch, 1983; Black, 1975; Kramm, 1978; Potdevin & Caron, 1986). Paragonite was considered an important part in the clay mineral fraction of ophiolite sedimentary and magmatic rocks (Dietrich, 1966, 1969; Black, 1975; Frey, 1978). XRD peaks between illite (002) and paragonite (002) where initially interpreted as mixed-layered interstratifications (Frey, 1978; Seidel, 1978; Merriman & Roberts, 1985). After having shown chemical limitations based on the miscibility gap describrd by Eugster et. al. (1972) to a possible mixed-layer compositional structure (Guidotti, 1984) it was indirectly evidenced by Livi et. al. (1997) that the recorded XRD peaks in-between illite and paragonite refer to domains of Na- and K-mica sheet structures. These XRD peaks moreover were interpreated as a metastable disordered compositionally intermediate (DCI) phase (Jiang & Peacor, 1993). The"mixed paragonite/muscovite" domain model was thought to be the most frequent type (Robinson & Merriman, 1999), and Livi et. al. (2008) gave good additional arguments. Without a TEM/HRTEM evidence, the nature of these phases cannot be determined allone with XRD (Livi et al., 1997, see also Giorgetti et al., 2003; Árkai et al., 2004). Independent of this discussion, paragonite s.l. includes all forms discussed. Paragonite s.l. is observed in the highest-grade diagenetic zone in New Caledonia, in the low-grade anchizone in the lower structural nappes of the Austroalpine and in the Piemont-Liguria Ocean nappe of the Platta nappe, and sporadically detected in the high-grade anchizone of the Helvetic nappes in formations of an open marine basin. The lowest grade occurrence is found in the diagnetic zone at temperatures around 200 °C, same tempratures are reviewed by Livi et. al. (2008). The availability of Na is considered to have a major influence on paragonite formation, however the paragenesis with blueschist facies minerals in New Caledonia and in the lower structural units of the Platta nappe also suggest the context of an early subduction event overprinted by a normal thermal orogenic event (Dietrich, 1969; Ferreiro Mählmann, 2001; Potel et al., 2006).

Due to the compilation result of this study, paragonite in the clay mineral fraction is considered a fingerprint pointing to a subduction history, e.g. found for deeply buried and accreted units of distal continental nappes (lower structural Austroalpine nappes) close to the continent-ocean transition and the ophiolite Platta nappe. The subsequent orogenic event caused a pressure decrease at same temperatures shifting the gradient to normal geothermal conditions (Frey & Ferreiro Mählmann, 1999; Oberhänsli et al., 2004). OM and most clay minerals then adapted to a new structural and chemical equilibrium during this second event (D2, see Sect. 3.2). Adaption is more advanced in the Lower Autroalpine and Platta nappe due to the longer time span of metamorphism than during the shorter event in New Caledonia. In New Caledonia even the illite *b* parameter still reflects the former subduction history. **Epidote** is discussed in the same way in these units. Epidote in the ophiolite Platta nappe is not considered. In the Platta nappe it was formed in the assemblage with prehnite, chlorite, albite during an oceanic metamorphism and later with pumpellyite and actinolite (some clinozoisite) again during subduction and Alpine metamorphism (Ferreiro Mählmann, 1994, 2001; Ferreiro Mählmann & Giger, 2012).

Low temperature albite and **microcline** were determined by XRD in 152 dolomitic-limestones, shales, and slates of the anchi- and epizone. In clayey and marly sandstones or silty marls and shales it is not possible to differentiate between its authigenic or detrital formation. In 25 thin sections and TEM analysis, sediment rock inclusions indicate an authigenic formation partly approaching idiomorphic habitus, but mostly an amoeboid to sub-idiomorphic habitus is typical. In some formations Peters (1963), and Kürmann (1993) have determined both minerals and suggested an authigenic origin. In the present compilation both were assigned to higher grade in the studied areas, microcline occurred in the highest grade of the diagenetic zone (Fig. 9) and albite in the high-grade anchizone. The results confirmed previous analyses of

Wenk & Keller (1969), and Trommsdorff (1983a, 1983b). In the diagenesis albite typically preserves a detrital core (Füchtbauer, 1950). By XRD high-albite is sometimes detected. The tendency to higher An-content in electron microprobe analyses on the same 25 samples is related to the small grain size, the volatile nature of Na_2O during analysis and the carbonate bearing clay or marl matrix captured by the electron beam (mixed analysis). In the anchizone, rounded (i.e., detrital) orthoclase cores may show microcline overgrowth rims (Lippmann & Savascin, 1969). As shown by Brauckmann (1984) and in line with the present study (Fig. 9), microcline occurs earlier than albite with increasing metamorphic grade.

In the epizone of the Austroalpine microcline dominates, while in the South Penninic albite-oligoclase is the dominant phase (Wenk, 1958; 1962). In the epizonal southern Platta nappe the peristerite miscibility gap (An_2 to An_{10}) was detected (thin sections), e.g. low albite and orthoclase in agreement with Wenk (1962). The gap is commonly determined by optical microscopy within greenschist facies rocks (Orville, 1974; Smith & Brown, 1988), but in Na-rich pelites the gap may already occur at low-grade epizonal conditions (i.e., sub-greenschist prehnite-pumpellyite facies according to Trommsdorff and Evans 1974; Trommsdorff & Dietrich 1980, see also Dietrich 1956). The earlier occurrence of feldspars in the Lower Austroalpine than in the Northern Calcareous Alps and in the Helvetic domain is again related to the longer duration of crystallisation at steady state conditions.

7 Conclusion

Equations 1c, 2, 3, 5 and 6 are based on a large dataset controlled by T, P, and t of orogenic heat flow and metamorphic conditions. These controlling factors should allow that different clay mineral and organic matter indices are used to determine the degree of orogenic diagenesis to incipient metamorphism at normal heat flow condition.

Based on a range of nappe stacks within orogenic mountain belt settings, it is proposed that correlation results can also be applied to other orogenic structural units within a similar geodynamic setting and history (Alpine Type Orogenes, Bucher & Frey, 1994) to make predictions on organic matter maturity, clay mineral reaction progress and formation, as well as estimations on temperature and pressure. Restricted to normal heat-flow case studies (orogenic settings) the results may better help to understand differences to sedimentary burial as also subduction related thermal maturity and clay mineral genesis.

Hyperthermal alteration or contact metamorphism can easily be differentiated by their VR vs. KI data if compared to the findings shown for normal thermal geodynamic P–t evolutions, because VlBR reacts faster to very short temperature pulses than VR. As follows equilibrium between VlBR, VR and the KI and CM paragenesis needs some myr to be reached. A time span < 5 my is not sufficient, while equilibration may be attained in tectonic units with a diagenetic to metamorphic period of 5 to 10 myr duration. For durations > 10 my VR will still increase very moderately, but also the sharpness ratio of the illite 10-Å peak is probably able to further aggradate. Thus, without any significant change in VR (i.e. steady state approached) the KI (HWHM) will decrease.

During low-grade diagenetic conditions, illitisation is progressing very fast (< 5 my) but decreases within high-grade diagenetic conditions, and the last 10% of smectite transforms very sluggishly within the anchizone, especially Ca-smectite in calcite- or dolomite-rich rocks. In the low-grade diagenetic zone, smectite transformation is a very sensible index for the determination of the diagenetic grade, however the effects of syn-sedimentary facies, meteoric and low-temperature hydrothermal alterations need to be discriminated.

In the high-grade diagenetic zone to high-grade anchizone VlBR is a diagnostic method. If vitrinite is missing VlB is an excellent alternative to determine maturity, if virtinite is present it may be used as an additional controlling parameter. We agree with the statement by Burnham (2019) that reflectance measurements from vitrinite should be preferred in rocks containing predominantly humic OM when calibrating paleothermal models. The variance and the standard deviation of the mean VR value have a higher significance than the scattering value of a corresponding VlBR.

The correlation of illite/muscovite *b* parameter with fluid inclusion, organic matter and clay mineral data allows to precisely determine the grade of diagenesis and incipient metamorphism from high-grade diagenesis to low-grade epizone. For the low-grade diagenetic zone, a much higher sample number is needed for the discrimination techniques used. The *b* parameter may still preserve information of a former HP event prior to orogenic collisional diagenesis and metamorphism. In New Caledonia the *b* parameter is linked to the meta-stable blueschist facies assemblage and was not re-equilibrated during the subsequent sub-greenschist facies metamorphism. Thus, the *b* parameter can help to determine an earlier lower temperature event if temperatures were not considerable higher during a second thermal phase.

Differences in index correlations and first appearances of clay- and metamorphic minerals compared to standard

textbook literature and reviews can be explained by the focus on a majority of existing studies on very low-grade metamorphism being related to hydrocarbon prospection and geothermal sites of hyperthermal settings. The here included datasets from the Helvetic and Austroalpine domain (European Alps) focus on areas dominated by normal geothermal orogenic diagenesis to very low-grade metamorphism.

Orogenic diagenesis after sedimentary burial categorically changes the relationships among organic matter indices known from sedimentary basins. The preservation of optical characteristics at higher maturity compared to sedimentary basins is probably related to the higher lithostatic pressure and conservation of hydrogen in the liptinite macerals and solid bitumen. Thus, the correlation between VR and VlBR shows lower VlB values than observed in sedimentary basins.

Considering VR maturity and temperature models, pure temperature dependent models are furthest away from the here presented calibration. Empirical time–temperature models (TTI) are closer to the measured data, while numerical kinetic-based models show an even better fit to the calibration (EASY%R_o). For orogenic diagenesis the time–temperature–pressure model (Dalla Torre et al., 1997) generated the best fit. As known from experimental studies the pressure retardation effect on reflectance decreases with increasing maturity and longer maturation periods. In the P–T–t model this is not respected at incipient metamorphism, probably leading to discrepant results to FI and reaction iso-grades. Future model developments must integrate a better pressure factor.

Abbreviations

AD	Alpine deformation
b	K-white mica *b* cell dimension
CIS	Crystallinity index standards
CM	Clay minerals
FI	Fluid inclusion
FIT	Fluid inclusion temperature
FT	Fission track
FWHM	Full width at half maximum of the 10 Å illite peak intensity
HP	High pressure
HT	High temperature
I/Sm	Illite/smectite
I/Sm-ml	Illite/smectite mixed layer
KI	Kübler-Index
OM	Organic matter
SB	Solid bitumen
SBR	Solid bitumen reflectance
VlBR	Vitrinite like solid bitumen reflectance
VLGM	Very low-grade metamorphic
VR	Vitrinite reflectance
XRD	X-ray diffraction
$\%R_r$	% of random reflectance under monochromatic white light
$\%R_{max}$	% of maximum reflectance at polarised light

Acknowledgements

Prof. Hans Krumm at the 1991 Alps excursion. He was the first field-oriented petrologist in recognizing the potential of KI/VR mapping in nappe tectonic settings (Photograph: R. Ferreiro Mählmann).

This study was dedicated to Professor Hans Krumm at his 90th birthday and presented at the 4th Frey-Kübler Symposium at Eroclay 2019 in Paris. He sadly passed away on 27.01.2021. RFM, RP and MR have collaborated as scholars intensively with him and LNT and SP feel to be scientific grandsons. He was an excellent teacher of great humaneness. We like to thank Dr. Susanne Theodora Schmidt (Universities Basel and Geneva, Switzerland) for continuous help in microprobe analyses and interpretation. Her peacefull death after long terminal illness on 24.05.2023 left us wanting without a carismatic collaborator, friend, and powerful woman. We are indepted to Prof. Christoph Spötl (University Innsbruck, Austria) for TEM measurements on feldspars. Very valuable help was provided by Prof. Rudolf Hänny (University Basel) who made accessible the scientific legacy of Martin Frey, besides many years after his retirement. We like to thank Prof. Jan Środoń (Krakov) for the stimulating discussion at Euroclay 2019 and claiming to publish the study and to Prof. Peter Árkai (Budapest) motivating RFM to be persistent in compiling data. RFM likes to point out that it was not possible to get scientific funding for compilation studies when moving from Basel to Darmstadt but benefited from financial help of the "Fonds zur Förderung des akademischen Nachwuchses" of the Univerity Basel during the time he worked at both universities and in Basel by the travel grants (Reisefonds der Universität Basel) until 2003 as representative of Martin Frey having passed away in 2000, and the help by the Freiwillige Akademische Gesellschaft (FAG) Basel. Very important was the constructive review of Prof. Fernando Nieto (Granada) and we appreciate the work done by an anonymous reviewer.

Author contributions
All authors have approved the submitted version and contributed to the conception of the study. RFM was mainly responsible for the organic petrological part. RFM with RP and LNT for the clay mineral results and correlation presentations. Data acquisition and analyses from the Austroalpine units were compiled by RFM and RP, from the Helvetic units by MR and SP, and from New Caledonia by SP. New unpublished data was included by RFM. MR substantially revised the manuscript.

Funding
Open Access funding enabled and organized by Projekt DEAL. The compilation project did not found funding.

Availability of data and materials
New data from RFM and LNT during this study are included in this published article in tables. Older data are compiled from the PhD studies of MR, RP, RFM and SP and from PhD studies and publications cited in the text. Despite that, the datasets used and/or analysed during the current study are available from the corresponding author on reasonable request.

Declarations

Ethics approval and consent to participate
The study does not use research involving human participants, human material, or human data.

Consent for publication
Not applicable.

Competing interests
The authors declare that they have no competing interests.

Author details
[1]Technical and Low Temperature Petrology, Technische Univ. Darmstadt, 64287 Darmstadt, Germany. [2]Swiss Federal Nuclear Safety Inspectorate, 5200 Brugg, Switzerland. [3]Basins-Reservoirs-Resources (B2R) EA 7511, UniLaSalle, 60026 Beauvais, France. [4]Department of Geosciences, Goethe University, 60438 Frankfurt am Main, Germany.

Received: 20 December 2023 Accepted: 21 April 2024
Published online: 12 September 2024

References

Abad, I., Nieto, F., & Gutiérrez-Alonso, G. (2003). Textural and chemical changes in slate-forming phyllosilicates across the external–internal zones transition in the lowgrade metamorphic belt of the NW Iberian Variscan Chain. *Schweizerische Mineralogische und Petrographische Mitteilungen, 83*(1), 63–80.

Abart, R., & Ramseyer, K. (2002). Deformation induced quartz-fluid oxygen isotope exchange during low-grade metamorphism: An example from the Glarus thrust, E Switzerland. *Schweizerische Mineralogische und Petrographische Mitteilungen, 82*(2), 273–290.

Abraham, H. (1918). *Asphalts and allied substances: Their occurrence, modes of production, uses in the arts and methods of testing* (1st ed., p. 606). D. Van Nostrand Company Inc.

Achtnich, T. (1982). Die Jurabreccien der Eisenspitze. *Geologisch Paläontologische Mitteilungen Universität Innsbruck, 12*(2), 41–70.

Aitchison, J. C., Clarke, G. L., Meffre, S., & Cluzel, D. (1995). Eocene arc-continent collision in New Caledonia and implications for regional southwest Pacific tectonic evolution. *Geology, 23*(2), 161–164.

Akker, I. V., Berger, A., Zwingmann, H., Todd, A., Schrank, C. E., Jones, M. W. M., Kewish, C. M., Schmid, T. C., & Herwegh, M. (2021). Structural and chemical resetting processes in white mica and their effect on K-Ar data during low temperature metamorphism. *Tectonophysics, 800*, 20. https://doi.org/10.1016/j.tecto.2020.228708.

Allen, Ph. A., & Allen, J. R. (2005). *Basin analysis: Principles and applications* (p. 560). Blackwell.

Alpern, B., & Lemos De Sousa, M. J. (1970). Sur le pouvoir reflecteur de la vitrinite et de la fusinite des houilles. *Comptes rendus de l'Académie des sciences, Paris, Série D, 271*, 956–959.

Altaner, S. P., Hower, J., Whitney, G., & Aronson, J. L. (1984). Model for K-bentonite formation: Evidence from zoned K-bentonites in the disturbed belt, Montana. *Geology, 12*(7), 412–415.

Ampferer, O. (1902). Grundzüge der Geologie des Mieminger Gebirges. *Verhandlungen der k. k. geologischen Reichsanstalt, Wien, 1912*, 170–180.

Ampferer, O. (1914). Über den Bau der westlichen Lechtaler Alpen. *Jahrbuch der k.k. geologischen Reichsanstalt, Wien, 64*, 307–326.

Ampferer, O. (1940). Probleme der Arosa Zone im Rätikongebirge. *Mitteilungen der geologischen Gesellschaft, Wien, 33*, 97–112.

Ampferer, O., & Hammer, W. (1911). Geologischer Querschnitt durch die Ostalpen vom Allgäu bis zum Gardasee. *Jahrbuch der k.k. geologischen Reichsanstalt, Wien, 61*, 531–645.

Apps, G. M., Peel, F., & Elliott, T. (2004). The structural setting and palaeogeographical evolution of the Gres d'Annot Basin. Deep-water sedimentation in the Alpine Basin of SE France; new perspectives on the Gres d'Annot and related systems. *Geological Society London, Special Publication, 221*, 65–96.

Aprahamian, J. (1974). La cristallinite de l'illite et les minéraux argileux en bordure des massifs cristallins externes de Belledonné et du Pelvoux (variations et relations possible avec des evénements tectoniques et métamorphiques alpins). *Géologie Alpine, 50*, 5–15.

Aprahamian, J. (1988). Cartographie du métamorphisme faible à trés faible dans les Alpes françaises externes par l'utilisation de la cristallinité de l'illite. *Geodinamica Acta, 2*(1), 25–32.

Aprahamian, J., Pairis, B., & Pairis, J. L. (1975). Nature des minéraux argileux et cristallinité des illites dans le massif de Platé et le revers occidental des Aiguilles Rouges: Implications possibles d'un point de vue sédimentaire, structural, et métamorphique. *Annales du Centre Université de Savoie, II*, 95–119.

Árkai, P. (1991). Chlorite crystallinity: An empirical approach and correlation with illite crystallinity, coal rank and mineral facies as exemplified by Palaeozoic and Mesozoic rocks of northeast Hungary. *Journal of Metamorphic Geology, 9*, 723–734.

Árkai, P., Abad, I., Nieto, F., Németh, T., Horváth, P., Kis, V., Judik, K., & Jiménez-Millán, J. (2012). Retrograde alteration of phyllosilicates in low-grade metapelites: A case study from the Szendrô Paleozoic, NE-Hungary. *Swiss Journal of Geosciences, 105*(2), 263–282. https://doi.org/10.1007/s00015-012-0097-1

Árkai, P., Balogh, K., & Frey, M. (1997). The effect of tectonic strain on crystallinity, apparent mean crystallite size and lattice strain of phyllosilicates in low-temperature metamorphic rocks. A case study from the Glarus overthrust, Switzerland. *Schweizerische Mineralogische und Petrologische Mitteilungen, 77*(1), 27–40.

Árkai, P., Ferreiro Mählmann, R., Suchý, V., Balogh, K., Sykorova, J., & Frey, M. (2002). Possible effects of tectonic shear strain on phyllosilicates: A case study from the Kanderesteg area, Helvetic domain, Central Alps, Switzerland. *Schweizerische Mineralogische und Petrologische Mitteilungen, 82*(2), 273–290.

Árkai, P., Livi, K. J. T., Frey, M., Brukner-Wein, A., & Sajgó, Cs. (2004). White micas with mixed interlayer occupancy: A possible cause of pitfalls in applying illite Kübler index "crystallinity" for the determination of metamorphic grade. *European Journal of Mineralogy, 16*, 469–482.

ASTM D7708-23, American Society for Testing and Materials. (2015). Standard test method for microscopical determination of the reflectance of vitrinite dispersed in sedimentary rocks. *Annual book of ASTM standards: Petroleum products, lubricants, and fossil fuels; gaseous fuels; coal and coke,* sec. 5, v. 5.06. ASTM International. Retrieved February 14, 2016, from http://www.astm.org/Standards/D7708.htm

ASTM D7708-14, American Society for Testing and Materials. (2014). *Standard test method for microscopical determination of the reflectance of vitrinite dispersed in sedimentary rocks*. ASTM International. https://doi.org/10.1520/D7708-14

Bailey, W. (1982). Nomenclature for regular interstratifications. *Clays and Clay Minerals, 30*, 76–78.

Balling, N. P. (1985). Thermal structure of the lithosphere beneath the Norwegian-Danish basin and the southern baltic shield: A major transition zone. *Terra Cognita, 5*, 377–378.

Barféty, J.-C., Gidon, M., Lemoine, M., & Mouterde, R. (1979). Tectonique synsédimentaire liasique dans les massifs cristallins de la zone externe des Alpes occidentales françaises: La faille du col d'Ornon. *Comptes Rendus de l'Académie des Sciences Paris, 289*, 1207–1210.

Barker, C. E. (1988). Geothermics of petroleum systems: Implications of the stabilization of kerogen thermal maturation after a geologically brief heating duration at peak temperature. US geological survey bulletin. In L. B. Magoon (Ed.), *Petroleum systems of the United States* (Vol. 1870, pp. 26–29). U.S. Geological Survey.

Barker, C. E., & Pawlewicz, M. J. (1993). An empirical determination of the minimum number of measurements needed to estimate the mean random vitrinite reflectance of disseminated organic matter. *Organic Geochemistry, 20*, 643–651. https://doi.org/10.1016/0146-6380(93)90050-L

Barker, C.E., & Pawlewicz, M.J. (1994). Calculation of vitrinite reflectance from thermal histories and peak temperatures. In Mukhopadhyay, P.K., & Dow, W.G. (Eds.). *Vitrinite reflectance as a maturity parameter, applications and limitations*. American Chemical Society Symposium Series, 570 (pp. 216–229).

Bell, T. H., & Brothers, R. N. (1985). Development of P-T prograde and P-retrograde, T-prograde isogradic surfaces during blueschist to eclogite regional deformation/metamorphism in New Caledonia, as indicated by progressively developed porphyroblast microstructures. *Journal of Metamorphic Geology, 3*(1), 59–78.

Belmar, M., & Morata, D. (2005). Nature and P-T-t constraints of very low-grade metamorphism in the Triassic-Jurassic basins, Coastal Range, central Chile. *Andean Geology (Revista Geológica de Chile), 32*(2), 189–205.

Belmar, M., Schmidt, S.Th., Ferreiro Mählmann, R., Mullis, J., Stern, W. B., & Frey, M. (2002). Diagenesis, low-grade and contact metamorphism in the Triassic-Jurassic of the Vichuquén-Tilicura and Hualacén Gualleco basins, Coastal Range of Chile. *Schweizerische Mineralogische und Petrologische Mitteilungen, 82*(2), 375–392.

Berger, G., Lacharpagne, J. C., Velde, B., Beaufort, D., & Lanson, B. (1997). Kinetic constraints on illitization reactions and the effects of organic diagenesis in sandstone/shale sequences. *Applied Geochemistry, 12*(1), 23–35. https://doi.org/10.1016/S0883-2927(1096)00051-00050

Bertrand, R. (1990). Correlations among the reflectances of vitrinite, chitinozoans, graptolites and scolecodonts. *Organic Geochemistry, 15*, 565–574. https://doi.org/10.1016/0146-6380(90)90102-6

Bertrand, R. (1993). Standardization of solid bitumen reflectance to vitrinite in some Paleozoic sequences of Canada. *Energy Sources, 15*, 269–287. https://doi.org/10.1080/00908319308909027

Bertrand, R., & Héroux, Y. (1987). Chitinozoan, graptolite, and scolecodont reflectance as an alternative to vitrinite and pyrobitumen reflectance in Ordovician and Silurian strata, Anticosti Island, Quebec, Canada. *American Association of Petroleum Geologists Bulletin, 71*, 951–957.

Bertrand, R., & Malo, M. (2001). Source rock analysis, thermal maturation and hydrocarbon generation in the Siluro-Devonian rocks of the Gaspé Belt basin, Canada. *Bulletin of Canadian Petroleum Geology, 49*, 238–261. https://doi.org/10.2113/49.2.238

Bertrand, R., & Malo, M. (2012). Dispersed organic matter reflectance and thermal maturation in four hydrocarbon exploration wells in the Hudson Bay Basin: Regional implications. *Geological Survey of Canada, Open File, 7066*, 54. https://doi.org/10.4095/289709

Bevins, R. E., & Robinson, D. (1988). Low grade metamorphism of the Welsh Basin Lower Palaeozoic succession: An example of diastathermal metamorphism. *Journal of the Geological Society London, 145*, 363–366.

Black, P. M. (1974). Oxygen isotope study of metamorphic rocks from Ouégoa District, New Caledonia. *Contributions to Mineralogy and Petrology, 47*, 197–206.

Black, P. M. (1975). Mineralogy of New Caledonia metamorphic rocks. IV. Sheet silicates from Ouégoa district. *Contributions to Mineralogy and Petrology, 49*, 269–284.

Boles, J. R., & Franks, S. G. (1979). Clay diagenesis in Wilcox sandstones of Southwest Texas; implications of smectite diagenesis on sandstone cementation. *Journal of Sedimentary Research, 49*(1), 55–70.

Bostick, N. H., Cashman, S. M., McCulloh, T. H., & Waddell, C. T. (1978). Gradients of vitrinite reflectance and present temperature in the Los Angeles and Ventura basins, California. In Oltz (Ed.), *Symposium in geochemistry: Low temperature metamorphism of kerogen and clay minerals* (Vol. 1979, pp. 65–96). Society for Sedimentary Geology, SEPM Pacific Section.

Bozkaya, Ö., & Yalçin, H. (2000). Very low grade metamorphism of Upper Paleozoic-Lower Mesozoic sedimentary rocks related to burial and thrusting in the central Taurus belt, Konya, Turkey. *International Geology Review, 42*(4), 353–367.

Bozkaya, Ö., & Yalcin, H. (2004a). Diagenesis and very low-grade metamorphism of the Antalya unit: Mineralogical evidence of Triassic rifting, Antalya-Gazipaşa, central Taurus belt, Turkey. *Journal of Asian Earth Sciences, 25*, 109–119.

Bozkaya, Ö., & Yalcin, H. (2004b). Diagenetic to low-grade metamorphic evolution of clay mineral assemblages in Palaeozoic to early Mesozoic rocks of the Eastern Taurides, Turkey. *Clay Minerals, 39*(4), 481–500.

Bozkaya, Ö., & Yalçın, H. (2010). Geochemistry of mixed-layer illite-smectites from an extensional basin, Antalya unit, Southwestern Turkey. *Clays and Clay Minerals, 58*(5), 644–666.

Bozkaya, Ö., Yalçin, H., Başibüyük, Z., & Bozkaya, G. (2007). Metamorphic-hosted pyrophyllite and dickite occurrences from the hydrous Al-silicate deposits of the Malatya-Pütürge region, central eastern Anatolia, Turkey. *Clays and Clay Minerals, 55*(4), 423–442.

Bozkaya, Ö., Yalçin, H., & Göncüoğlu, M. C. (2002). Mineralogical and organic responses to stratigraphic irregularities: An example from the Lower Paleozoic very low-grade metamorphic units of the Eastern Taurus Autochthon, Turkey. *Schweizerische Mineralogische und Petrologische Mitteilungen, 82*(2), 355–373.

Bozkaya, Ö., Yalçin, H., & Göncüoğlu, M. C. (2012a). Diagenetic and very low-grade metamorphic characteristics of the Palaeozoic series of the Istanbul Terrane (NW Turkey). *Swiss Journal of Geosciences, 105*(2), 183–202.

Bozkaya, Ö., Yalçin, H., & Göncüoğlu, M. C. (2012b). Mineralogic evidences of a mid-Paleozoic tectono-thermal event in the Zonguldak Terrane, NW Turkey: Implications for the dynamics of some Gondwana-derived terranes during the closure of the Rheic Ocean. *Canadian Journal of Earth Sciences, 49*, 559–575. https://doi.org/10.1139/E11-076

Brandon, M. T., Roden-Tice, M. K., & Garver, J. I. (1998). Late Cenozoic exhumation of the Cascadia accretionary wedge in the Olympic Mountains, northwest Washington State. *Geological Society of America Bulletin, 110*(8), 985–1009.

Brauckmann, F. J. (1984). Hochdiagenese im Muschelkalk der Massive von Bramsche und Vlotho. *Bochumer Geologische und Geotechnische Arbeiten, 14*, 1–195.

Breitschmid, A. (1982). Diagenese und schwache Metamorphose in den sedimentären Abfolgen der Zentralschweizer Alpen (Vierwaldstätter See, Urirotstock). *Eclogae Geologicae Helvetiae, 75*, 331–380.

Brothers, R. N. (1970). Lawsonite–albite schists from northernmost New Caledonia. *Contributions to Mineralogy and Petrology, 25*, 185–202.

Brothers, R. N., & Black, N. C. (1973). Tertiary plate tectonics and high-pressure metamorphism in New Caledonia. *Tectonophysics, 17*, 337–358.

Brown, G. (1961). *The X-ray identification and crystal structure of clay minerals* (p. 544). Mineral Society.

Bucher, K., & Frey, M. (1994). *Petrogenesis of metamorphic rocks* (6th ed., p. 318). Springer-Verlag.

Bürgisser, J. (1998). *Deformation in foreland basins of the Western Alps (Pelvoux massif, SE France); significance for the development of the Alpine arc* (p. 151). Unpublished Ph.D. thesis, ETH Zürich.

Burkhard, J. M. (1987). Ore Minerals and Geochemistry in the Serpentinites of the Eastern Central Alps (Davos to the Val Malenco) compared to occurrences in the Klamath Mountains (California and Oregon). *Heidelberger Geowissenschaftliche Abhandlungen, 12*, p. 345.

Burnham, A. K. (2019). Kinetic models of vitrinite, kerogen, and bitumen reflectance. *Organic Geochemistry, 131*, 50–59. https://doi.org/10.1016/j.orggeochem.2019.03.007

Butler, R. W. H. (1989). The influence of pre-existing basin structure on thrust system evolution in Western Alps. *Geological Society London, Special Publications, 44*, 105–122.

Cardott, B., Landis, Ch. R., & Curtis, M. E. (2015). Post-oil solid bitumen network in the Woodford Shale, USA—A potential primary migration pathway. *International Journal of Coal Geology, 139*, 106–113. https://doi.org/10.1016/j.coal.2014.08.012

Caron, M., Doessegger, R., Steiger, R., & Trümpy, R. (1982). Das Alter der jüngsten Sedimente der Ortler-Decke (Oberostalpin) in der Val Trupchun (Schweizerischer Nationalpark, Graubünden). *Eclogae Geologicae Helvetiae, 75*(1), 159–169.

Ceriani, S., Fügenschuh, B., Potel, S., & Schmid, S. M. (2003). Tectono-metamorphic evolution of the Frontal Penninic units of the Western Alps: Correlation between low-grade metamorphism and tectonic phases. *Schweizerische Mineralogische und Petrographische Mitteilungen, 83*(1), 111–131.

Channell, J. E. T., Brandner, R., Spieler, A., & Smathers, N. P. (1990). Mesozoic paleogeography of the Northern Calcareous Alps—Evidence from paleomagnetism and facies analysis. *Geology, 18*, 828–831.

Chermak, J. A., & Rimstidt, J. D. (1990). The hydrothermal transformation rate of kaolinite to muscovite/illite. *Geochimica et Cosmochimica Acta, 54*(11), 2979–2990.

Čičel, B., & Novak, I. (1977). Dissolution of smectites in hydrochloric acid. I. Half-time of dissolution as a measure of reaction rate. In: Konta, J. (Ed.) *Proceedings of the 7th conference on clay mineralogy and petrology* (pp. 161–171). Charles University, Prague.

Ciulavu, M., Ferreiro Mählmann, R., Seghedi, A., Schmid, S. M., Hofmann, H., & Frey, M. (2008). Metamorphic evolution of a very low- to low-grade metamorphic core complex (Danubian window) in the South Carpathians. Geological Society London, Special Publication. In S. Siegesmund, B. Fügenschuh, & N. Froitzheim (Eds.), *Tectonic aspects of the Alpine–Dinaride–Carpathian system* (Vol. 298, pp. 281–315). Geological Society.

Clarke, G. L., Aitchison, J. C., & Cluzel, D. (1997). Eclogites and blueschists of the Pam Peninsula, NE New Caledonia: A reappraisal. *Journal of Petrology, 38*, 843–876.

Clauer, N., Środoń, J., Francu, J., & Šucha, V. (1997). K-Ar dating of illite fundamental particles separated from illite-smectite. *Clay Minerals, 32*(2), 181–196. https://doi.org/10.1180/claymin.1997.1032.1182.1102

Cluzel, D., Aitchison, J., Clarke, G., Meffre, S., & Picard, C. (1994). Point de vue sur l'évolution tectonique et géodynamique de la Nouvelle-Calédonie (Pacifique, France). *Comptes Rendus de l'Académie des Sciences, 319*, 683–690.

Cluzel, D., Aitchison, J. C., & Picard, C. (2001). Tectonic accretion and underplating of mafic terranes in the Late Eocene intraoceanic forearc of New Caledonia (Southwest Pacific): Geodynamic implications. *Tectonophysics, 340*, 23–59.

Cluzel, D., & Meffre, S. (2002). The Boghen terrane (New Caledonia, SW Pacific): A Jurassic accretionary complex. Preliminary U-Pb radiochronological data on detrital zircon. *Comptes Rendus Geoscience, 334*(11), 867–874.

Coimbra, R., Rocha, F., Immenhauser, A., Olóriz, F., Terroso, F., & Horikx, M. (2021). Carbonate-hosted clay minerals: A critical re-evaluation of extraction methods and their possible bias on palaeoenvironmental information. *Earth-Science Reviews, 214*, 103502. https://doi.org/10.1016/j.earscirev.2021.103502

Coward, M. P., Gillcrist, R., & Trudgill, B. (1991). Extensional structures and their tectonic inversion in the Western Alps. *Geological Society London, Special Publications, 56*(1), 93–112.

Dalla Torre, M., De Capitani, C., Frey, M., Underwood, M. B., Mullis, J., & Cox, R. (1996). Very low-temperature metamorphism of shales from the Diabolo Range, Franciscan Complex, California: New constraints on the exhumation path. *Geological Society of America Bulletin, 108*(5), 578–601.

Dalla Torre, M., Ferreiro Mählmann, R., & Ernst, W. G. (1997). Experimental study on the pressure dependence of vitrinite maturation. *Geochimica Cosmochimica Acta, 61*(14), 2921–2928. https://doi.org/10.1016/S0016-7037(97)00104-X

Dallmeyer, R. D., Neubauer, F., & Fritz, H. (2008). The Meliata suture in the Carpathians: Regional significance and implications for the evolution of high-pressure wedges within collisional orogens. *Geological Society London, Special Publications, 298*(1), 101–115.

Davies, V. M. (1982). Interaction of thrusts and basement faults in the French external Alps. *Tectonophysics, 88*, 325–331.

Debrand-Passard, S., Courbouleix, S., & Lienhardt, M. J. (1984). Synthèse géologique du Sud-Est de la France. *Mémoire du Bureau de recherches géologiques et minières*, p. 126.

Deer, W. A., Howie, R. A., & Zussmann, J. (1962). *Rock forming minerals, vol. 3: Sheet silicates* (p. 270). Longman.

Dercourt, J., Zonenshain, L. P., Ricou, L. E., Kazmin, V. G., Pichon, X. L., Knipper, A. L., Grandjacquet, C., Sbortshikov, I. M., Geyssant, J., Lepvrier, C., Pechersky, D. H., Boulin, J., Sibuet, J. C., Savostin, L. A., Sorokhtin, O., Westphal, M., Bazhenov, M. L., Lauer, J. P., & Biju-Duval, B. (1986). Geological evolution of the Tethys belt from the Atlantic to the Pamirs since the Lias. *Tectonophysics, 123*, 241–315.

Diessel, C. F. K., Brothers, R. N., & Black, P. M. (1978). Coalification and graphitization in high pressure schists in New Caledonia. *Contributions to Mineralogy and Petrology, 68*, 63–78.

Dietrich, R. V. (1956). Trigonal paragonite from Campbell and Franklin Counties, Virginia. *American Mineralogist, 41*, 940–942.

Dietrich, R.V. (1966). Minerals of Virginia. *Research Division Bulletin, Virginia Polytechnic Institute*, 47–55, p. 325.

Dietrich, V. J. (1969). *Die Ophiolithe des Oberhalbsteins (Graubünden) und das Ophiolithmaterial der ostschweizerischen Molasseablagerungen, ein petrographischer Vergleich* (p. 179). Europäische Hochschulschriften, Herbert Lang & Cie AG.

Dietrich, V. J., Vaugnat, M., & Bertrand, J. (1974). Alpine metamorphism of mafic rocks. *Schweizerische Mineralogische und Petrographische Mitteilungen, 54*(2), 291–332.

Dong, H., & Peacor, D. R. (1996). TEM observations of coherent stacking relations in smectite, I/S and illite of shales: Evidence for MacEwan crystallites and dominance of 2M1 polytypism. *Clays and Clay Minerals, 44*(2), 257–275.

Dunoyer De Segonzac, G. (1970). The transformation of clay minerals during diagenesis and low-grade metamophism: A review. *Sedimentology, 15*, 282–346.

Dunoyer De Segonzac, G., & Bernoulli, D. (1976). Diagenèse et métamorphisme des argiles dans le Rhétien Sud-alpin et Austroalpin (Lombardie et Grisons). *Bulletin de la Société géologique de France, 18*(5), 1283–1293.

Eberl, D. D., Środoń, J., Kralik, M., Taylor, B. E., & Peterman, Z. E. (1990). Ostwald ripening of clays and metamorphic minerals. *Science, 248*, 474–477.

Eggert, P., Grebe, H., Teichmüller, M., & Teichmüller, R. (1976). Inkohlungsuntersuchungen an Treibholz aus der Unteren Junghansen-Serie (Unterkreide) der Feuerstätter Decke (Nordpenninikum) westlich Oberstdorf/Allgäu. *Neues Jahrbuch für Geologie und Paläontologie – Abhandlungen, 152*(1), 112–136.

Ehrenberg, S. N., Aagaard, P., Wilson, M. J., Fraser, A. R., & Duthie, D. M. L. (1993). Depth-dependent transformation of kaolinite to dickite in sandstones of the Norwegian continental shelf. *Clay Minerals, 28*, 325–352.

Elliott, W. C., Aronson, J. L., Matisoff, G., & Gautier, D. L. (1991). Kinetics of the smectite to illite transformation in the Denver basin: Clay mineral, K/Ar, and mathematical model results. *American Association of Petroleum Geologists Bulletin, 75*, 436–462.

Elliott, W. C., & Matisoff, G. (1996). Evaluation of kinetic models for the smectite to illite transformation. *Clays and Clay Minerals, 44*(1), 77–87.

Eppel, H., & Abart, R. (1997). Grain-scale stable isotope disequilibrium during fluid-rock interaction; 2, an example from the Penninic-Austroalpine tectonic contact in eastern Switzerland. *American Journal of Science, 297*(7), 707–728.

Erdelbrock, K. (1994). *Diagenese und schwache Metamorphose im Helvetikum der Ostschweiz (Inkohlung und Illit-"Kristallinität")* (p. 220). Unpublished Ph.D. thesis, RWTH Aachen.

Ernst, W. G., & Ferreiro Mählmann, R. (2004). Vitrinite alteration rate as a function of temperature, time, starting material, aqueous fluid pressure, and oxygen fugacity—Laboratory corroboration of prior work. The Geochemical Society, Publication. In R. J. Hill, J. Leventhal, M. J. Aizenshtat, G. Baedecker, G. Claypool, R. Eganhouse, M. Goldhaber, & K. Peters (Eds.), *Geochemical investigations in earth and space sciences: A tribute to Isaac, R. Kaplan* (Vol. 9, pp. 341–375). Elsevier.

Essene, E. J. (1989). The current status of thermobarometry in metamorphic rocks. Geological Society London, Special Publication. In J. S. Daly, R. A. Cliff, & B. W. D. Yardley (Eds.), *Evolution of metamorphic belts* (Vol. 43, pp. 1–44). Geological Society.

Eugster, H. P., Albee, A. L., Bence, A. E., Thompson, J. B., & Waldbaum, D. R. (1972). The two phase region and excess mixing properties of paragonite ± muscovite crystalline solutions. *Journal of Petrology, 13*, 147–179.

Ferreiro Mählmann, R. (1994). Zur Bestimmung von Diagenesehöhe und beginnender Metamorphose - Temperaturgeschichte und Tektogenese des Austroalpins und Süpenninikums in Vorarlberg und Mittelbünden. *Frankfurter Geowissenschaftliche Arbeiten, Serie C, 14*, p. 498.

Ferreiro Mählmann, R. (1995). Das Diagenese-Metamorphose-Muster von Vitrinitreflexion und Illit-"Kristallinität" in Mittelbünden und im

Oberhalbstein. Teil 1: Bezüge zur Stockwerktektonik. *Schweizerische Mineralogische und Petrologische Mitteilungen, 75*(1), 85–122.
Ferreiro Mählmann, R. (1996). Das Diagenese-Metamorphose-Muster von Vitrinitreflexion und Illit-"Kristallinität" in Mittelbünden und im Oberhalbstein. Teil 2: Korrelation kohlenpetrographischer und mineralogischer Parameter. *Schweizerische Mineralogische und Petrologische Mitteilungen, 76*(1), 23–47.
Ferreiro Mählmann, R. (2001). Correlation of very low-grade data to calibrate a thermal maturity model in a nappe tectonic setting, a case study from the Alps. *Tectonophysics, 334*, 1–33. https://doi.org/10.1016/S0040-1951(01)00022-1
Ferreiro Mählmann, R., Bozkaya, Ö., Potel, S., Le Bayon, R., Šegvić, B., & Nieto, F. (2012). The pioneer work of Bernard Kübler and Martin Frey in very low-grade metamorphic terranes: Paleo-geothermal potential of variation in Kübler-Index/organic matter reflectance correlations. A review. *Swiss Journal of Geosciences, 105*(2), 121–152. https://doi.org/10.1007/s00015-012-0115-3
Ferreiro Mählmann, R., & Frey, M. (2012). Standardisation, calibration and correlation of the Kübler-index and the vitrinite/bituminite reflectance: An inter-laboratory and field related study. *Swiss Journal of Geosciences, 105*(2), 153–170. https://doi.org/10.1007/s00015-012-0110-8
Ferreiro Mählmann, R., & Giger, M. (2012). The Arosa zone in Eastern Switzerland: Oceanic, syn-sedimentary, accretional and orogenic very-low grade patterns in a tectono-metamorphic mélange. *Swiss Journal of Geosciences, 105*(2), 203–233. https://doi.org/10.1007/s00015-012-0103-7
Ferreiro Mählmann, R., & Le Bayon, R. (2016). Vitrinite and vitrinite like solid bitumen reflectance in thermal maturity studies: Correlations from diagenesis to incipient metamorphism in different geodynamic settings. *International Journal of Coal Geology, 157*(1), 52–73. https://doi.org/10.1016/j.coal.2015.12.008
Ferreiro Mählmann, R., Petrova, T. V., Pironon, J., Stern, W. B., Ghanbaja, J., Dubessy, J., & Frey, M. (2002). Transmission electron microscopy study of carbonaceous material in a metamorphic profile from diagenesis to amphibolite facies (Bündnerschiefer, Eastern Switzerland). *Schweizerische Mineralogische und Petrographische Mitteilungen, 82*, 253–272.
Fitzherbert, J. A., Clarke, G. L., & Powell, R. (2003). Lawsonite–omphacite-bearing metabasites of the Pam Peninsula, NE New Caledonia: Evidence for disrupted blueschist-to eclogite-facies conditions. *Journal of Petrology, 44*(10), 1805–1831.
Foscolos, A. E. (1990). Catagenesis of argillaceous sedimentary rocks: Diagenesis. Reprint series 4. *Geoscience Canada*, pp 177–188.
Frank, W. (1983). Argumente für ein neues Entwicklungsmodell des Ostalpins. Jahrbericht, 1982, *Hochschulschwerpunkt Leoben*. S15(4), 246–262.
Frank, W., Kralik, M., Scharbert, S., & Thöni, M. (1987). Geochronological data from the Eastern Alps. In H. W. Flügel & P. Faupl (Eds.), *Geodynamics of the Eastern Alps, 272–281* (p. 418). F. Deuticke.
Frey, M. (1969). A mixed-layer paragonite/phengite of low-grade metamorphic origin. *Contributions to Mineralogy and Petrology, 24*(1), 63–65. https://doi.org/10.1007/BF00398753
Frey, M. (1970). The step from diagenesis to metamorphism in pelitic rocks during Alpine orogenesis. *Sedimentology, 15*, 261–279.
Frey, M. (1978). Progressiv low-grade metamorphism of a black shale formation, Central Swiss Alps, with special references to pyrophyllite and margarite bearing assemblages. *Journal of Petrology, 19*, 95–137.
Frey, M. (1987a). Very low-grade metamorphism of clastic sedimentary rocks. In M. Frey (Ed.), *Low temperature metamorphism, 9–58* (p. 351). Blackie & Son Ltd.
Frey, M. (1987b). The reaction-isograd kaolinite + quartz = pyrophyllite + H_2O, Helvetic Alps. *Schweizerische Mineralogische und Petrologische Mitteilungen, 67*(1), 1–11.
Frey, M. (1988). Discontinuous inverse metamorphic zonation, Glarus Alps, Switzerland: Evidence from illite "cristallinity" data. *Schweizerische Mineralogische und Petrologische Mitteilungen, 68*(1), 171–183.
Frey, M., Bucher, K., Frank, E., & Mullis, J. (1980a). Alpine metamorphism along the Geotraverse Basel-Chiasso—A review. *Eclogae Geologicae Helvetiae, 73*(2), 527–546.
Frey, M., & Burkhard, M. (1992). Mineralogisch-petrologische Exkursion zur progressiven alpinen Metamorphose der Zentralalpen. *Berichte der Deutschen Mineralogischen Gesellschaft, 1992*(2), 103–122.
Frey, M., De Capitani, C., & Liou, J. G. (1991). A new petrogenetic grid for low-grade metabasites. *Journal of Metamorphic Geology, 9*, 497–509. https://doi.org/10.1111/j.1525-1314.1991.tb00542.x
Frey, M., Desmons, J., & Neubauer, F. (1999). Alpine metamorphic map 1:500,000. *Schweizerische Mineralogische und Petrographische Mitteilungen, 79*(1), 1–4.
Frey, M., & Ferreiro Mählmann, R. (1999). Alpine metamorphism of the Central Alps. *Schweizerische Mineralogische und Petrologische Mitteilungen, 79*(1), 135–154.
Frey, M., Hunziker, C., Roggwiller, P., & Schindler, C. (1973). Progressive niedriggradige Metamorphose glauconitführender Horizonte in den helvetischen Decken der Ostschweiz. *Beiträge zur Mineralogie und Petrographie, 39*, 185–218.
Frey, M., Jäger, E., & Niggli, E. (1976). Gesteinsmetamorphose im Bereich der Geotraverse Basel–Chiasso. *Schweizerische Mineralogische und Petrographische Mitteilungen, 56*(3), 649–659.
Frey, M., & Kisch, H. J. (1987). Scope of subject. In M. Frey (Ed.), *Low temperature metamorphism, 1–8* (p. 351). Blackie & Son Ltd.
Frey, M., & Niggli, E. (1971). Illit-Kristallinität, Mineralfazien und Inkohlungsgrad. *Schweizerische Mineralogische und Petrographische Mitteilungen, 51*(1), 229–234.
Frey, M., & Robinson, D. (1999). *Low-grade metamorphism* (p. 313). Blackwell Science.
Frey, M., Teichmüller, M., Teichmüller, R., Mullis, J., Künzi, B., Breitschmid, A., Gruner, U., & Schwizer, B. (1980b). Very low-grade metamorphism in external parts of the Central Alps: Illite crystallinity, coal rank and fluid inclusion data. *Eclogae Geologicae Helvetiae, 73*(1), 173–203.
Frey, M., & Wieland, B. (1975). Chloritoid in autochthon-parautochthonen Sedimenten des Aarmassivs. *Schweizerische Mineralogische und Petrographische Mitteilungen, 55*(3), 407–418.
Frisch, W. (1979). Tectonic progradation and plate tectonic evolution of the Alps. *Tectonophysics, 60*, 121–139.
Froitzheim, N., & Manatschal, G. (1996). Kinematics of Jurassic rifting, mantle exhumation, and passive-margin formation in the Austroalpine and Penninic nappes (eastern Switzerland). *Geological Society of America Bulletin, 108*, 1120–1133.
Froitzheim, N., Schmid, S. M., & Conti, P. (1994). Repeated change from crustal shortening to orogen-paralell extension in the Austroalpine units of Graubünden. *Eclogae Geologicae Helvetiae, 87*(2), 559–6912.
Füchtbauer, H. (1950). Die nicht karbonatischen Bestandteile des Göttinger Muschelkalkes mit besonderer Berücksichtigung der Mineralneubildungen. *Heidelberger Beiträge zur Mineralogie und Petrographie, 2*(3), 235–254.
Fügenschuh, B., Loprieno, A., Ceriani, S., & Schmid, S. M. (1999). Structural analysis of the Subbriançonnais and Valais units in the area of Moûtiers (Savoy, Western Alps): Paleogeographic and tectonic consequences. *International Journal of Earth Sciences (Geologische Rundschau), 88*(2), 201–218.
Fügenschuh, B., & Schmid, S. M. (2003). Late stages of deformation and exhumation of an orogen constrained by fission-track data: A case study in the Western Alps. *Geological Society of America Bulletin, 115*(11), 1425–1440.
García-Romero, E., Lorenzo, A., García-Vicente, A., Morales, J., García-Rivas, J., & Suárez, M. (2021). On the structural formula of smectite: A review and new data on the influence of axchangeable cations. *Journal of Applied Crystallography, 54*, 12. https://doi.org/10.1107/S1600576720016040
García-Romero, E., Suárez, M., Santarén, J., & Alvarez, A. (2007). Crystallochemical characterization of the palygorskite and sepiolite from the Allou Kagne deposit, Senegal. *Clays and Clay Minerals, 55*(6), 606–617.
Gaupp, R. H. (1982). Sedimentgeschichte und Paläotektonik der kalkalpinen Mittelkreide (Allgäu, Tirol, Vorarlberg). *Zitteliana, 8*, 33–72.
Gaupp, R. H., & Batten, D. J. (1985). Maturation of organic matter in Cretaceous strata of the Northern Calcareous Alps. *Neues Jahrbuch für Geologie und Paläonologie. Monatshefte, 1985/3*, 157–175.
Ghent, E. D., Roddick, J. C., & Black, P. M. (1994). 40Ar/39Ar dating of white micas from the epidote to the omphacite zones, northern New Caledonia: Tectonic implications. *Canadian Journal of Earth Sciences, 31*, 995–1001.
Gillcrist, R., Coward, M., & Mugnier, J. L. (1987). Structural inversion and its controls; examples from the Alpine Foreland and the French Alps. *Geodinamica Acta, 1*, 5–34.

Giorgetti, G., Monecke, T., Kleeberg, R., & Herzig, P. M. (2003). Intermediate sodium-potassium mica in hydrothermally altered rocks of the Waterloo deposit, Australia: A combined SEM-EMP-XRD-TEM study. *Contributions to Mineralogy and Petrology, 146*, 159–173.
Green, H., Šegvić, B., Zanoni, G., Omodeo-Salé, S., & Adatte, T. (2020). Evaluation of shale source rocks and clay mineral diagenesis in the Permian basin, USA: Inferences on basin thermal maturity and source rock potential. *Geosciences, 10*(10), 381. https://doi.org/10.3390/geosciences10100381
Grim, R. E. (1968). *Clay mineralogy* (2nd ed., p. 596). Mc Graw-Hill Book Comp.
Grobe, A., Urai, J. L., Littke, R., & Lünsdorf, N. K. (2016). Hydrocarbon generation and migration under a large overthrust: The carbonate platform under the Semail Ophiolite, Jebel Akhdar, Oman. *International Journal of Coal Geology, 168*(1), 3–19. https://doi.org/10.1016/j.coal.2016.1002.1007
Guggenheim, St., Bain, D. C., Bergaya, F., Brigatti, M. F., Drits, V. A., Eberl, D. D., Formoso, M. L. L., Galán, E., Merriman, R. J., Peacor, D. R., Stanjek, H., & Watanabe, T. (2002). Report of the association internationale pour l'étude des argiles (AIPEA) nomenclature committee for 2001: Order, disorder and crystallinity in phyllosilicates and the use of the 'crystallinity index.' *Clays and Clay Minerals, 50*, 406–409.
Guidotti, C. V. (1984). Micas in metamorphic rocks. Reviews in mineralogy, 13, 357–467. In S. W. Bailey (Ed.), *Micas* (p. 754). Mineralogical Society of America.
Guidotti, C. V., & Sassi, F. P. (1976). Muscovite as a petrogenetic indicator mineral in pelitic schists. *Neues Jahrbuch für Mineralogie Abhandlungen, 127*, 97–142.
Guidotti, C. V., & Sassi, F. P. (1986). Classification and correlation of metamorphic facies series by means of Muscovite b(o) data from low-grade metapelites. *Neues Jahrbuch für Mineralogie. Abhandlungen, 153*(3), 363–380.
Gupta, S. (1997). Tectonic control on paleovalley incision at the distal margin of the early Tertiary Alpine foreland basin, southeastern France. *Journal of Sedimentary Research, 67*, 1030–1043.
Hackley, P. C., Araujo, C. V., Borrego, A. G., Bouzinos, A., Cardott, B., Cook, A. C., Eble, C., Flores, D., Gentzis, T., Gonçalves, P. A., Mendonça Filho, J. G., Hámor-Vidó, M., Jelonek, I., Kommeren, K., Knowles, W., Kus, J., Mastalerz, M., Menezes, T. R., Newman, J., … Valentine, B. J. (2015). Standardization of reflectance measurements in dispersed organic matter: Results of an exercise to improve interlaboratory agreement. *Marine and Petroleum Geology, 59*, 22–34.
Hackley, P. C., & Cardott, B. J. (2016). Application of organic petrography in North American shale petroleum systems: A review. *International Journal of Coal Geology, 163*, 8–51. https://doi.org/10.1016/j.coal.2016.06.010
Hackley, P. C., & Lewan, M. (2018). Understanding and distinguishing reflectance measurements of solid bitumen and vitrinite using hydrous pyrolysis: Implications to petroleum assessment. *American Association of Petroleum Geologists, 102*(6), 1119–1140.
Handy, M. R., Herwegh, M., Kamber, B., Tietz, R., & Villa, I. (1996). New constraints on the evolution of the Lower Austroalpine-Penninic suture from a study of the Err, Platta and Margna nappes (Eastern Switzerland). *Schweizerische Mineralogische und Petrographische Mitteilungen, 76*(3), 453–474.
Handy, M. R., Schmid, S. M., Bousquet, R., Kissling, E., & Bernoulli, D. (2010). Reconciling plate-tectonic reconstructions of Alpine Tethys with the geological–geophysical record of spreading and subduction in the Alps. *Earth-Science Reviews, 102*(3–4), 121–158.
Haq, B. U., Hardenbol, J., & Vail, P. R. (1987). Chronology of fluctuating sea levels since the Triassic. *Science, 235*, 1156–1167.
Hartkopf-Fröder, C., Königshof, P., Littke, R., & Schwarzbauer, J. (2015). Optical thermal maturity parameters and organic geochemical alteration at low grade diagenesis to anchimetamorphism: A review. *International Journal of Coal Geology, 150–151*, 74–119. https://doi.org/10.1016/j.coal.2015.06.005
Henrichs, C. (1993). Sedimentpetrographische Untersuchungen zur Hochdiagenese in der Kössen-Formation (Ober Trias) der westlichen Ostalpen und angrenzenden Südalpengebiete. *Bochumer geologische und geotechnische Arbeiten, 40*, p. 206.
Henrichs, C., & Richter, D. K. (1993). Illitkristallinität und Petrovarianz - ein Vergleich siliziklastischer und karbonatischer Gesteine. *Kurzfassung: Sedimente 93, Marburg. 8 Sedimentologentreffen, Geologica et Paleontologica, 1993*, 43–44.
Herbert, H. J., Kasbohm, J., Nguyen-Thanh, L., Meyer, L., Hoang-Minh, T., Xie, M., & Ferreiro Mählmann, R. (2016). Alteration of expandable clays by reaction with iron while being percolated by high brine solutions. *Applied Clay Sciences, 121–122*, 174–187.
Hillier, S., Mátyás, J., Matter, A., & Vasseur, G. (1995). Illite/smectite diagenesis and its variable correlation with vitrinite reflection in the Pannonian Basin. *Clays and Clay Minerals, 43*, 174–183.
Hiltmann, W., Kuckelkorn, K., & Wehner, H. (1995). Thermische Entwicklung und KW-Bildungspotential der in der Bohrung Hindelang 1 (Allgäuer Alpen) durchteuften tektonischen Einheiten. *Geologica Bavarica, 100*, 175–197.
Hoang-Minh, T., Kasbohm, J., Nguyen-Thanh, L., Thi Nga, P., Thi Lai, L., Thuy Duong, N., Duc Thanh, N., Thi Minh Tuyet, N., Duy Anh, D., Pusch, R., Knutsson, S., & Ferreiro Mählmann, R. (2019). Use of TEM-EDX for structural formula identification of clay minerals: A case study of Di Linh bentonite, Vietnam. *Journal of Applied Crystallography, 52*(1), 133–147.
Hoffman, E., & Jenkner, A. (1932). Die Inkohlung und ihre Erkennung im Mikrobild. *Glückauf, 68*, 81.
Hoffman, J., & Hower, J. (1979). Clay mineral assemblages as low grade metamorphic geothermometers: Application to the thrust faulted disturbed belt of Montana, USA. In P. A. Scholle & P. R. Schluger (Eds.), *Aspects of diagenesis* (Vol. 26, pp. 55–79). Society of Economic Paleontologists and Mineralogists Special Publication.
Hoffman, J., Hower, J., & Aronson, J. L. (1976). Radiogenic dating of thrust faults in the Disturbed Belt, Montana. *Geology, 4*, 16–21.
Hower, J., Eslinger, E. V., Hower, M. E., & Perry, E. A. (1976). Mechanism of burial metamorphism of argillaceous sediment: 1. Mineralogical and chemical evidence. *Geological Society of America Bulletin, 87*, 725–737.
Huang, W. L. (1996). Experimental study of vitrinite maturation: Effects of temperature, time, pressure, water, and hydrogen index. *Organic Chemistry, 24*, 233–241.
Huang, W. L., Longo, J. M., & Pevear, D. R. (1993). An experimentally derived kinetic model for smectite-to-illite conversion and its use as a geothermometer. *Clays and Clay Minerals, 41*, 162–177.
Hunziker, J. C., Desmons, J., & Hurford, A. J. (1992). Thirty-two years of geochronological work in the Central and Western Alps: A review on seven maps. *Mèmoires de Gèologie, (Lausanne), 13*, 73.
Hunziker, J. C., Frey, M., Clauer, N., Dallmeyer, R. D., Friedrichsen, H., Flehmig, W., Hochstrasser, P., Roggwiler, P., & Schwander, H. (1986). The evolution of illite to muscovite: Mineralogical and isotopic data from the Glarus Alps, Switzerland. *Contributions to Mineralogy and Petrology, 92*, 157–180.
Hürzeler, J. P., & Abart, R. (2008). Fluid flow and rock alteration along the Glarus thrust. *Swiss Journal of Geosciences, 101*(2), 251–268.
Huyghe, P., & Mugnier, J. L. (1995). A comparison of inverted basins of the Southern North Sea and inverted structures of the external Alps. Geological Society London, Special Publication. In J. G. Buchanan & P. G. Buchanan (Eds.), *Basin inversion* (Vol. 88, pp. 339–353). Geological Society. https://doi.org/10.1144/GSL.SP.1995.1088.1101.1119
Inoue, A., Velde, B., Muenier, A., & Touchard, G. (1988). Mechanism of illite formation during smectite to illite conversion in a hydrothermal system. *American Mineralogist, 73*, 1325–1334.
Jacob, H. (1967). Petrologie von Asphaltiten und asphaltischen Pyrobitumen. *Erdöl und Kohle, 20*, 393–400.
Jacob, H. (1989). Classification, structure, genesis and practical importance of natural solid oil bitumen ("migrabitumen"). *International Journal of Coal Geology, 11*, 65–79.
Jacob, H., & Hiltmann, W. (1985). Dispers bitumen solids as an indicator for migration and maturity within the scope of prospecting for petroleum and natural gas—A model for NW Germany. DGMK project 267. *Deutsche Gesellschaft für Mineralölwissenschaft und Kohlechemie e.V., Hamburg, final report*, p. 54.
Jagodzinski, H. (1949). Eindimensionale Fehlordnung in Kristallen und ihr Einfluss auf die Röntgeninterferenzen. I. Berechnung des Fehlordnungsgrades aus den Röntgenintensitäten. *Acta Crystallographica, 2*, 201–207.
Jakob, J. (1923). Vier Mangansilikate aus dem Val d'Err (Kt. Graubünden). *Schweizerische Mineralogische und Petrographische Mitteilungen, 3*(1), 227–237.
Jennings, S., & Thompson, G. R. (1986). Diagenesis in Plio-Pleistocene sediments in the Colorado River delta, 37 southern California. *Journal of Sedimentary Petrology, 56*, 89–98.
Jiang, W. T., & Peacor, D. R. (1993). Formation and modification of metastable intermediate sodium potassium mica, paragonite, and muscovite in hydrothermally altered metabasalts from northern Wales. *American Mineralogist, 78*, 782–793.

Jones, B. F., & Galán, E. (1988). Sepiolite and palygorskite. Reviews in mineralogy and geochemistry. In S. W. Bailey (Ed.), *Hydrous phyllosilicates (exclusive of micas)* (Vol. 19, pp. 631–674). De Gruyter, Inc.
Kahr, G., Frey, M., & Madsen, F. T. (1996). Thermoanalytical dehydroxylation of clays and combustion of organic compounds in a prograde metamorphic Liassic black shale formation, Central Swiss Alps. *Schweizerische Mineralogische und Petrographische Mitteilungen, 76*(2), 165–173.
Karpova, G. V. (1966). Paragonite hydromicas in terrigenous rocks of the greater Doubas. *Doklady of the Academy of Sciences of the USSR Earth Science Sections, 171*, 185–187.
Kaufhold, S., & Dohrmann, R. (2008). Detachment of colloidal particles from bentonites in water. *Applied Clay Science, 39*(1–2), 50–59.
Kisch, H. J. (1980a). Illite crystallinity and coal rank associated with lowest-grade metamorphism of Taveyanne greywacke in the Helvetic zone of the Swiss Alps. *Eclogae Geologicae Helvetiae, 73*, 753–777.
Kisch, H. J. (1980b). Incipient metamorphism of Cambro-Silurian clastic rocks from the Jamtland Supergroup, central Scandinavian Caledonides, western Sweden: Illite crystallinity and 'vitrinite' reflectance. *Journal of the Geological Society London, 137*, 271–288.
Kisch, H. J. (1981). Coal rank and illite crystallinity associated with the zeolite facies of Southland and the pumpellyite bearing facies of Otago, southern New Zealand. *New Zealand Journal of Geology and Geophysics, 24*, 349–360.
Kisch, H. J. (1983). Mineralogy and petrology of burial diagenesis (burial metamorphism) and incipient metamorphism in clastic rocks. In G. Larsen & G. V. Chilinger (Eds.), *Diagenesis in sediments and sedimentary rocks* (2nd ed., pp. 289–493). Elsevier.
Kisch, H. J. (1987). Correlation between indicators of very low grade metamorphism. In M. Frey (Ed.), *Low temperature metamorphism, 227–300* (p. 351). Blackie & Son Ltd.
Kisch, H. J. (1991). Illite crystallinity: Recommendations on sample preparation, X-ray diffraction settings, and interlaboratory samples. *Journal of Metamorphic Geology, 9*(6), 723–734.
Kisch, H. J., Árkai, P., & Brime, C. (2004). On the calibration of the illite Kübler-Index (illite "crystallinity"). *Schweizerische Mineralogische und Petrographische Mitteilungen, 84*(3), 323–331.
Kisch, H. J., Sassi, R., & Sassi, F. P. (2006). The b0 lattice parameter and chemistry of phengites from HP/LT metapelites. *European Journal of Mineralogy, 18*(2), 207–222. https://doi.org/10.1127/0935-1221/2006/0018-0207
Kralik, M., Krumm, H., & Schramm, M. (1987). Low grade and very low grade metamorphism in the Northern Calcareous Alps and in the Greywacke zone: Illite-crystallinity data and isotopic ages. In H. W. Flügel & P. Faupl (Eds.), *Geodynamics of the Eastern Alps, 164–178* (p. 418). F. Deuticke.
Kralik, M., & Schramm, M. (1994). Illitwachstum: Übergang Diagenese - Metamorphose in Karbonat- und Tongesteinen der Nördlichen Kalkalpen – Mineralogie und Isotopengeologie (Rb-Sr, K-Ar und C-O). *Jahrbuch der Geologischen Bundesanstalt, 137*, 105–137.
Kramm, U. (1978). Die Metamorphose Mn-reicher Pelite der Wippraer Zone/ Unterharz. *Fortschritte der Mineralogie, 56*(1), 67–68.
Krumm, H. (1969). A scheme of clay mineral stability in sediments based on clay mineral distribution in Triassic sediments of Europe. *Proceedings of the International Clay Conference, Tokyo, 1*, 313–324.
Krumm, H. (1977). Problems and results in "illite crystallinity". In *Procedings of the third European clay conference, Oslo*, pp 91–92.
Krumm, H. (1984). Anchimetamorphose im Anis und Ladin (Trias) der Nördlichen Kalkalpen zwischen Arlberg und Kaisergebirge - ihre Verbreitung und deren baugeschichtliche Bedeutung. *Geologische Rundschau, 73*(1), 223–257.
Krumm, H., Petschick, R., Esselborn, J., & Krückhans, G. (1995). Die Schichtsilikate und ihr Diageneseverhalten in der Bohrung Hindelang 1 (Allgäuer Alpen). *Geologica Bavarica, 100*, 219–250.
Krumm, H., Petschick, R., & Wolf, M. (1988). From diagenesis to anchimetamorphism, upper Austroalpine sedimentary cover in Bavaria and Tyrol. *Geodinamica Acta, 2*(1), 33–47.
Krumm, S., & Buggisch, W. (1991). Sample preparation effects on illite crystallinity measurement: Grain-size gradation and particle orientation. *Journal of Metamorphic Geology, 9*, 671–677.
Kübler, B. (1964). Les argiles, indicateurs de métamorphisme. *Revue de l'Institut Français du Pétrole, 19*, 1093–1112.
Kübler, B. (1967). La cristallinité de l'illite et les zones tout à fait supérieures du métamorphisme. *Etages Tectoniques* (pp. 105–122). Baconniere.
Kübler, B. (1968). Evaluation quantitative du métamorphisme par la cristallinité de l'illite. *Bulletin du Centre de Recherches de Pau, SNPA, 2*, 385–397.
Kübler, B., Betrixe, M. A., & Monnier, F. (1979a). Les premiers stades de la diagenese organique et là diagenese minérale: Une tentative d'équivalence. 1ere partie: Zonéographie par la maturation de là matiere organique'. *Bulletin der Vereinigung Schweizerischer Petroleumgeologen und Petroleumingenieure, 45*, 1–22.
Kübler, B., Pittion, J.-L., Héroux, Y., Charollais, J., & Weidmann, M. (1979b). Sur le pouvoir réflecteur de la vitrinite dans quelques roches du Jura, de la Molasse et des Nappes préalpines, helvétiques et penniniques. *Eclogae Geologicae Helvetiae, 72*(2), 347–373.
Kuckelkorn, K., & Hiltmann, W. (1990). Zur Maturität und Erdölbildung in den Allgäuer Alpen, 2. *Erdöl Erdgas Kohle, 106*(2), 54–57.
Kuckelkorn, K., Hiltmann, W., & Schwerd, K. (1990). Zur Maturität und Erdölbildung in den Allgäuer Alpen I. *Erdöl Erdgas Kohle, 106*(1), 7–11.
Kulbicki, G., & Millot, G. (1959). Appoint des minéraux argileux interstratifiés à la géologie des séries sédimentaires. *Bulletin du Groupe français des Argiles, 11*(6), 47–52.
Kürmann, H. (1993). Zur Hochdiagenese und Anchimetamorphose in Permotrias-Sedimenten des Austroalpins westlich der Tauern. Ph.D. thesis, University of Bochum. *Bochumer geologische geotechnische Arbeiten*, 41, p. 328.
Lahfid, A., Beyssac, O., Deville, E., Negro, F., Chopin, C., & Goffe, B. (2010). Evolution of the Raman spectrum of CM in low-grade metasediments of the Glarus Alps (Switzerland). *Terra Nova, 22*, 354–360.
Landis, C. A., & Castaño, J. R. (1995). Maturation and bulk chemical properties of a suite of solid hydrocarbons. *Organic Geochemistry, 22*, 137–150.
Laubscher, H. P. (1983). Detachment, shear, and compression in the central Alps. *Geological Society of America Memoir, 158*, 191–211.
Laubscher, H. P., & Bernoulli, D. (1982). History and deformation of the Alps. In K. J. Hsü (Ed.), *Mountain building processes* (pp. 169–180). Academic Press.
Lazarre, J., Tricart, P., Courrioux, G., & Ledru, P. (1996). Héritage téthysien et polyphasage alpin; réinterprétation tectonique du "synclinal" de l'aiguille de Morges (massif du Pelvoux, Alpes occidentales, France). *Comptes Rendus de l'Académie des Sciences, Série II Sciences de la Terre et des Planètes, 323*, 1051–1058.
Le Bayon, R., Adam, Ch., & Ferreiro Mählmann, R. (2012a). Experimentally determined pressure effects on vitrinite reflectance at 450 °C. *International Journal of Coal Geology, 92*, 69–81.
Le Bayon, R., Brey, G. P., Ernst, W. G., & Ferreiro Mählmann, R. (2011). Experimental kinetic study of organic matter maturation: Time and pressure effects on vitrinite reflectance at 400°C. *Organic Geochemistry, 42*, 340–355.
Le Bayon, R., Buhre, St., Schmidt, B. C., & Ferreiro Mählmann, R. (2012b). Experimental organic matter maturation at 2 kbar: Heat-up effect to low temperatures on vitrinite reflectance. *International Journal of Coal Geology, 92*, 45–53.
Lewan, M. D., & Pawlewicz, M. J. (2017). Reevaluation of thermal maturity and stages of petroleum formation of the Mississippian Barnett Shale, Fort Worth Basin, Texas. *American Association of Petroleum Geologists Bulletin, 2017*, 1945–1970. https://doi.org/10.1306/01251716053
Li, G., Essene, E. J., Peacor, D. R., & Coombs, D. S. (2002). Reactions leading to the formation and breakdown of stilpnomelane in the Otago Schist, New Zealand. *Journal of Metamorphic Geology, 18*(4), 393–407. https://doi.org/10.1046/j.1525-1314.2000.00263.x
Liniger, M., & Nievergelt, P. (1990). Stockwerk-Tecktonik im südlichen Graubünden. *Schweizerische Mineralogische und Petrographische Mitteilungen, 70*(1), 95–101.
Lippmann, F., & Savaşçin, M. Y. (1969). Mineralogische Untersuchungen an Lösungsrückständen eines württembergischen Keupergipsvorkommens. *Tschermaks Mineralogische und Petrographische Mitteilungen, 13*(2), 165–190.
Littke, R. (1993). *Deposition, diagenesis and weathering of organic matter-rich sediments* Lecture notes in earth science (Vol. 47, p. 216). Springer.
Liu, J. G., Shigenori, M., & Moonsup, C. (1987). Very-low grade metamorphism of volcanic and volcanoclastic rocks—Mineral assemblages and mineral facies. In M. Frey (Ed.), *Low temperature metamorphism, 59–113* (p. 351). Blackie & Son Ltd.
Livi, K. J. T., Christidis, G. E., Árkai, P., & Veblen, D. R. (2008). White mica domian formation: A model for paragonite, and muscovite formation during prograde metamorphism. *American Mineralogist, 93*, 520–527.

Livi, K. J. T., Veblen, D. R., Ferry, J. M., & Frey, M. (1997). Evolution of 2:1 layered silicates in low-grade metamorphosed Liassic shales of Central Switzerland. *Journal of Metamorphic Geology, 15*(3), 323–344. https://doi.org/10.1111/j.1525-1314.1997.00019.x

Loeschke, J., & Weber, K. (1973). Geochemie und Metamorphose paläozoischer Tuffe und Tonschiefer aus den Karawanken (Österreich). *Neues Jahrbuch für Geologie und Paläontologie – Abhandlungen, 142*, 115–138.

Lopatin, N. V. (1971). Temperature and geologic time as factors in coalification. *Akad. Nauk SSSR Isv. Ser. Geol., 3*, 95–106. in Russian.

López-Munguira, A., & Nieto, F. (2000). Transmission electron microscopy study of very low-grade metamorphic rocks in Cambrian sandstones and shales, Ossa-Morena Zone, Southwest Spain. *Clays and Clay Minerals, 48*(2), 213–223.

Lu, G., Fellin, M. G., Winkler, W., Rahn, M., Guillong, M., von Quandt, A., & Willett, S. (2018). Revealing exhumation of the central Alps during the Early Oligocene by detrital zircon U-Pb age and fission-track double dating in the Taveyannaz formation. *International Journal of Earth Sciences, 109*, 2425–2446. https://doi.org/10.1007/s005310002001910t

Maison, T., Potel, S., Malié, P., Ferreiro Mählmann, R., Chanier, F., Mahieux, G., & Bailleul, J. (2019). Low-grade evolution of clay minerals and organic matter in fault zones of the Hikurangi prism (New Zealand). *Clay Minerals, 53*, 579–602.

Malinconico, M. L., Sanford, W. E., & Horten, J. W. (2009). Postimpact heat conduction and compaction-driven fluid flow in the Chesapeake Bay impact structure based on downhole vitrinite reflectance data, ICDP-USGS Eyreville deep core holes and Cape Charles test holes. The Geological Society of America, Special Paper. In G. S. Gohn, C. Koeberl, K. G. Miller, & W. U. Reimold (Eds.), *The ICDP-USGS deep drilling project in the chesapeake bay impact structure: Results from the eyreville core holes* (Vol. 458, pp. 905–930). Geological Society of America.

Mastalerz, M., Drobniak, A., & Stankiewicz, A. B. (2018). Origin, properties and implications of solid bitumen in source-rock reservoirs: A review. *International Journal of Coal Geology, 195*, 14–36. https://doi.org/10.1016/j.coal.2018.05.013

Maurizot, P., Eberlé, J. M., Habault, C., & Tessarollo, C. (1989). *Carte géol. Territoires d'Outre-Mer, Nouvelle-Calédonie (1/50000), feuille Pam-Ouégoa* (2nd ed., p. 81). Bureau de Recherches Géologiques et Minières.

Merriman, R. J. (1991). Very low-grade metamorphism. *Journal of Metamorphic Geology, Special Issue, 9*(6), 663–790.

Merriman, R. J. (2002). Contrasting clay mineral assemblages in British Lower Palaeozoic slate belts: The influence of geotectonic setting. *Clay Minerals, 37*(2), 207–219.

Merriman, R. J. (2005). Clay minerals and sedimentary basin history. *European Journal of Mineralogy, 17*(1), 7–20.

Merriman, R. J., & Frey, M. (1999). Patterns of very low-grade metamorphism in metapelitic rocks, 61–107. In M. Frey & D. Robinson (Eds.), *Low-grade metamorphism* (p. 313). Blackwell Science.

Merriman, R. J., & Kemp, S. J. (1996). Clay minerals and sedimentary basin maturity. *Mineralogical Society Bulletin, 111*, 7–8.

Merriman, R. J., & Peacor, D. R. (1999). Very low-grade metapelites: Mineralogy, microfabrics and measuring reaction progress, 10–60. In M. Frey & D. Robinson (Eds.), *Low-grade metamorphism* (p. 313). Blackwell Science.

Merriman, R. J., & Roberts, B. (1985). A survey of white mica crystallinity and polytypes in pelitic rocks of Snowdonia and Llŷn, North Wales. *Mineralogical Magazine, 49*, 305–319.

Miyashiro, A. (1961). Evolution of metamorphic belts. *Journal of Petrology, 2*(3), 277–311.

Montmartin, C., Faure, F., & Raimbourg, H. (2021). Paleotemperature investigation of the Variscan southern external domain: The case of the Montagne Noire (France). *BSGF—Earth Sciences Bulletin, 192*(3), 43. https://doi.org/10.1051/bsgf/2020043

Moore, D. M., & Reynolds, R. C. (1989). *X-ray diffraction and the identification and analysis of clay minerals* (p. 400). Oxford University Press (OUP).

Moore, D. M., & Reynolds, R. C. (1997). *X-ray diffraction and the identification and analysis of clay minerals* (2nd ed., p. 378). Oxford University Press.

Morse, J. W., & Casey, W. H. (1988). Ostwald processes and mineral paragenesis in sediments. *American Journal of Science, 288*(6), 537–560.

Müller-Wolfskeil, P., & Zacher, W. (1984). Neue Ergebnisse zur Tektonik der Allgäuer und Vilser Alpen. *Geologische Rundschau, 73*(1), 321–335.

Mullis, J. (1979). The system methane-water as a geologic thermometer and barometer from the external part of the Central Alps. *Bulletin de Minéralogie, 102*, 526–536.

Mullis, J., Ferreiro Mählmann, R., & Wolf, M. (2017). Fluid inclusion microthermometry to calibrate vitrinite reflectance (between 50 and 270°C), illite Kübler-Index data and the diagenesis/anchizone boundary in the external part of the Central Alps. *Applied Clay Science, 143*, 307–319.

Mullis, J., Rahn, M. K., Schwer, P., de Capitani, Ch., Stern, W. B., & Frey, M. (2002). Correlation of fluid inclusion temperatures with illite "crystallinity" data and clay mineral chemistry in sedimentary rocks from the external part of the Central Alps. *Schweizerische Mineralogische und Petrologische Mitteilungen, 82*(2), 325–340.

Nadeau, P. H., Wilson, M. J., McHardy, W. J., & Tait, J. (1984). Interstratified clays as fundamental particles. *Science, 225*, 923–925.

Nguyen-Thanh, L., Ferreiro Mählmann, R., Hoang-Minh, T. H., Petschick, R., Reischmann, T., Nesbor, H. D., Ruttmann, M., & Fritsche, J. G. (2021). Clay mineral formation in Permian rocks of a geothermal borehole at Northern Upper Rhine Graben, Germany. *International Journal of Earth Sciences (Geologische Rundschau)*. https://doi.org/10.1007/s00531-021-02022-y

Nguyen-Thanh, L., Herbert, H. J., Kasbohm, J., Hoang-Minh, T., & Ferreiro Mählmann, R. (2014). Effects of chemical structure on the stability of smectites in short-term alteration experiments. *Clays and Clay Minerals, 62*, 425–446.

Nguyen-Thanh, L., Hoang-Minh, Th., Herbert, H. J., Kasbohm, J., Lai, L. T., Ngoc Nguyen, M., & Ferreiro Mählmann, R. (2017). Development of Fe-rich clay minerals in a weathering profile derived from serpentinized ultramafic rocks in Nui Nua massif, Vietnam. *Geoderma, 308*(1), 159–170.

Nieto, F., Mata, M. P., Bauluz, B., Giorgetti, G., Árkai, P., & Peacor, D. R. (2005). Retrograde diagenesis, a widespread process on a regional scale. *Clay Minerals, 40*(1), 93–104.

Nieto, F., Ortega-Huertas, M., Peacor, D. R., & Arostegui, J. (1996). Evolution of illite/smectite from early diagenesis through incipient metamorphism in sediments of the Basque-Cantabrian Basin. *Clays and Clay Minerals, 44*(3), 304–323.

Nieto, F., & Peacor, D. R. (1993). Regional retrograde alteration of prograde pelite sequences to lower grade hydrated assemblages. *Terra Abstracts, 5*, 419.

Nieto, F., Velilla, N., Peacor, D. R., & Huertas, M. O. (1994). Regional retrograde alteration of sub-greenschist facies chlorite to smectite. *Contributions to Mineralogy and Petrology, 115*(3), 243–252.

Nievergelt, P., Liniger, M., Froitzheim, N., & Ferreiro Mählmann, R. (1996). Early to Mid Tertiary crustal extension in the Central Alps: The Turba Mylonite Zone (Eastern Switzerland). *Tectonics, 15*(2), 329–340.

Niggli, E., & Zwart, H. J. (1973). *Metamorphic map of the Alps, scale 1:1 000 000.* Subcommission for the cartography of the metamorphic belts of the world. Sheet 17 of the metamorphic map of Europe. Leiden//UNESCO, Paris.

Oberhauser, R. (1968). Beiträge zur Kenntnis der Tektonik und der Paläogeographie während der Oberkreide und im Paläogen im Ostalpenraum. *Jahrbuch der Geologischen Bundesanstalt Wien, 111*, 115–145.

Oberhänsli, R., Bousquet, R., Engi, M., Goffé, B., Gosso, G., Handy, M., Häck, V., Koller, F., Lardeaux, J. M., Polino, R., Rossi, P., Schuster, R., Schwartz, S., & Spalla, M. I. (2004). Explanatory note to the map "Metamorphic structure of the Alps, 1:1,000,000." Mitteilungen der Österreichischen Mineralogischen GesellschaftIn R. Öberhänsli (Ed.), *Metamorphic structure of the Alps* (Vol. 149, pp. 112–226). CGMW.

Ortner, H. (2003). Cementation and tectonics in the Inneralpine Molasse of the Lower Inn valley. *Geologisch-Paläontologische Mitteilungen Inssbruck, 26*, 71–89.

Ortner, H., & Gaupp, R. (2007). Synorogenic sediments of the western Northern Calcareous Alps. *Geo. Alp, 4*(4), 133–148.

Orville, P. M. (1974). The "peristerite gap" as an equilibrium between ordered albite and disordered plagioclase solution. *Société Française de Mineralogie et de Cristallographie Bulletin, 97*, 386–392.

Padan, A., Kisch, H. J., & Shagam, R. (1982). Use of the lattice parameter b0 of dioctahedral illite/muscovite for the characterization of P/T gradients of incipient metamorphism. *Contributions to Mineralogy and Petrology, 79*(1), 85–95.

Paris, J. P. (1981). Géologie de la Nouvelle-Calédonie, un essai de synthèse. *Mémoires du Bureau de Recherches géologiques et minières, 113*, 278.

Perriaux, J., & Uselle, J. P. (1968). Quelques données sur la sédimentologie des gres du Champsaur (Hautes-Alpes). *Geologie Alpine, 44*, 329–332.
Peters, Tj. (1963). Mineralogie und Petrographie des Totalpserpentins bei Davos. *Schweizerische Mineralogische und Petrographische Mitteilungen, 43*, 529–686.
Petersen, H. I., Schovsbo, N. H., & Nielsen, A. (2013). Reflectance measurements of zooclasts and solid bitumen in Lower Paleozoic shales, southern Scandinavia: Correlation to vitrinite reflectance. *International Journal of Coal Geology, 114*, 1–18. https://doi.org/10.1016/j.coal.2013.1003.1013
Petrova, T. V., Ferreiro Mählmann, R., Stern, W. B., & Frey, M. (2002). Application of combustion and TGA–DTA analysis to the study of metamorphic organic matter. *Schweizerische Mineralogische und Petrographische Mitteilungen, 82*(1), 33–53.
Petschick, R. (1989). Zur Wärmegeschichte im Kalkalpin Bayerns und Nordtirols (Inkohlung und Illit-Kristallinität). *Frankfurter Geowissenschaftliche Arbeiten, C, 10*, p. 259.
Petschick, R., Kuhn, G., & Gingele, F. (1996). Clay mineral distribution in surface sediments of the South Atlantic: Sources, transport, and relation to oceanography. *Marine Geology, 130*(3–4), 203–229. https://doi.org/10.1016/0025-3227(95)00148-4
Pfiffner, A. (2009). *Geologie der Alpen* (p. 359). Verlag UTB.
Pickel, W., Kus, J., Flores, D., Kalaitzidis, S., Christanis, K., Cardott, B., Misz-Kennan, M., Rodrigues, S., Hentschel, A., Hamor-Vido, M., Crosdale, P., Wagner, N., ICPP. (2017). Classification of liptinite—ICCP system 1994. *International Journal of Coal Geology, 169*, 40–61. https://doi.org/10.1016/j.coal.2016.11.004
Piqué, A., & Wybrecht, E. (1987). Origine des chlorites de l´épizone héritage et cristallisation synschisteuse. Exemple des grauwackes cambriennes du Maroc occidental. *Bulletin de Minéralogie, 110*, 665–682.
Pollastro, R. M. (1993). Considerations and applications of the illite/smectite geothermometer in hydrocarbon-bearing rocks of Miocene to Mississippian age. *Clays & Clay Minerals, 41*, 119–133. https://doi.org/10.1346/CCMN.1993.0410202
Potdevin, J. L., & Caron, J. M. (1986). Transfert de matière et déformation synmétamorphique dans un pli. I. Structures et bilans de matière. *Bulletin de Minéralogie, 109*(4), 395–410.
Potel, S. (2001). *Very low-grade metamorphism of the northern New Caledonia* (p. 207). Unpublished Ph.D. thesis, University Basel.
Potel, S. (2007). Very low-grade metamorphic study in the pre-Late Cretaceous terranes of New Caledonia (southwest Pacific Ocean). *Island Arc, 16*(2), 291–305.
Potel, S., Ferreiro Mählmann, R., Stern, W. B., Mullis, J., & Frey, M. (2006). Very low-grade metamorphic evolution of pelitic rocks under high-pressure/low-temperature conditions. *Journal of Petrology, 47*(5), 991–1015. https://doi.org/10.1093/petrology/egl001
Potel, S., Maison, T., Maillet, M., Sarr, A. C., Doublier, M. P., Trullenque, G., & Ferreiro Mählmann, R. (2016). Reliability of very low-grade metamorphic methods to decipher basin evolution: Case study from the Markstein basin (southern Vosges, NE France). *Applied Clay Science, 134*(3), 175–185.
Potel, S., Schmith, S. Th., & de Capitani, C. (2002). Composition of pumpellyite, epidote and chlorite from New Caledonia—How important are metamorphic grade and whole rock composition? *Schweizerische Mineralogische und Petrologische Mitteilungen, 82*(2), 229–252.
Potel, S., & Trullenque, G. (2012). Very low-grade metamorphism in the para-autochtonous sedimentary cover of the Pelvoux massif (Western Alps, France). *Swiss Journal of Geosciences, 105*(2), 235–247.
Pytte, A. M. (1982). The kinetics of the smectite to illite reaction in contact metamorphic shales. *M.A. thesis, Dartmouth College, Hanover, NH*, p. 78.
Pytte, A.M., & Reynolds, R.C. (1989). The thermal transformation of smectite to illite. In Naeser, N.D.M. & McCulloh, T.H. (Eds.). *Thermal History of Sedimentary Basins: Methods and Case Histories* (pp. 133–140). Springer, New York. https://doi.org/10.1007/978-1-4612-3492-0_8
Rahn, M. K. (1994). *Incipient Metamorphism of the Glarus Alps: Petrology of the Taveyanne Greywacke and fission track dating* (p. 209). Unpublished Ph.D. thesis, University Basel, Switzerland.
Rahn, M. K., Brandon, M. T., Batt, G. E., & Garver, J. I. (2004). A zero-damage model for fission-track annealing in zircon. *American Mineralogist, 89*(4), 473–484.
Rahn, M. K., Hurford, A. J., & Frey, M. (1997). Rotation and exhumation of a thrust plane: Apatite fission-track data from the Glarus thrust, Switzerland. *Geology, 25*(7), 599–602.
Rahn, M. K., Mullis, J., Erdelbrock, K., & Frey, M. (1994). Very low-grade metamorphism of the Taveyanne greywacke, Glarus Alps, Switzerland. *Journal of Metamorphic Geology, 12*, 625–641.
Rahn, M. K., Mullis, J., Erdelbrock, K., & Frey, M. (1995). Alpine metamorphism in the North Helvetic flysch of the Glarus Alps, Switzerland. *Eclogae geologicae Helvetiae, 88*(1), 157–178.
Rahn, M. K., Steinmann, M., & Frey, M. (2002). Cloritoid composition and formation in the eastern Central Alps: A comparison between Penninic and Helvetic occurences. *Schweizerische Mineralogische und Petrographische Mitteilungen, 82*(2), 253–272.
Rahn, M. K., Wang, H., & Dunkl, I. (2019). A natural long-term annealing experiment for the zircon fission track system in the Songpan-Garzê flysch, China. *Terra Nova, 31*(3), 295–305. https://doi.org/10.1111/ter.12399
Ravenne, C., Vially, R., Riche, P., & Tremolieres, P. (1987). Sédimentation et tectonique dans le bassin marin Eocene supérieur-Oligocene des Alpes du Sud. *Revue de l'Institut Français du Pétrole, 42*, 529–553.
Reynolds Jr., R. C. (1985). NEWMOD, a computer program for the calculation of one-dimensional diffraction patterns of mixed-layered clays.
Reinhardt, M. (1991). Vitrinite reflectance, illite-crystallinity and tectonics: Results from the Northern Appennines (Italy). *Organic Geochemistry, 17*(2), 175–184.
Reynolds, R. C., & Hower, J. (1970). The nature of interlayering in mixed layer illite-montmorillonite. *Clays and Clay Minerals, 18*, 25–36.
Richter, D. (1957). Gesteine und Vorkommen der Arosa Zone zwischen Arosa und Hindelang im Allgäu. *Geologische Rundschau, 46*(2), 413–420.
Roberson, H. E., & Lahann, R. W. (1981). Smectite to illite conversion rates. Effect of solution chemistry. *Clays and Clay Minerals, 29*, 129–135.
Robert, P. (1988). *Organic metamorphism and geothermal history—Microscopic study of organic matter and thermal evolution of sedimentary basins* (p. 309). Reidel Publication Company.
Robinson, D., & Merriman, J. (1999). Low-temperature metamorphism an overview. In M. Frey & D. Robinson (Eds.), *Low-grade metamorphism* (p. 313). Blackwell Science.
Rolandone, F., Jaupart, C., Mareschal, J. C., Gariépy, C., Bienfait, G., Carbonne, C., & Lapointe, R. (2002). Surface heat flow, crustal temperatures and mantle heat flow in the Proterozoic Trans-Hudson Orogen, Canadian Shield. *Journal of Geophysical Research, 107*(B12), 2341. https://doi.org/10.1029/2001JB000698
Roth, P., & Meisser, N. (2011). I minerali dell'Alpe Tanatz. Passo dello Spluga (Grigioni, Svizzera). *Rivista Mineralogica Italiana, 2*, 90–99.
Sanei, H., Haeri-Ardakani, O., Wood, J. M., & Curtis, M. E. (2015). Effects of nanoporosity and surface imperfections on solid bitumen reflectance (BRo) measurements in unconventional reservoirs. *International Journal of Coal Geology, 138*, 95–102. https://doi.org/10.1016/j.coal.2014.12.011
Sassi, F. P. (1972). The petrological and geological significance of the b0 values of potassic white micas in low-grade metamorphic rocks. An application to the Eastern Alps. *Tschermaks Mineralogische und Petrographische Mitteilungen, 18*(2), 105–113.
Sassi, F. P., & Scolari, A. (1974). The b0 value of the potassic white micas as a barometric indicator in low-grade metamorphism of pelitic schists. *Contributions to Mineralalogy and Petrology, 45*(1), 143–152. https://doi.org/10.1007/BF00371166
Schiffman, P., & Staudigel, H. (1995). The smectite to chlorite transition in a fossil seamount hydrothermal system: The basement complex of La Palma, Canary Islands. *Journal of Metamorphic Geology, 13*(4), 487–498.
Schmid, S. M., Bernoulli, D., Fügenschuh, B., Maţenco, L., Schefer, S., Schuster, R., Tischler, M., & Ustaszewski, K. (2008). The Alpine–Carpathian–Dinaridic orogenic system: Correlation and evolution of tectonic units. *Swiss Journal of Geosciences, 101*(1), 139–183. https://doi.org/10.1007/s00015-008-1247-3
Schmid, S. M., Fügenschuh, B., Kissling, E., & Schuster, R. (2004). Tectonic map and overall architecture of the Alpine orogen. *Eclogae Geologicae Helvetiae, 97*, 93–117.
Schmid, S. M., Pfiffner, O. A., Froitzheim, N., Schönborn, G., & Kissling, E. (1996). Geophysical-geological transect and tectonic evolution of the Swiss-Italien Alps. *Tectonics, 15*(5), 1036–1064.

Schmidt, J. S., Menezesl, T. R., Souza, F. V. A., Spigolon, A. L. D., Pestilho, A. L. S., & Coutinho, L. F. C. (2019). Comments on empirical conversion of solid bitumen reflectance for thermal maturity evaluation. *International Journal of Coal Geology, 201*, 44–50. https://doi.org/10.1016/j.coal.2018.11.012

Schönherr, J., Littke, R., Urai, J. L., Kukla, P. A., & Rawahi, Z. (2007). Polyphase thermal evolution in the Infra-Cambrian Ara Group (South Oman Salt Basin) as deduced by solid bitumen maturity. *Organic Geochemistry, 38*(8), 1293–1318.

Schramm, J. M. (1980). Frühalpidische Metamorphose in Gesteinen der Grauwackenzone und der Nördlichen Kalkalpen. *Jahrbericht 1979, Hochschulschwerpkt, S15, Salzburg, 1*, 77–82.

Schramm, J. M. (1982a). Zur Metamorphose des feinklastischen Permoskyth im Ostabschnitt der Nördlichen Kalkalpen (Österreich). *Verhandlungen der Geologischen Bundesanstalt, 1982*(2), 63–72.

Schramm, J. M. (1982b). Überlegungen zur Metamorphose des klastischen Permoskyth der Nörlichen Kalkalpen vom Alpenostrand bis zum Rätikon (Österreich). *Verhandlungen der geologischen Bundesanstalt, 1982*(2), 73–83.

Seidel, E. (1978). *Zur Petrologie der Phyllit-Quarzit-Serie Kretas. Technical University, Braunschweig* (p. 145). Unpublished Habilitation thesis.

Seward, D., Ford, M., Bürgisser, J., Lickorish, H., Williams, E. A., & Meckel, L. D., III. (1999). Preliminary results of fission—track analyses in the southern Pelvoux area, SE France. *Memorie di Scienze Geologiche, Padua University, 51*, 25–31.

Shaw, G. (1971). The chemistry of sporopollenin. In J. Brooks, P. Grant, M. D. Muir, G. Shaw, & P. van Gijzel (Eds.), *Sporopollenin* (pp. 305–350). Academic Press.

Smith, J. V., & Brown, W. L. (1988). *Feldspar minerals: Crystal structures, phsical, chemical, and microtextural properties. Revised* (2nd ed., p. 828). Springer Verlag.

Spackman, W. (1958). The maceral concept and the study of modern environments as a means of understanding the nature of coal. *Transactions of the New York Academy of Sciences, Series II, 20*(5), 411–423.

Spiegel, C., Siebel, W., Kuhlemann, J., & Frisch, W. (2004). Toward a comprehensive provenance analysis: A multi-method approach and ist implications for the evolution of the central Alps. *The Geological Society of America, Special Paper, 378*, 37–50.

Środoń, J. (1979). Correlation between coal and clay diagenesis in the Carboniferous of the Upper Silesian Coal Basin. *Developments in Sedimentology, 27*, 251–260. https://doi.org/10.1016/S0070-4571(08)70721-0

Środoń, J. (1984). X-ray powder diffraction identification of illitic materials. *Clays and Clay Minerals, 32*(5), 337–349.

Środoń, J. (1995). Reconstruction of maximum paleotemperatures at present erosional surface of the Upper Silesian Basin, based on the composition of illite/smectite in shales. *Studia Geologica Polonica, 108*, 9–20.

Środoń, J. (1996). Clay minerals in diagenetic processes. *Przegląd Geologiczny, 44*, 604–607. in Polish.

Środoń, J. (1999). Nature of mixed-layer clays and mechanisms of their formation and alteration. *Annual Review of Earth and Planetary Sciences, 27*, 19–53.

Środoń, J., Anczkiewicz, A. A., Dunkl, I., Vlahović, I., Velić, I., Tomljenović, B., Kawiak, T., Banaś, M., & von Eynatten, H. (2018). Thermal history of the central part of the Karst Dinarides, Croatia: Combined application of clay mineralogy and low-T thermochronology. *Tectonophysics, 744*, 155–176.

Środoń, J., Clauer, N., Banaś, M., & Wójtowicz, A. (2006). K-Ar evidence for a Mesozoic thermal event superimposed on burial diagenesis of the Upper Silesia Coal Basin. *Clay Minerals, 41*, 671–692.

Środoń, J., & Eberl, D. D. (1984). Illite. Reviews in mineralogy. In S. W. Bailey (Ed.), *Micas* (Vol. 13, p. 754). Mineralogical Society of America.

Stach, E. (1935). *Lehrbuch der Kohlenpetrographie* (p. 293). Gebrüder Bornträger.

Stalder, H. A., Wagner, A., Graeser, S., & Stuker, P. (1998). *Mineralienlexikon der Schweiz* (p. 298). Wepf.

Stampfli, G. M., Mosar, D., Marquer, D., Marchant, R., Baudin, T., & Borel, G. (1998). Subduction and obduction processes in the Western Alps. *Tectonophysics, 296*(1–2), 159–204.

Steck, A., & Hunziker, J. (1994). The Tertiary structural and thermal evolution of the Central Alps-compressional and extensional structures in an orogenic belt. *Tectonophysics, 238*(1), 229–254. https://doi.org/10.1016/0040-1951(1094)90058-90052

Stern, T., Smith, E. G. C., Davey, F. J., & Muirhead, K. J. (1987). Crustal and upper mantle structure of the northwestern North Island, New Zealand, from seismic refraction data. *Geophysical Journal of the Royal Astronimical Society, 91*, 913–936.

Strakhov, N. M. (1967). *Principles of lithogenesis* (p. 264). Oliver and Boyd.

Suárez-Ruiz, I., Flores, D., Graciano Mendonça Filho, J., & Hackley, P. C. (2012). Review and up-date of the applications of organic petrology: Part 1, geological applications. *International Journal of Coal Geology, 99*, 54–112. https://doi.org/10.1016/j.coal.2012.02.004

Šucha, V., Kraust, I., Gerthofferová, H., Peteš, J., & Sereková, M. (1993). Smectite to illite conversion in bentonites and shales of the East Slovak Basin. *Clay Minerals, 28*(2), 243–253. https://doi.org/10.1180/claymin.1993.028.2.06

Suchý, V., Frey, M., & Wolf, M. (1997). Vitrinite reflectance and shear-induced graphitization in orogenic belts: A case study from the Kandersteg area, Helvetic Alps, Switzerland. *International Journal of Coal Geology, 34*, 1–20.

Sue, C., Tricart, P., Dumont, T., & Pêcher, A. (1997). Raccourcissement polyphasé dans le massif du Pelvoux (Alpes occidentales): Exemple du chevauchement de socle de Villard-Notre-Dame Multistep shortening in the Pelvoux Massif (Western Alps): Case of the Villard-Notre-Dame Basement Thrust. *Comptes Rendus de l'Académie des Sciences - Series IIA - Earth and Planetary Science, 324*(10), 847–854.

Sweeney, J. J., & Burnham, A. K. (1990). Evaluation of a simple model of vitrinite reflectance based on chemical kinetics. *American Association of Petroleum Geologists Bulletin, 74*(10), 1559–1570.

Taff, J. A. (1909). Grahamite deposits of southeastern Oklahoma. In C. W. Hayes & W. Lindgren (Eds.), *Contributions to economic geology, 1908; Part I, metals and nonmetals, except fuels* (Vol. 380, pp. 286–297). G.P.O. https://doi.org/10.3133/b3380

Teichmüller, M. (1958). Métamorphism du charbon et prospection du pétrole. *Revue de l'industrie minérale numéro spécial, 1958*, 99–113.

Teichmüller, M. (1987). Organic material and very low-grade metamorphism. In M. Frey (Ed.), *Low temperature metamorphism, 114–161* (p. 351). Blackie & Son Ltd.

Thöni, M. (1981). Degree and evolution of the Alpine metamorphism in the Austroalpine unit W of the Hohe Tauern in the light of K/Ar and Rb/Sr age determinations on micas. *Jahrbuch der Geologischen Bundesanstalt Wien, 142*, 111–174.

Tollmann, A. (1959). Der Deckenbau der Ostalpen auf Grund der Neuuntersuchungen des Zentralalpinen Mesozoikums. *Mitteilungen der Gesellschaft der Geologie- und Bergbaustudenten in Österreich, 10*, 1–62.

Tollmann, A. (1976). *Der Bau der Nördlichen Kalkalpen - orogene Stellung und regionale Tektonik* (p. 449). F. Deuticke.

Tollmann, A. (1978). Plattentektonische Fragen in den Ostalpen und der plattentektonische Mechanismus des mediterranen Orogens. *Mitteilungen der Österreichischen Geologischen Gesellschaft, 69*, 291–351.

Tricart, P. (1986). Le Chevauchement de la zone briançonnaise au Sud-Est du Pelvoux; clé des rapports zone externe—zones internes dans les Alpes occidentales. *Bulletin de la Société Géologique de France, Huitième Série, 2*, 233–244.

Tricart, P. (2004). From extension to transpression during the final exhumation of the Pelvoux and Argentera massifs, Western Alps. *Eclogae Geologicae Helvetiae, 97*(1), 429–439.

Tricart, P., Bourbon, M., Chenet, P. Y., Cros, P., Delorme, M., & Dumont, T. (1988). Tectonique synsédimentaire triasico-jurassique et rifting téthysien dans la nappe briançonnaise de Peyre-Haute (Alpes occidentales). *Bulletin de la Société géologique de France, 4*, 669–680.

Trommsdorff, V. (1983a). Petrologic aspects of serpentinite metamorphism. *Rendiconti della Societa Italiana di Mineralogia e Petrologia, 38*, 549–559.

Trommsdorff, V. (1983b). Metamorphose magnesiumreicher Gesteine: Kritischer Vergleich von Natur, Experiment und thermodynamischer Datenbasis. *Fortschritte der Mineralogie, 61*(2), 283–308.

Trommsdorff, V., & Dietrich, V. (1980). Alpine metamorphism in a cross section between the Rhine and Valtellina valleys (Switzerland and Italy). Excursion No. 7. In R. Trümpy (Ed.), *Geology of Switzerland—A guidebook, Part B: Geological excursions* (pp. 317–341). Wepf.

Trommsdorff, V., & Evans, B. W. (1974). Alpine metamorphism of peridotitic rocks. *Schweizerische Mineralogische und Petrologische Mitteilungen, 54*, 333–352.

Trullenque, G. (2005). *Tectonic and microfabric studies along the Penninic Front between Pelvoux and Argentera Massifs (Western Alps, France)* (p. 301). Unpublished Ph.D. thesis, University Basel, Switzerland.
Trullenque, G., Kunze, K., Heilbronner, R., Stünitz, H., & Schmid, S. M. (2006). Microfabrics of calcite ultramylonites as records of coaxial and non-coaxial deformation kinematics: Examples from the Rocher de l'Yret shear zone (Western Alps). *Tectonophysics, 424*(1–2), 69–97.
Trümpy, R. (1975). Penninic–austroalpine boundary in the Swiss Alps: A presumed former continental margin and its problems. *American Journal of Science, 275*(A), 209–238.
Trümpy, R. (1980a). *Geology of Switzerland, a guide-book, Part A: An outline of the geology of Switzerland* (p. 104). Wepf & Co.
Trümpy, R. (1980b). *Geology of Switzerland, a guide-book, Part B: Geological excursions* (p. 230). Wepf & Co.
Velde, B. (1965). Experimental determination of muscovite polymorph stabilities. *American Mineralogist, 50*, 436–449.
Velde, B. (1977). *Clays and clay minerals in natural and synthetic systems, developments in sedimentology* (Vol. 21, p. 217). Elsevier Science Ltd.
Velde, B. (1985). Possible chemical controls of illite/smectite composition during diagenesis. *Mineral Magazine, 49*, 387–391.
Wada, H., Tomita, T., Matsuura, K., Iuchi, K., Ito, M., & Morikiyo, T. (1994). Graphitization of carbonaceous matter during metamorphism with references to carbonate and pelitic rocks of contact and regional metamorphism, Japan. *Contributions to Mineralogy and Petrology, 118*, 217–228.
Waibel, A. F. (1990). *Sedimentology, petrographic variability, and very-low-grade metamorphism of the Champsaur sandstone (Paleogene, Hautes-Alpes, France). Evolution of volcaniclastic foreland turbidites in the external Western Alps* (p. 140). Unpublished PhD thesis, Université de Genève.
Waliczek, M., Machowski, G., Poprawa, P., Świerczewska, A., & Więcław, D. (2020). A novel VRo, T, and S indices conversion formulae on data from the fold-and-thrust belt of the Western Outer Carpathians (Poland). *International Journal of Coal Geology, 234*(11–12), 103672. https://doi.org/10.1016/j.coal.2020.10367
Waliczek, M., Machowski, G., Więcław, D., Konon, A., & Wandycz, P. (2019). Properties of solid bitumen and other organic matter from Oligocene shales of the Fore-Magura Unit in Polish Outer Carpathians: Microscopic and geochemical approach. *International Journal of Coal Geology, 210*, 103206. https://doi.org/10.1016/j.coal.2019.05.01
Walther, J. V., & Orville, P. M. (1982). Volatile production and transport in regional metamorphism. *Contributions to Mineralogy and Petrology, 79*, 252–257.
Wang, H. (1994). *Diagenesis and incipient metamorphism of Helvetic Alps, Eastern Switzerland: Clay mineral data* (p. 88). Unpublished Ph.D. thesis, University Basel, Switzerland.
Wang, H., Frey, M., & Stern, W. B. (1996). Diagenesis and metamorphism of clay minerals in the Helvetic Alps of eastern Switzerland. *Clays and Clay Minerals, 44*(1), 96–112.
Waples, D. W. (1980). Time and temperature in petroleum formation: Application of Lopatin's method of petroleum exploration. *American Association of Petroleum Geologists Bulletin, 64*, 916–926.
Warr, L. N., & Ferreiro Mählmann, R. (2015). Recommendations for Kübler index standardization. *Clay Minerals, 50*, 282–285.
Warr, L. N., Primmer, T. J., & Robinson, D. (1991). Variscan very low-grade metamorphism in southwest England: A diastathermal and thrust-related origin. *Journal of Metamorphic Geology, 9*, 751–764.
Warr, L. N., & Rice, A. H. (1994). Interlaboratory standardization and calibration of clay mineral crystallinity and crystallite size data. *Journal of Metamorphic Geology, 12*, 141–152.
Weaver, C. E. (1960). Possible use of clay minerals in search for oil. *American Association of Petroleum Geologists Bulletin, 44*(9), 1505–1518.
Weaver, C. E. (1961). *Clay minerals of the Ouachita structural belt and adjacent foreland* (Vol. 6120, pp. 147–162). Bureau of Economic Geology, University of Texas.
Weaver, C. E. (1967). Potassium, illite and the ocean. *Geochimica et Cosmochimica Acta, 31*(11), 2181–2196.
Weaver, C. E. (1984). *Shale slate metamorphism in southern Appalachians* Developments in petrology (Vol. 10, p. 240). Elsevier Science Ltd.
Weber, K. (1972). Kristallinität des Illits in Tonschiefern und andere Kriterien schwacher Metamorphose im nordöstlichen Rheinischen Schiefergebirge. *Neues Jahrbuch für Geologie und Paläontologie – Abhandlungen, 141*(3), 333–363.
Weissert, H. J., & Bernoulli, D. (1985). A transform margin in the Mesozoic Tethys: Evidence from the Swiss Alps. *Geologische Rundschau, 74*(3), 665–679.
Wenger, L. M., & Baker, D. R. (1987). Variations in vitrinite reflectance with organic facies-examples from Pennsylvanian cyclothems of the Midcontinent, USA. *Organic Geochemistry, 11*(5), 411–416.
Wenk, E. (1958). Über Diskontinuitäten in Plagioklasserien metamorphen Ursprungs. *Schweizerische Mineralogische und Petrologische Mitteilungen, 38*(3), 494–498.
Wenk, E. (1962). Plagioklas als Indexmineral in den Zemtralalpen. Die Paragenese Calcit-Plagioklas. *Schweizerische Mineralogische und Petrologische Mitteilungen, 42*(1), 139–152.
Wenk, E., & Keller, F. (1969). Isograde in Amphibolitserien der Zentralalpen. *Schweizerische Mineralogische und Petrologische Mitteilungen, 49*, 157–198.
White, D., & Thiessen, R. (1913). *The origin of coal* (Vol. 38, p. 390). U.S. Government Printing Office.
Whitney, G. (1990). Role of water in the smectite to illite reaction. *Clays and Clay Minerals, 38*(4), 343–350.
Will, P., Lüders, V., Wemmer, K., & Gilg, H. A. (2016). Pyrophyllite formation in the thermal aureole of a hydrothermal system in the Lower Saxony Basin, Germany. *Geofluids, 16*(2), 349–363. https://doi.org/10.1111/gfl.12154
Winkler, H. G. F. (1979). *Petrogenesis of metamorphic rocks* (5th ed., p. 348). Springer Verlag.
Winkler, W. (1988). Mid- to early Late Cretaceous flysch and melange formations in the western part of the Eastern Alps; palaeotectonic implications. *Jahrbuch der Geologischen Bundesanstalt Wien, 131*(2), 341–389.
Wolf, M. (1975). Über die Beziehung Illit-Kristallinität und Inkohlung. *Neues Jahrbuch für Geologie und Paläonologie, Monatshefte, 7*, 437–447.
Yalçin, H., & Bozkaya, Ö. (2011). Sepiolite-palygorskite occurrences in Turkey. *Developments in Clay Science, 3*, 175–200.
Yokoyama, K., Brothers, R. N., & Black, P. M. (1986). Regional eclogite facies in the high-pressure metamorphic belt of New Caledonia. In B. W. Evans & E. H. Brown (Eds.), *Blueschists and eclogites. Geological Society of America Memoir* (Vol. 164, pp. 407–423).
Zerlauth, M., Bertrand, A., Rantitsch, G., Groß, D., Ortner, H., Pomella, H., & Fügenschuh, B. (2015). Thermal history of the westernmost Eastern Alps (Penninic Rhenodanubian Flysch nappes, Helvetic nappes, and subalpine Molasse thrust sheets). *International Journal of Earth Sciences, 105*, 1525–1547.
Zhang, S. Y., & Zhang, H. F. (2020). Genesis of the Baiyun pyrophyllite deposit in the Central Taihang Mountain, China: Implications for gold mineralization in wall rocks. *Ore Geology Reviews, 120*, 103313. https://doi.org/10.1016/j.oregeorev.2020.103313
Zhu, C., Rao, S., & Hu, S. (2016). Application of illite crystallinity for paleo-temperature reconstruction: A case study in the western Sichuan basin, SW China. *Carpathian Journal of Earth and Environmental Sciences, 11*(2), 599–608.
Zyndel, F. (1912). *Über den Gebirgsbau Mittelbündens*. Beiträge zur geologischen Karte der Schweiz, (N.F.) (p. 40). A. Francke (vorm. Schmid & Francke).

Publisher's Note